Silicon Carbide Oxidation in High Temperature Steam

by

ARCHIVES

Ramsey Paul Arnold

Bachelor of Science, Chemical Engineering
Carnegie Mellon University, 2009

Submitted to the Department of Nuclear Science and Engineering in Partial Fulfillment of the Requirements for the Degree of

MASTER OF SCIENCE IN NUCLEAR SCIENCE AND ENGINEERING

at the

MASSACHUSETTS INSTITUTE OF TECHNOLOGY

September 2011

© 2011 Massachusetts Institute of Technology. All rights reserved

Signature of Author: _____
Department of Nuclear Science and Engineering
August 19, 2011

Certified by: _____
Mujid S. Kazimi, Ph.D.
TEPCO Professor of Nuclear Engineering
Thesis Supervisor

Certified by: _____
Thomas J. McKrell, Ph.D.
Research Scientist
Thesis Reader

Accepted by: _____
Mujid S. Kazimi, Ph.D.
Chair, Department Committee on Graduate Students

This Page Left Intentionally Blank

Silicon Carbide Oxidation in High Temperature Steam

by

Ramsey P. Arnold

Submitted to the Department of Nuclear Science and Engineering
On August 19, 2011 in Partial Fulfillment of the
Requirements for the Degree of Master of Science in
Nuclear Science and Engineering

ABSTRACT

The commercial nuclear power industry is continually looking for ways to improve reactor productivity and efficiency and to increase reactor safety. A concern that is closely regulated by the Nuclear Regulatory Commission is the exothermic zircaloy-steam oxidation reaction which can potentially occur during a loss of coolant accident (LOCA), and may become autocatalytic beyond 1,200°C, thus generating a large amount of hydrogen. The concern for the zircaloy oxidation reaction has been heightened since the March 2011 events of Fukushima, Japan. One solution offering promising results is the use of silicon carbide (SiC) cladding in nuclear reactor fuel rod designs. SiC, a robust ceramic which reacts very slowly with water or steam, has many features that meet or exceed that of zircaloy including the ability to withstand higher temperatures due to a higher melting point and the ability to absorb fewer neutrons than zircaloy which would allow for increased safety margins and fuel burnup.

An experimental investigation of the oxidation performance of α-SiC during a postulated LOCA event was performed. The test facility was designed and fabricated to test the oxidation rates of zircaloy and SiC in a high temperature, high-purity, flowing steam environment. Studies of zircaloy-4 oxidation were conducted to validate the test facility for this purpose. Thirty six zircaloy-4 tests lasting up to 30 minutes, at temperatures ranging from 800°C to 1,200°C, were completed and compared to existing models and literature data. Additionally, six longer duration α-SiC tests lasting from 8 hours to 48 hours, at temperatures of 1,140°C and 1,200°C, were completed.

These tests clearly show that, from an oxidation perspective, SiC significantly outperforms zircaloy in high-flowing, superheated steam. For zircaloy, results from the most intense temperature/duration testing combination of 1,200°C for 30 minutes show 15.6 percent weight gain. For the most intense SiC tests at 1,200°C for eight hours, a weight loss of two orders of magnitude less occurred, a 0.077 percent weight loss. The four 24 hour and 48 hour SiC tests at 1,140°C also correlate well with the expected paralinear oxidation trend and further confirm that SiC is more resistant to oxidation in high temperature steam than zircaloy.

Thesis Supervisor: Mujid Kazimi
Title: TEPCO Professor of Nuclear Engineering

This Page Left Intentionally Blank

Acknowledgements

I would like to thank my thesis advisor, Professor Kazimi, for his academic support and for his guidance, encouragement, and valuable insight into my research. I am equally grateful to Dr. McKrell for his continuous support, patience, and direction in helping me design and implement my experimental approach. Both have helped me develop a strong research oriented background and continued to advance my professional development.

I would like to thank my lab mates that worked on this MIT LOCA study with me: Chao Yue, Youho Lee, and Faris Toqan. The collaborative and open nature of our team made for a positive and productive work environment and allowed me to learn a lot from each of you. I would also like to thank Herb Feinroth and *Ceramic Tubular Products* for the many useful discussions about our studies and providing us with the SiC samples.

I would like to thank my parents, sister, and girlfriend for the constant support that I've received over the past year. I am also grateful for the great camaraderie I've developed with my classmates in the classrooms, labs, and offices as well as on the fields and courts. I don't know how I would have completed this without all of you.

Finally, I would like to thank the Defense Nuclear Facilities Safety Board for their professional and financial support during my studies at MIT.

This Page Left Intentionally Blank

Table of Contents

List of Figures

List of Tables

Nomenclature

atm	atmosphere(s)
BWR	boiling water reactor
°C	degrees Celsius
CFR	Code of Federal Regulations
cm	centimeter(s)
CTP	Ceramic Tubular Products
CVD	chemical vapor deposition
DBA	design basis accident
ECCS	emergency core cooling systems
ECR	equivalent cladding reacted
°F	degrees Fahrenheit
g	gram(s)
(g)	gas
ΔH_{rxn}	enthalpy/heat of reaction
K	Kelvin
kgU	kilogram(s) of Uranium
kJ	kilojoule(s)
LBLOCA	large break loss of coolant accident
LOCA	loss of coolant accident
LWR	light water reactor
m	meter
MIT	Massachusetts Institute of Technology
mL	milliliter(s)
mm	millimeter(s)
mol	mole
MPa	megapascal(s)
MWd	megawatt-day(s)
MW_{th}	megawatt(s)-thermal
NRC	Nuclear Regulatory Commission
PWR	pressurized water reactor
s	second(s)
(s)	solid
SEM	scanning electron microscope
SiC	silicon carbide
SiO_2	silicon dioxide/silica
U-235	uranium-235
U.S.	United States of America
UO_2	uranium dioxide
ZrO_2	zirconium dioxide
W	watt(s)

This Page Left Intentionally Blank

1. Introduction

1.1 Motivation for this Research

The promising results from ongoing research involving silicon carbide (SiC) cladding at Massachusetts Institute of Technology (MIT) and in the private sector acquired increased importance for the commercial nuclear power industry since the March 2011 events of Fukushima, Japan, as new cladding designs and materials are being considered for use in nuclear reactors [Carpenter 2010; Dobisesky 2011; Stempien 2011]. Equally important to the nuclear power industry is the challenge of improving the productivity and efficiency of a reactor, which can be accomplished by increasing the burnup of the fuel, improving characteristic properties of heat transfer in the reactor, and developing advanced materials. For example, in an ongoing Lightbridge and MIT study, the development of a helical cruciform fuel rod design has been seen to allow for a higher core power density by increasing the surface-to-volume ratio of a fuel rod which results in more efficient heat dissipation of the fuel rod, a lower fuel rod heat flux, and a lower centerline temperature of the fuel rod [Kazimi 2011]. Another way to possibly improve reactor productivity and efficiency and to increase reactor safety is the implementation of SiC cladding into a reactor which is also the focus of this thesis. Assuming it is accepted by the Nuclear Regulatory Commission (NRC), it is speculated that SiC cladding would enable the fuel to safely achieve a higher burnup because of its superior material properties in comparison to present zircaloy claddings. Additionally, SiC can maintain its strength at high temperatures which could be useful for light water reactor (LWR) emergency scenarios and for use in future reactor designs. The underlying goal of this study is to examine the oxidation reaction of SiC in high temperature steam.

1.1.1 Current Cladding of LWR Fuel

Nuclear fuel rods consist of two parts: cylindrical fuel pellets, most often made of uranium dioxide (UO_2), and cladding consisting of a hollow tube into which the fuel pellets are stacked. The primary function of the cladding is to physically separate the fuel from the coolant and act as a barrier that prevents the release of fission products into the primary coolant system. The Seabrook PWR Nuclear Power Plant located in Seabrook, New Hampshire, has an output of 3,400 MW_{th} and contains more than 50,000 fuel rods in its core, each with a height of 4 m, a cladding outer diameter of 9.5 mm, a cladding thickness of 0.572 mm, and a fuel-cladding gap of

0.0826 mm [Todreas 2011]. For this reason, it is vital that the fuel rods have a low failure rate and the ability to be manufactured precisely, within the necessary industry tolerances.

In an LWR, the structural integrity of the cladding is one of the most important aspects of the reactor design. A major constraint on core thermal performance is the need to protect the cladding from the harsh environment of a reactor which includes a variety of thermal and mechanical stresses, damaging chemical reactions, and radiation exposure [Duderstadt 1976]. The ideal cladding material would have a high melting point in order to maintain its structural integrity both during normal operating conditions and during the harshest design basis accidents (DBAs) and would have a small neutron capture cross-section so that the cladding has minimal impact on the neutron population of the reactor [Glasstone 1981]. Because of its suitable material properties, zirconium alloys, referred to as zircaloy, have been used as the cladding material of choice for commercial nuclear power reactors since the early 1960's [Simnad 1981]. Ongoing improvements to the material have continually been developed since then. The majority of U.S. reactors utilize either zircaloy-2 (1.5% Sn, 0.12% Fe, 0.1% Cr, balance Zr) in boiling water reactors (BWRs) or zircaloy-4 (1.5% Sn, 0.2% Fe, 0.1% Cr, balance Zr) in pressurized water reactors (PWRs); however, in the past twenty years, two new zirconium alloys with improved properties have been accepted for use in the U.S.: Zirlo, from *Westinghouse Electric Company* in 1991, and M5, from *Framatome ANP* in 2003 [NRC 2003; Pickman 1972; Yueh 2005]. Although current claddings used in LWR fuel are able to meet the required safety regulations of the NRC, there is an interest in improving the cladding materials and design which could increase safety margins and improve the productivity and efficiency of a reactor.

1.1.2 Loss of Coolant Accidents

The underlying goal of this study is to examine how fast SiC would react with high temperature, flowing steam during one of the most studied DBAs, a loss of coolant accident (LOCA). Although a LOCA event is not expected to occur at any point during the lifetime of a reactor, reactors must still be designed with layers of safety systems to protect them in the unlikely event that such an accident does occur. With a small break LOCA, pressures in the primary coolant system can remain close to the normal operating pressure for quite some time – approximately 7.6 MPa for a BWR and 15.5 MPa for a PWR. Conversely, the most severe DBA, a large break LOCA (LBLOCA), is where a double-ended guillotine pipe rupture of the reactor primary

coolant system occurs. A LBLOCA is characterized by four phases that are brought on by the accident itself coupled with the safety systems that are in place and are intended to mitigate the event [Todreas 2011]. The first phase is the "blowdown phase" which lasts for approximately 20 seconds and occurs when the contents of the reactor are blown down into containment through a break in the pipe which causes a prompt pressure drop of the primary coolant system and a pressure increase in the containment. Next is the "refill phase" which lasts for 10 to 20 seconds and results in the lower plenum of the reactor core refilling with water from the emergency core cooling systems (ECCS). The third phase is the "reflood phase" which rewets the fuel rods by water from the ECCS as the core continues to fill. The final phase is the "long term core cooling phase" which circulates water through the core by the ECCS process. Typically, during a LBLOCA, the pressure of the primary loop coolant system drops dramatically to approximately 0.2 to 0.3 MPa within the first two to three minutes, while the pressure of the containment increases to the same final pressure. It is important to note that during the blowdown phase, as water is emptying from the reactor core, the fuel rods begin to become uncovered and remain at least partially uncovered until the core has been completely reflooded during the long term core cooling phase. During this time, conservative calculations show that the peak clad temperature could approach 1,200°C (2,200°F), as seen in Figure 1 [Nero 1979].

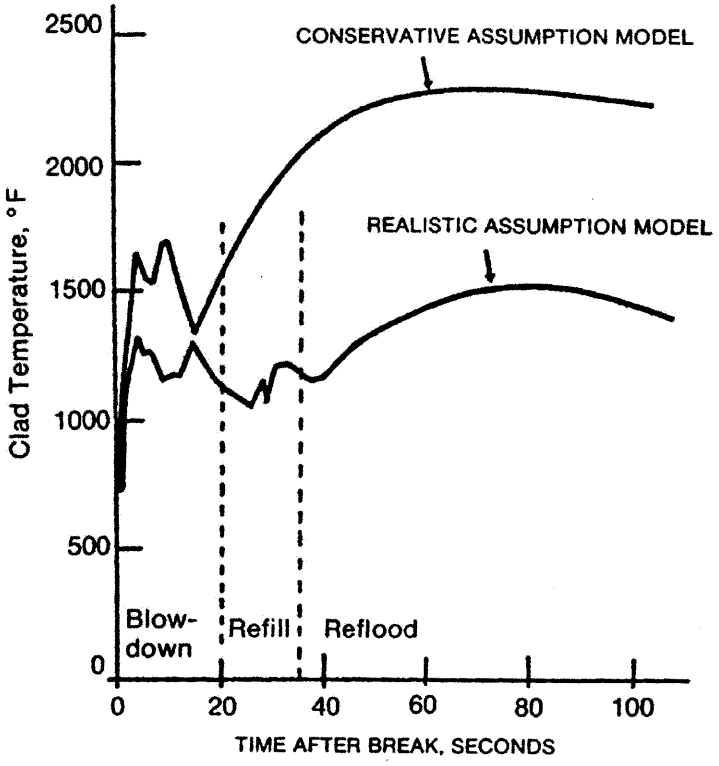

Figure 1 – Calculated fuel clad temperatures for a PWR LOCA [Nero 1979]

A PWR LOCA environment can be characterized by elevated fuel temperatures and a superheated steam-water mixture as its primary chemical constituent with other vaporized or aerosolized chemicals and impurities that are present in the primary coolant loop of a nuclear reactor during its operation. Prior to the cladding being rewetted by a rising water level from the ECCS, it is susceptible to steam oxidation in the sections where film boiling is occurring and above the water level where steam is naturally flowing. During the blowdown phase of a LOCA, the steam has been shown to be flowing at velocities of up to 32 m/s; however, once cladding temperatures have become stable, which should occur within approximately three minutes into the accident, the steam velocity is reduced to less than 5 m/s [Feng 2007]. In terms of temperature, Figure 2 summarizes the core materials degradation that will occur in the different temperature regimes that could occur during a LOCA if the ECCS did not function properly. To summarize, a PWR LOCA environment prior to cladding rewetting consists of high temperature, superheated, flowing steam as well as other vaporized or aerosolized constituents with a range of resulting pressures.

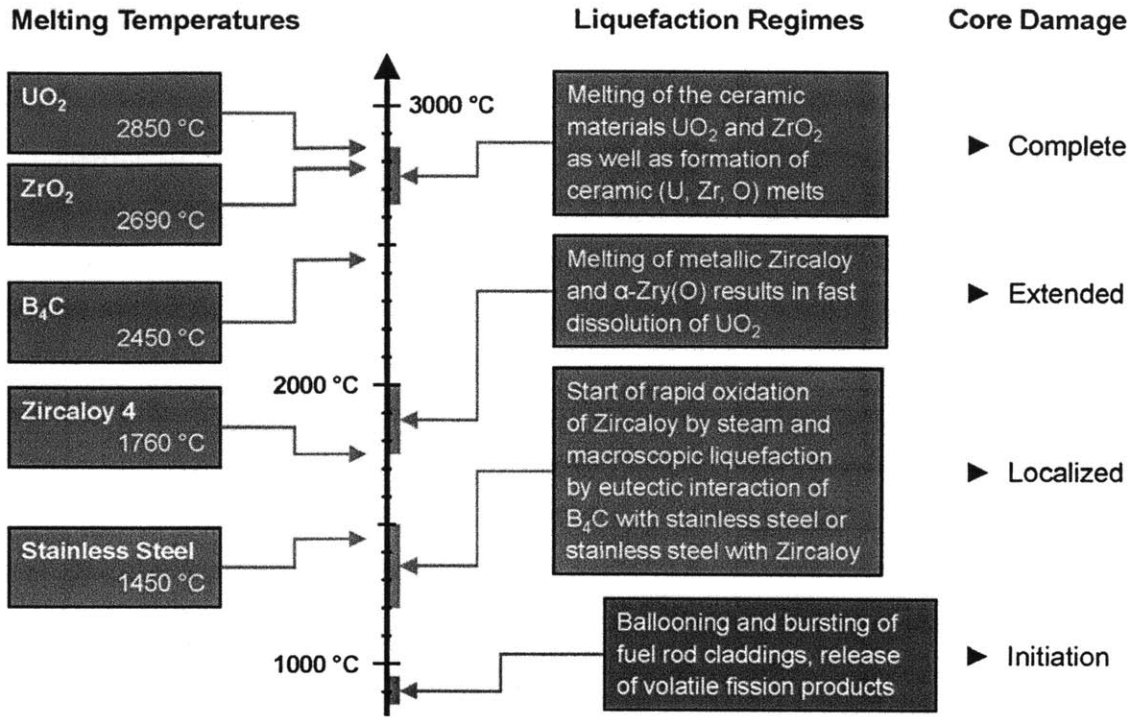

Figure 2 – Core materials degradation temperature regimes [KIT 2011]

1.1.3 Safety Regulations

There are two NRC safety regulations that are related to and a direct result of current zircaloy cladding limitations. First, the current fuel rod discharge burnup limit in the U.S. is 62 MWd/kgU average for the peak rod with the most advanced cladding types [NRC 2003]. Although the average discharge burnup among PWRs as of 2002 was 45.7 MWd/kgU while utilizing fuels with U-235 enrichments of less than four percent by weight, research within the nuclear power community suggests that there is the potential to further enhance the productivity and efficiency of LWRs by raising the maximum allowable burnup and increasing uranium enrichment limits [EPRI 2008; Olander 2001]. However, with safety as the primary concern of the commercial nuclear power industry, such regulatory enhancements would have to be extensively analyzed before any changes could be implemented.

The second NRC safety regulation that involves fuel cladding requires that reactor ECCS have a calculated cooling performance that meets the following criteria in the event of a LOCA: the maximum fuel element cladding temperature shall not exceed 1,200°C, the total oxidation of the

cladding shall nowhere exceed 17 percent of the total thickness of the cladding before oxidation, the maximum hydrogen generation shall not exceed one percent of the amount that would be generated if all of the metal in the cladding were to react, any change in the core geometry must be calculated to result in a coolable geometry, and the long-term cooling must be sufficient to control decay heat and cool the core to acceptable levels [10 CFR § 50.46]. These constraints are needed because zircaloy begins to undergo a highly exothermic oxidation reaction (ΔH_{rxn} is approximately 6,500 kJ/kg Zr) with steam at temperatures beyond 1,200°C, as seen in Equation 1.1 [Collier 1987; Hoffman 1989; Perry 2008]. The exothermic nature of Equation 1.1 beyond 1,200°C means the reaction is autocatalytic and therefore the rate of hydrogen generation and material loss is greatly accelerated. Additionally, hydrogen generation renders the cladding brittle due to hydrogen embrittlement. The limits imposed by 10 CFR § 50.46 will insure that some ductility will remain in the zircaloy cladding which will allow the core to remain intact during the ECCS process in the event of a LOCA [Waeckel 2000].

$$Zr_{(s)} + 2\,H_2O_{(g)} \rightarrow ZrO_{2(s)} + 2\,H_{2(g)} + 596.4\ \text{kJ/mol Zr} \qquad \text{Equation 1.1}$$

1.2 Silicon Carbide as LWR Cladding

Although research and development of zircaloy has continuously been improving the material for use as cladding, there remain a number of annual cladding failures in recent reactor operation history. Several challenges that may be the cause of this include higher power levels, increased discharge burnups, longer fuel cycles, higher enrichments, and more aggressive water chemistry conditions intended to reduce corrosion in other areas of the primary coolant system [Yang 2006]. For this reason as well as the previously discussed drawbacks of zircaloy, new cladding designs and materials should be evaluated for use in nuclear reactors to improve safety margins and increase productivity and efficiency. SiC, a robust ceramic, has several features that greatly improve upon those of zircaloy including its ability to withstand higher temperatures due to its melting point of 2,545°C, as compared to 1,850°C for zircaloy-4 [ATI Wah Chang 2003; Snead 2007]. Also, SiC is less chemically active, it does not interact with steam in a similar intense fashion as zircaloy does, and it is less susceptible to thermal and mechanical loads due to its modest thermal conductivity, low thermal expansion coefficient, and low creep rate [Carpenter 2008; Stempien 2011]. In comparison to Figure 2 with SiC cladding substituted for zircaloy, a more positive depiction of the potential temperature regimes results. Because SiC maintains its

strength at much higher temperatures than zircaloy and does not expand significantly due to thermal stresses, ballooning and bursting of fuel rod cladding would likely not occur until much higher temperatures are reached where the strength of SiC begins to weaken [Snead 2007]. Also, as will be shown in this study, rapid oxidation of SiC does not occur which prevents weakening of the cladding and significant production of hydrogen. Finally, because SiC is a ceramic, its melting point occurs in the same temperature regime as that of UO_2 which is a substantial improvement over zircaloy. For these reasons, SiC cladding research has continued to be of interest to MIT and the commercial nuclear power industry.

Over the past several years, a group of researchers and companies in the U.S. has taken on a new initiative to investigate SiC cladding as a potential improvement over and replacement for zircaloy cladding. One such company with which MIT has been collaborating during this study is *Ceramic Tubular Products* (*CTP*), located in Rockville, Maryland. *CTP* has a goal to develop SiC cladding for use in existing and future LWR designs that will allow for improvements in the service of the fuel rods. The particular design that they have been studying consists of three layers of SiC in different forms and is referred to as triplex cladding. Different design iterations have been tested under LWR in-core conditions and some designs were seen to be stable under irradiation and coolant chemistry conditions [Carpenter 2010]. Figure 3 shows a cross-sectional view of the triplex cladding design. The inner layer is a monolith SiC tube that provides most of the strength and stiffness to the cladding. It is the primary barrier to prevent fission product release. The middle layer is a SiC fiber-matrix composite that provides protection to the inner layer and impedes crack propagation. This layer consists of SiC fibers that are wound around the tube and a SiC matrix that is applied by chemical vapor deposition (CVD). The outer layer is a thin CVD SiC coating that provides further protection from the coolant and a uniform surface finish. The dimensions for each layer and the SiC phase, either α or β, have not been finalized as the triplex design is still under development. For this reason, it would be useful to better understand the differences of the two phases of SiC – in particular, how they would perform during a LOCA event in comparison to zircaloy.

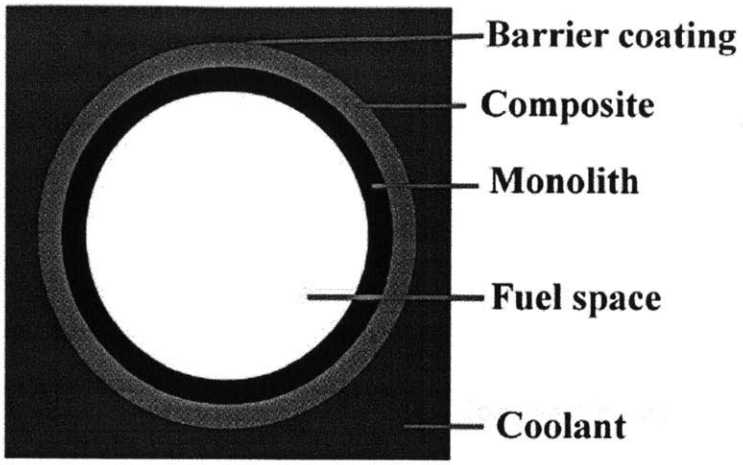

Figure 3 – Triplex SiC cladding design [Carpenter 2010]

1.3 Objective and Scope

The objective of this work is to experimentally investigate the oxidation performance of SiC during a postulated LOCA event. Oxidation rates will be determined for α-SiC samples in a steam environment at temperatures from 1,140°C to 1,200°C at atmospheric pressure. Also, a scanning electron microscope (SEM) materials analysis will be performed on the samples to better understand the driving reaction mechanisms and morphology of the oxidation. It is expected that SiC will outperform zircaloy under these conditions. The design, construction, validation, and operation of an experiment that is capable of subjecting samples to a steam environment at temperatures up to 1,600°C will be conducted. Once completed, correlations of the oxidation rate of SiC samples as a function of exposure time and temperature in the LOCA superheated, flowing steam environment will be experimentally determined and compared to analogous zircaloy-4 data acquired in this study and published in literature. Also, parabolic and linear recession rate constants and the development of a paralinear kinetic model as a function of temperature and steam flow rate will be investigated.

A primary testing material of Hexoloy tubes, made of α-phase SiC and manufactured by *Saint-Gobain Ceramics* located in Niagara Falls, New York, was chosen due to its availability, relevancy, and suitability for benchmarking with similar *CTP* data. These primary test material samples will be run at a furnace temperature of 1,140°C and 1,200°C. Also, for each test temperature, samples will be run at several different time durations. Each sample time and temperature combination will be tested at least twice for redundancy. Approximately 40 samples

will be needed for the initial batch of primary sample testing. Secondary testing materials include α-phase SiC rectangular blocks and β-phase SiC tubes for future testing. In order to validate and benchmark the design of the test facility, 36 zircaloy-4 tube samples will be tested and then the results will be compared to those of relevant studies relating to zircaloy oxidation in steam. Completion of these tests will allow for comparisons between zircaloy and SiC and between the MIT experimental results and those of *CTP*.

1.4 Thesis Organization

Consisting of six chapters, this thesis explores the past studies relating to cladding oxidation and describes the design, operation, and results of experiments completed at the MIT oxidation test facility.

Chapter Two reviews general background information on the silicon carbide oxidation kinetics and reaction mechanisms including differences between low and high temperature regimes and the effect of steam flow rate on the oxidation. Also, a discussion of the thermodynamics of a SiC-steam system is presented.

Chapter Three presents the experimental approach and design of the oxidation test facility at MIT. The different equipment and procedures are described as well as the pre-analysis that went into properly designing the facility.

Chapter Four describes the different tests that were conducted in order to validate and benchmark the test facility. A comparison between the zircaloy tests of this study and previous zircaloy studies is included.

Chapter Five discusses the different SiC tests that were completed and future tests to be completed that were beyond the timeline of this thesis work that will add to a better understanding of SiC oxidation in high temperature flowing steam. A comparison of results between MIT and *CTP* is included.

Chapter Six summarizes the findings and conclusions of this work. A discussion also follows that suggests further SiC oxidation testing and ways to improve the MIT oxidation test facility.

This Page Left Intentionally Blank

2. Silicon Carbide Oxidation

2.1 General Background

In order to study SiC oxidation, it was necessary to understand the results of previous studies in this field. A background review was completed of studies that characterize SiC oxidation kinetics and reaction mechanisms in high temperature steam environments. SiC has been previously studied extensively for uses in semiconductors and for combustion applications. SiC research for nuclear applications has also been looked at but not as extensively in the area of high temperature oxidation. A thermodynamic analysis was also completed using the *FactSage* software suite to further understand the different reaction mechanisms that are involved in SiC oxidation. It is important to note that there are distinct differences between low and high temperature testing regimes including the major reaction mechanisms and the oxidation kinetics that are involved. For the purpose of this study, high temperatures will be used to refer to temperatures greater than 1,127°C while low temperatures will be used to describe temperatures below this. It has been seen in SiC-water vapor thermodynamics analyses that this temperature is the limit between two different reaction regimes [Opila 1999]. Therefore, since all SiC testing that is completed in this study is at 1,140°C or greater, all experiments can be considered to be high temperature steam LOCA tests. For a summary and discussion of low temperature SiC oxidation testing, please refer to the Ph.D. dissertation of Dr. David Carpenter, *An Assessment of Silicon Carbide as a Cladding Material for Light Water Reactors*, which was completed at MIT in 2010.

To begin to understand SiC oxidation, it is first useful to look at the Deal-Grove model which examines the thermal-oxidation kinetics of silicon, Si [Deal 1965]. The oxidation model takes into account the reactions occurring at the two boundaries of the oxide layer, the diffusion process in the oxide layer, and that the oxidation process is controlled by the inward movement of the oxidant species, either molecular oxygen, O_2, or water, H_2O, in the cases of dry- and wet-oxygen oxidation, respectively. This is referred to as diffusion controlled kinetics. The model assumes the transported oxidant species must go through the following stages: it is transported from the bulk of the oxidizing gas to the outer surface of oxide where it reacts or is adsorbed; it is transported across the oxide film towards the unreacted silicon; and it reacts at the silicon surface to form a new layer of silicon dioxide (SiO_2) which is also referred to as silica. Each of

these three steps can be described as independent flux, F, equations which model each stage of the oxidant species transport, as seen in Figure 4. By assuming that all three fluxes are equal to one another in the steady state condition, the result is shown in Equation 2.1 where k is the reaction rate at the Si/SiO_2 surface per mole, C^* is the equilibrium concentration of the oxidant in the oxide as determined by Henry's law, h is the gas-phase transport coefficient, x_o is the total oxide layer thickness, and D_{eff} is the effective diffusion coefficient. With some manipulation, Equation 2.1 can be solved and rearranged to yield the more useful Equation 2.2 where t is time, N is the number of oxidant molecules in a unit volume of the oxide layer, and x_i is the initial thickness of the oxide layer.

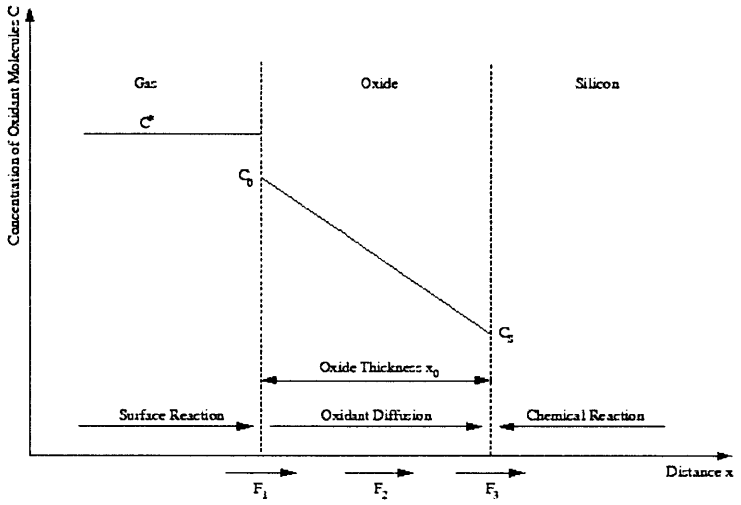

Figure 4 – One-dimensional model for the oxidation of silicon [Deal 1965]

$$F_1 = F_2 = F_3 = F = \frac{k \cdot C^*}{1 + k/h + k \cdot x_o / D_{eff}} \qquad \text{Equation 2.1}$$

$$x_o{}^2 + A \cdot x_0 = B \cdot (t + \tau) \qquad \text{Equation 2.2}$$

where $A = 2 \cdot D_{eff} \cdot (1/k + 1/h)$

$B = 2 \cdot D_{eff} \cdot C^*/N$

$\tau = (x_i{}^2 + A \cdot x_i)/B$

Equation 2.2 can be further manipulated to yield Equation 2.3 which is an expression for the oxide thickness in terms of oxidation time. Looking at relatively large times, i.e., $t \gg A^2/4 \cdot B$ and

$t \gg \tau$, Equation 2.4 can be achieved, a form of the parabolic oxidation law where B is referred to as the parabolic rate constant, k_p, and can be measured through experimentation.

$$x_o = \frac{A}{2} \cdot \left[\left(1 + \frac{t+\tau}{A^2/4 \cdot B} \right)^{1/2} - 1 \right] \quad \text{Equation 2.3}$$

$$x_o{}^2 = B \cdot t \quad \text{Equation 2.4}$$

In general, Si and SiC oxidation vary with temperature and the partial pressure of water, p_{H_2O}. Although the Deal-Grove model is a useful representation of Si oxidation, there are differences between Si and SiC oxidation. Deal and Grove demonstrated that the oxidation kinetics for silicon in a H_2O/O_2 mixture is essentially the same as that in a H_2O/argon mixture which implies that the oxidizing species is only water vapor. It has been seen that this is not the case for SiC as O_2 can act as a primary oxidant, although, H_2O further enhances the oxidation kinetics beyond that of O_2 [Opila 1999]. SiC oxidation, which has been studied since the early 1960's, is also more complex than Si oxidation in that more reactions can occur between SiC or SiO_2 and the oxidants, either H_2O or O_2 [Jorgensen 1961]. High temperature SiC oxidation kinetics and reaction mechanisms will be further discussed in section 2.3.

2.2 Silicon Carbide Thermodynamics

A thermodynamic analysis was completed using the *FactSage* software suite to help understand the different reaction mechanisms that are involved in high temperature SiC oxidation. *FactSage* allows users to calculate the conditions for multiphase, multicomponent equilibrium using multiple databases of thermodynamic properties for a user-specified system of compounds. With *FactSage*, a thermodynamic interpretation of the possible key reactions could be gained; however, it is important to realize that the tests of this study are not in equilibrium as there is a constant, steady state flow of steam moving across the sample and a continual recession and removal of the forming oxide layer. Therefore, constituent concentrations are dynamic, never reaching equilibrium, and reaction kinetics cannot be determined from this analysis. Although the *FactSage* analysis is useful to the background of this study, it alone does not answer the question of what oxidation kinetics and reaction mechanisms are taking place during the tests of this study.

For the analysis, the equilibrium compounds in a SiC-H_2O system were investigated at four pressures: 1 atm, 20 atm, 70 atm, and 155 atm. Sufficient oxygen was assumed so graphite would not be seen as a possible product – a H_2O to SiC molecular ratio of ten to one was used for the analysis. Figure 5 and Figure 6 show the chemical equilibrium results of the SiC-H_2O system at the normal operating pressures of a BWR and PWR, respectively. Both plots are normalized to the concentration of SiO_2 and it can be seen that the different compound curves have the same general shapes. However, with a PWR operating at its normal pressure, the concentration curves of H_2O, H_2, CO_2, and CO drop off more dramatically at low temperatures than the BWR curves.

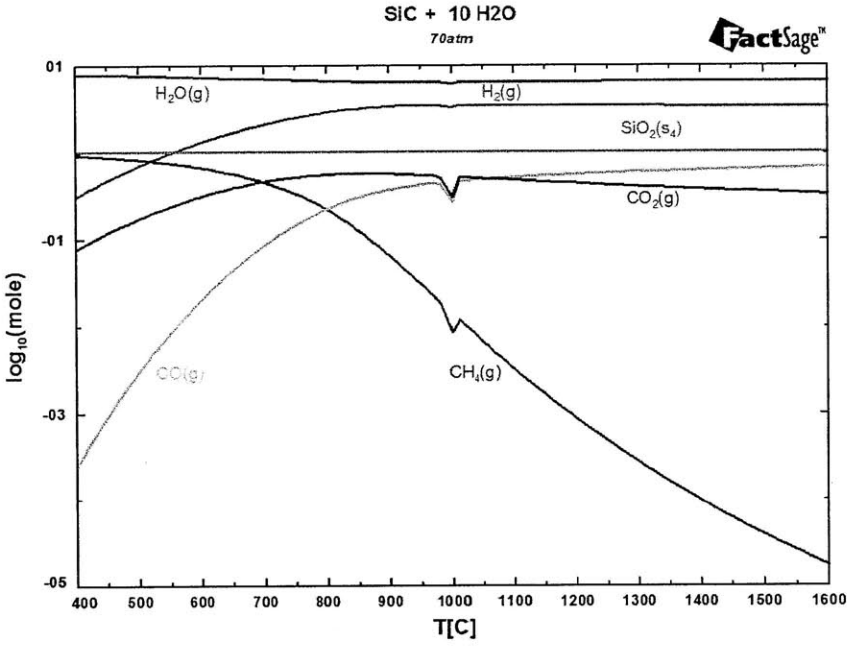

Figure 5 – BWR SiC chemical equilibrium as a function of temperature (70 atm)

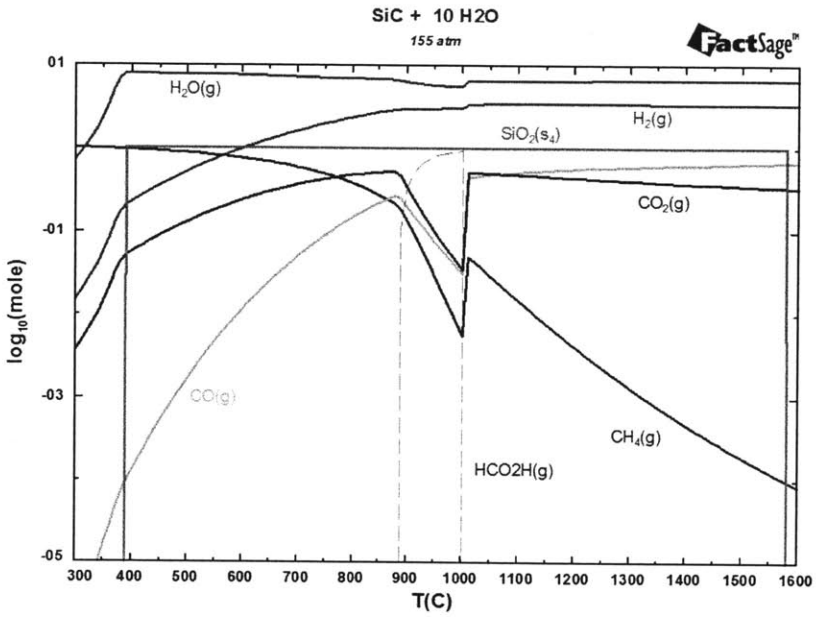

Figure 6 – PWR SiC chemical equilibrium as a function of temperature (155 atm)

As discussed in section 1.1.2, a LOCA event will cause a significant drop in pressure; during a LBLOCA, approximate pressures of 2 to 3 atm can be seen shortly after the event commences. Accordingly, Figure 7 and Figure 8 show the chemical equilibrium results of the SiC-H_2O system at the pressures that could be seen during a LOCA and a LBLOCA, respectively. There is little difference between the two graphs. One useful point is that beyond approximately 1,050°C, the oxidation reaction favors the formation of CO over CO_2. An important difference between the LOCA and LWR plots is that at higher pressures, the oxidation reaction that results in the formation of CH_4 is more likely to occur at higher temperatures – at 1 atm, the intersection of the CO and CH_4 compound curves occurs at approximately 550°C, while at 155 atm it occurs at approximately 950°C. This means that at 1 atm, CH_4 formation is favored below 550°C while above this temperature CO formation is favored. Although the *FactSage* analysis is insightful into all of the possible reaction mechanisms that occur during SiC oxidation, it alone does not answer the question of what oxidation kinetics and actual reaction mechanisms are taking place in the LOCA tests.

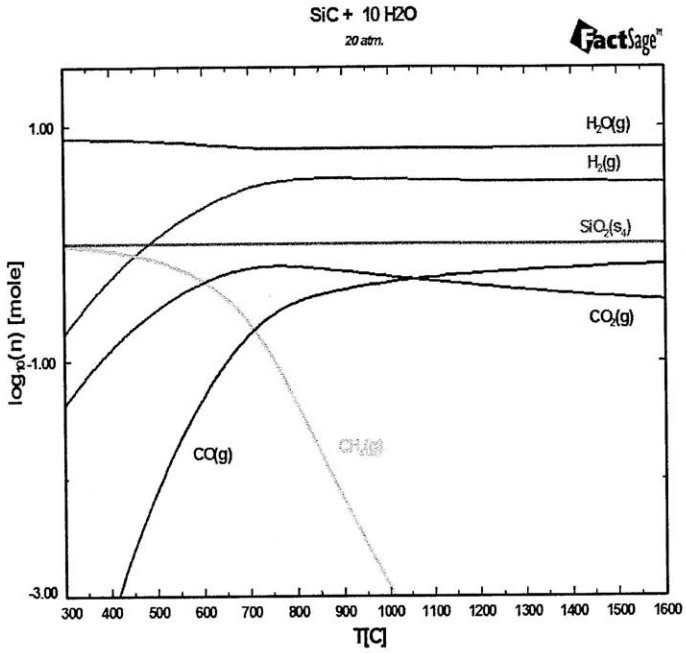

Figure 7 – LOCA SiC chemical equilibrium as a function of temperature (20 atm)

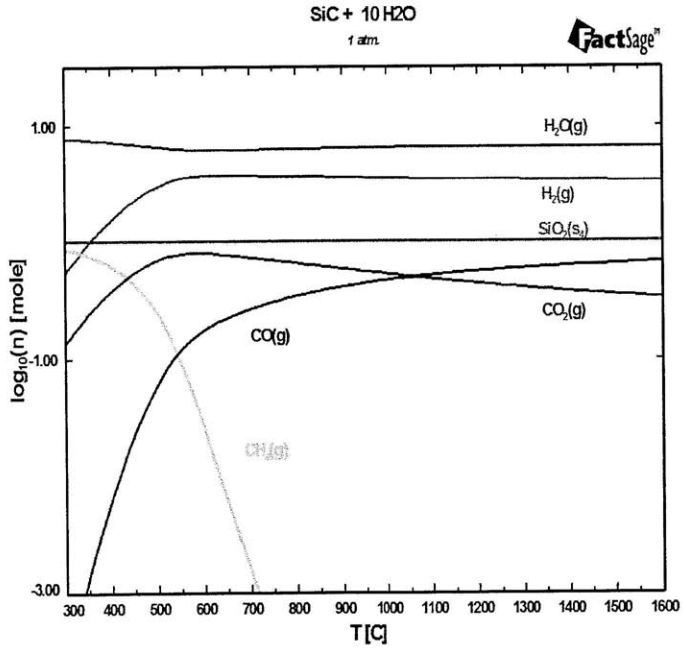

Figure 8 – LBLOCA SiC chemical equilibrium as a function of temperature (1 atm)

2.3 High Temperature Oxidation

Previous studies to characterize the oxidation of SiC in different environments as a function of temperature, pressure, and steam velocity can be found in the literature. Factors that have been varied in these studies include the total pressure, the gas chemistry by varying the partial pressures of water vapor, oxygen, and inert gases, the temperature, and the velocity of the flowing gas atmosphere. Table 1 summarizes the different experimental conditions of five studies and ongoing MIT testing [Opila 1994, Opila 1995, Opila 1999, Robinson 1999, Tortorelli 2003]. Although more studies were reviewed, many of them have similar testing conditions, so the ones depicted below are a good representation of the SiC oxidation studies that have been completed. Figure 9 and Figure 10 show two comparisons of testing parameters of the reviewed studies and this study – temperature versus velocity and water concentration versus velocity. These two graphs are useful in showing what testing has been completed by the scientific community and what gaps exist. It can be seen that without the results of this MIT study, a large gap centered on a flowing steam velocity of 1 m/s is apparent. This high-flowing velocity is important to nuclear reactors especially when considering a LOCA event. It can also be seen that very little testing has occurred at temperatures of 1,400°C and beyond – of the four studies depicted in the table and figures, a minimal amount of 1,400°C tests were successfully completed due to equipment failures. Finally, no studies have been completed in a 100 percent steam gas flow and only two studies with a steam concentration of greater than 15 percent. From this gap analysis, it can be seen that no SiC oxidation testing at the combination of temperatures, gas composition, and flow rates that have been proposed in this study have been previously conducted.

Table 1 – Summary of experimental testing parameters between SiC oxidation studies [Opila 1994, Opila 1995, Opila 1999, Robinson 1999, Tortorelli 2003]

Study	Velocity [m/s]	Temp. [°C]	P [atm]	H_2O Concentration [%]	Duration [hr]
MIT '11	0.89 - 1.19	1,140 - 1,200	1	100	8 - 48
Opila '94	0.0044	1,200 - 1,400	1	10	100
Opila '95	0.044	1,200 - 1,400	1	50	100
Opila '99	0.032 - 0.084	1,000 - 1,400	1	10 - 90	24 - 194
Robinson '99	20	1,200 - 1,450	5.7	12	100
Tortorelli '03	0.0005	1,200	10	15	500

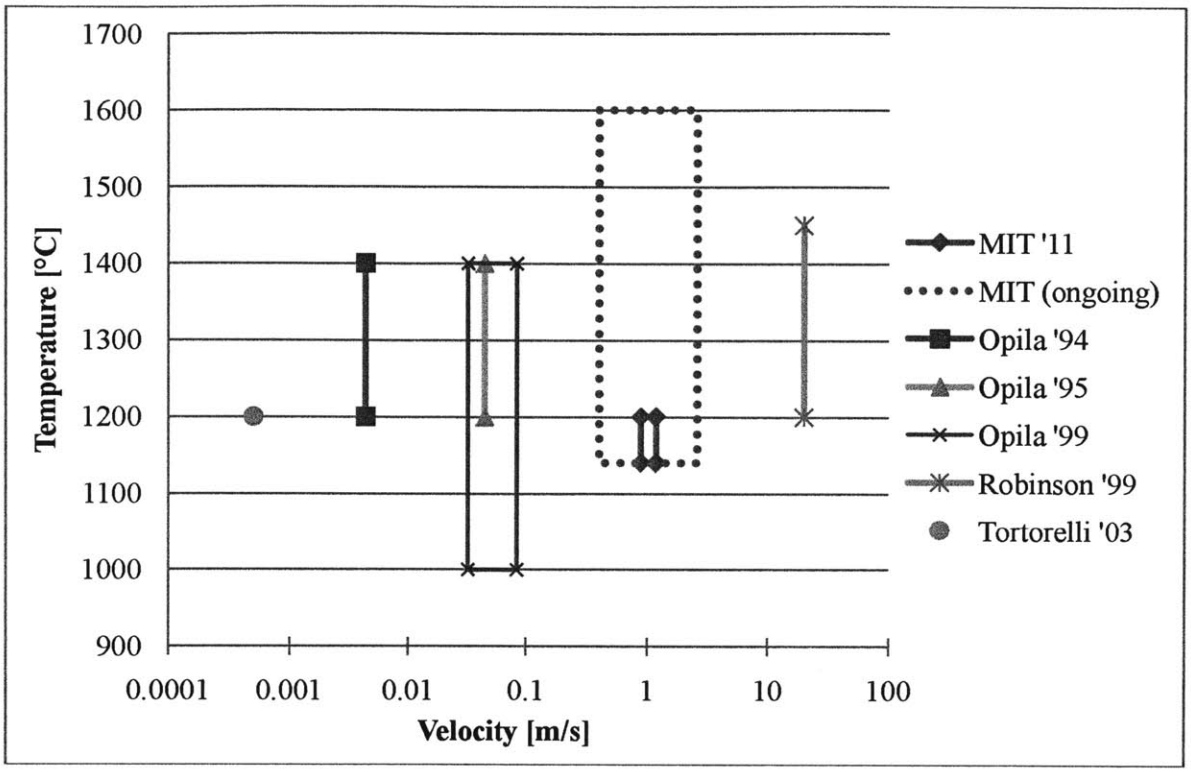

Figure 9 – Comparison of studies: temperature versus velocity

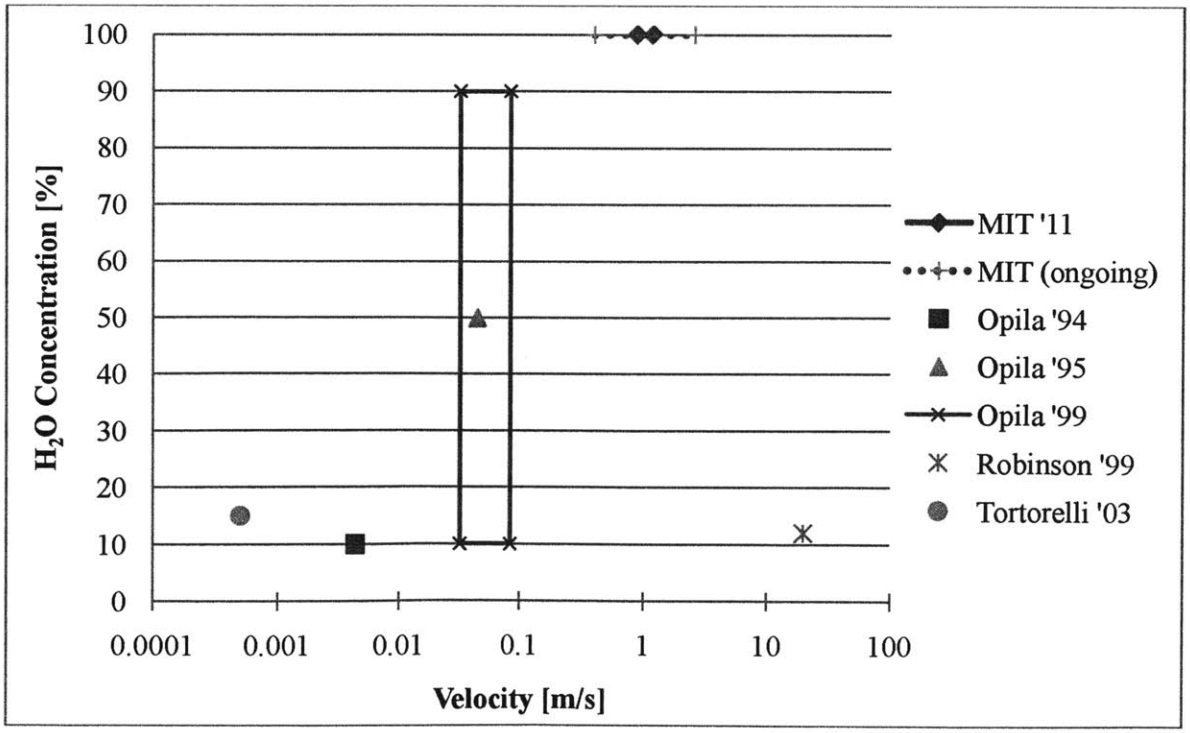

Figure 10 – Comparison of studies: H_2O concentration versus velocity

In general, SiC oxidation is similar to Si oxidation and progresses in three basic steps: transport of the oxidant inward through the oxide, reaction of the oxidant at the oxide/ceramic interface, and transport of the carbon containing species outward [Jacobson 1997]. This process is depicted in Figure 11 with O_2 as the oxidant.

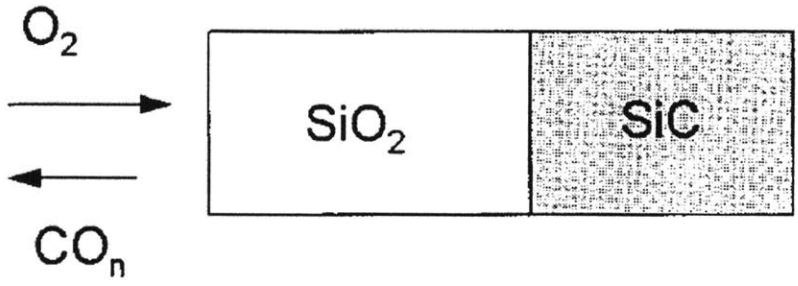

Figure 11 – Schematic showing transport of gases through the oxide on SiC [Jacobson 1997]

One study numerically investigated and modeled the active-passive regime transition in the oxidation of α- and β-phase SiC at high temperatures from 1,000°C to 1,700°C in a helium atmosphere with low oxygen or water partial pressures [Eck 2008]. A transition between two different reaction regimes seen in SiC oxidation depends on the SiC type, either α- or β-phase, the total pressure, and the partial pressure of the oxidant. If the oxidant partial pressure, either p_{O_2} or p_{H_2O}, is high enough, the oxidation is passive and a protective silica layer is formed on the surface of the SiC as can be seen in Equation 2.5 and Equation 2.6. There is a general agreement of relevant studies that passive SiC oxidation initially shows linear kinetics and then slows to a parabolic rate. This behavior suggests that the ceramic/oxide interface reaction is initially rate controlling and then oxidant diffusion through the oxide becomes rate controlling as the silica layer thickens making it harder for the oxidant to diffuse through it. In contrast to the passive regime, if the p_{O_2} or p_{H_2O} is too low, the oxidation is active and the SiC vaporizes to form a gaseous oxide as seen in Equation 2.7. In the active regime, SiC is left unprotected and a faster recession rate occurs because either the oxidant is able to react directly with SiC rather than having to diffuse through the silica layer or a very thin silica layer exists and diffusion occurs rapidly.

$$SiC + 1.5\ O_{2(g)} \rightarrow SiO_2 + CO_{(g)} \qquad \text{Equation 2.5}$$

$$SiC + 3\ H_2O_{(g)} \rightarrow SiO_2 + CO_{(g)} + 3\ H_{2(g)} \qquad \text{Equation 2.6}$$

$$SiC + O_{2\,(g)} \rightarrow SiO_{(g)} + CO_{(g)} \qquad \text{Equation 2.7}$$

Another parameter that has an effect on the reaction mechanisms is steam flow rate. It has been seen that at higher steam flow rates, the silica layer volatizes as a gaseous hydroxide as seen in Equation 2.8 [Opila 1997]. During this study, experiments will be operating in the passive regime due to the temperature and partial pressure of the flowing steam and Equation 2.6 will be one of two reactions that will likely occur along with Equation 2.8 due to the high flow rate regime at which experiments will be operated. It is expected that the volatile layer of silica that is being formed will simultaneously be vaporized by the flowing superheated steam to form gaseous silicon hydroxide.

$$SiO_2 + 2\ H_2O_{(g)} \rightarrow Si(OH)_{4(g)} \qquad \text{Equation 2.8}$$

Previous studies have also been conducted to characterize the reaction kinetics of SiC in superheated steam. In general, the thickness of the silica layer, x, that forms as a result of the oxidation of SiC over time, t, is controlled by the parabolic rate constant, k_p, which varies linearly with the logarithm of the partial pressure of water vapor as seen in Equation 2.9 and Equation 2.10 [Jorgensen 1961]. In another study, a thin, dense vitreous SiO_2 layer, known as a cristobalite layer, was seen to form and remain constant in thickness after the recession rate reaches a steady state even as the porous SiO_2 layer grows. The thickness of the dense SiO_2 layer, d, is described by the Equation 2.11 [Tortorelli 2003]. It has also been seen that SiC oxidation is enhanced with the presence of impurities, e.g., it was shown that experiments that used an alumina reaction tube increased oxidation rates when compared to experiments that used a less volatile, quartz reaction tube [Opila 1994]. The parabolic rate constant is also dependent on temperature and this effect will be investigated in this study and future MIT studies.

$$x^2 = k_p t \qquad \text{Equation 2.9}$$

$$k_p = A \ln p_{H_2O} + B \qquad \text{Equation 2.10}$$

$$x = k_p/2 \cdot k_1 \qquad \text{Equation 2.11}$$

In a high-flowing superheated steam environment such as the one that is created by the MIT oxidation test facility, the recession rate of the silica layer is affected by the $Si(OH)_4$ forming, silica volatilization reaction, Equation 2.8, which is controlled by the linear recession rate constant, k_l, and is proportional to the temperature, p_{H_2O}, and the steam flow velocity, as seen in Equation 2.12 where v is the velocity of the flowing steam, ΔH_{vol} is the enthalpy of the volatilization reaction, and T is the temperature [Opila 1997, Opila 2003]. The coupling of the parabolic rate constant and the linear rate constant, which relate to the reactions in Equation 2.6 and Equation 2.8 respectively, results in a paralinear kinetic model, as seen in Equation 2.13 [Opila 2003, Opila 2006]. The paralinear model is initially controlled by the parabolic rate constant; then, as the parabolic reaction rate begins to slow down, the negative, linear recession reaction rate begins to dominate. As will be shown in this study, negatively linear silica volatilization kinetics is the rate controlling reaction mechanism in high-flowing superheated steam and produces a weight loss.

$$k_l \propto \frac{v^{1/2} \cdot {p_{H_2O}}^2}{{p_{total}}^{1/2}} \cdot \exp\left(\frac{-\Delta H_{vol}}{R \cdot T}\right) \qquad \text{Equation 2.12}$$

$$\frac{\mathrm{dx}}{\mathrm{dt}} = \frac{k_p}{2\mathrm{x}} - k_l \qquad \text{Equation 2.13}$$

This Page Left Intentionally Blank

3. Experimental Approach and Facility Design

3.1 Oxidation Test Facility

The purpose of the oxidation test facility is to test the oxidation rates of various materials such as zircaloy and SiC in a high temperature flowing steam environment. In the initial design stages, it was determined that two key constraints had to be met in order for the facility to be useful to this study. First, the facility has to be able to generate a steady flow rate of high-purity, dry steam at a rate that does not starve the steam-sample reaction. Second, the samples must be safely subjected to temperatures of up to 1,600°C. With these two overarching design requirements in mind, an extensive amount of planning and design was completed that included reviewing past studies with similar experimental objectives, continuously iterating the facility design, and selecting and determining the capabilities of equipment.

3.1.1 Design Criteria

To begin designing the oxidation test facility, it was necessary to review past studies that dealt with producing high temperature steam to test oxidation rates of materials. Throughout the literature review, many experimental setups were analyzed to develop some general ideas for the oxidation test facility [Aomi 1999; Aomi 2000; Chuto 2008; Nagase 2000; Opila 1999; Ozawa 2000; Urbanic 1978]. Although this was a good start for the design of this study, there were several important differences between the reviewed designs. The maximum operating temperature of completed tests of the designs that were reviewed was 1,400°C and the studies that operated at this temperature did so minimally. Setups were seen to break and become nonfunctional because of the thermal stresses associated with this high temperature. Because the facility of this study aims to attain testing temperatures of up to 1,600°C, an understanding of material properties and interactions is critical for all materials used in the design. Another common feature of the designs that were reviewed is horizontal orientation of the reaction tube which leads to a horizontal flow of steam and allows for a relatively simple insertion and placement of samples. This is not the case for the design of this study design due to the material selection of the reaction tube.

Two materials were considered for the reaction tube due to their ability to withstand high temperatures and an oxidizing environment: alumina and fused quartz. After further

consideration, fused quartz was chosen as it does not react with the steam and introduce impurities into the system that could potentially contaminate the results as alumina does. This decision had a large implication on the resulting orientation of the facility and reaction tube. Because quartz begins to flow at temperatures beyond 1,250°C, it would be necessary to implement a vertical orientation to mitigate the issue of a sagging reaction tube. This would have significant implications for the design of the sample holder as discussed in section 3.4.

After considerable thought, it was decided that the facility would be open to the atmosphere. This would allow for a simple steam generator design which would facilitate sample insertion and removal, would not have to be pressurized, and would not add any significant cost to the facility due to the safety requirements that must be met with pressurized vessels. As discussed in section 3.1.3, this limits the testing environment to atmospheric pressure; however, the oxidation rate data that will be determined in this study will further improve the engineering community's understanding of SiC behavior at high temperatures and is relevant to a LBLOCA.

3.1.2 General Overview

Figure 12 shows the experimental setup of the oxidation test facility while Figure 13 shows a picture of this setup. In general, the oxidation facility was designed to have the ability to boil water and superheat the resulting steam to temperatures that approach 1,600°C. This is done in four heating stages. The first stage consists of a steam generator that boils water to generate the required steam mass flux that will not starve the steam-sample oxidation reaction for the test. Then, the steam is heated in stages two through four in the reaction tube with a total length of 1.18 m. The steam passes through the reaction tube which is wrapped with heat tape rated to 760°C. Then, the steam passes through the preheater furnace and the sample furnace which surround the reaction tube. The preheater furnace is rated to 1,200°C and the sample furnace to 1,700°C. However, because fused quartz softens around at 1,680°C and melts at 1,710°C, the maximum experiment temperature was chosen to be 1,600°C [Quartz Products 2006]. Test samples will be suspended in the sample furnace with either a K-type thermocouple wire for temperatures below 1,200°C or an alumina sample holder for temperatures above 1,200°C. As discussed in section 3.3.2, a straight gas adapter was chosen over the L-shaped adapter shown in the picture to connect the steam generator to the reaction tube.

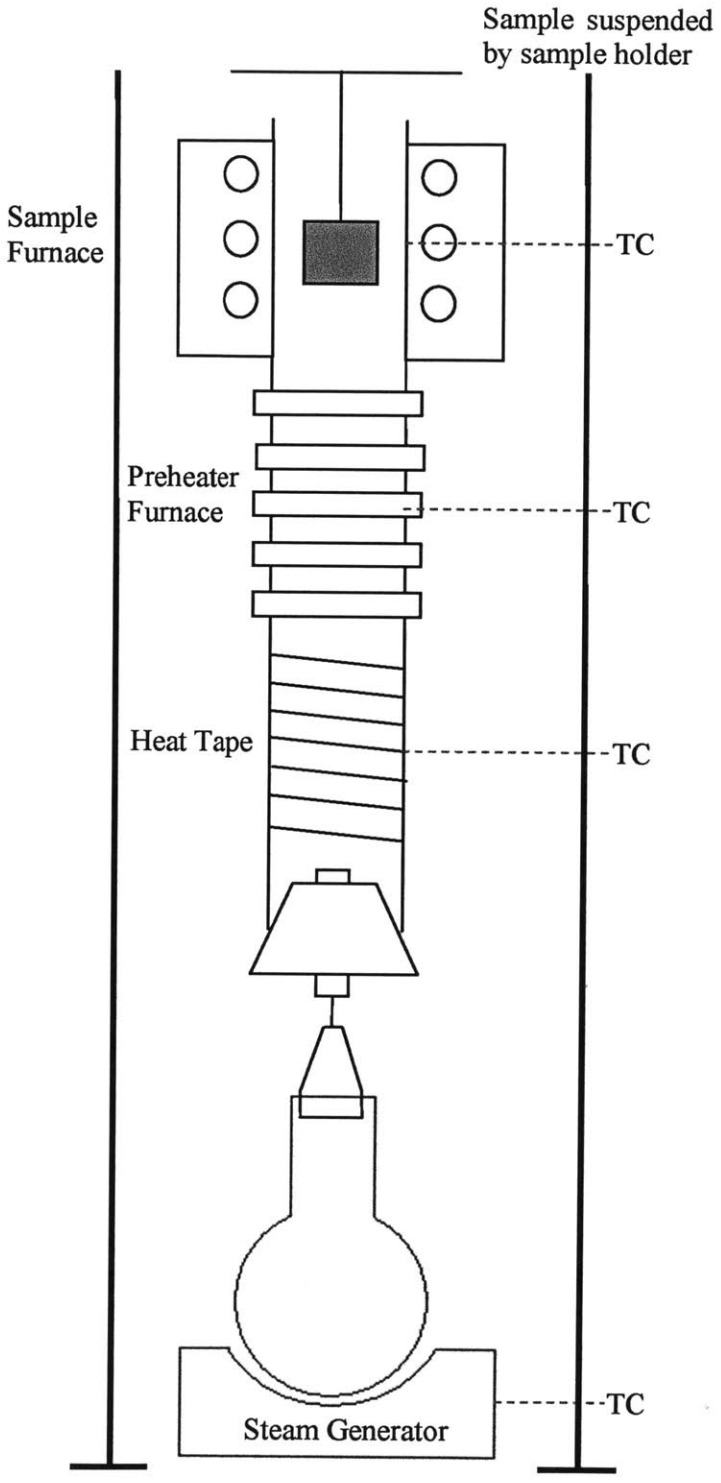

Figure 12 – Experimental setup of oxidation test facility with four heating stages

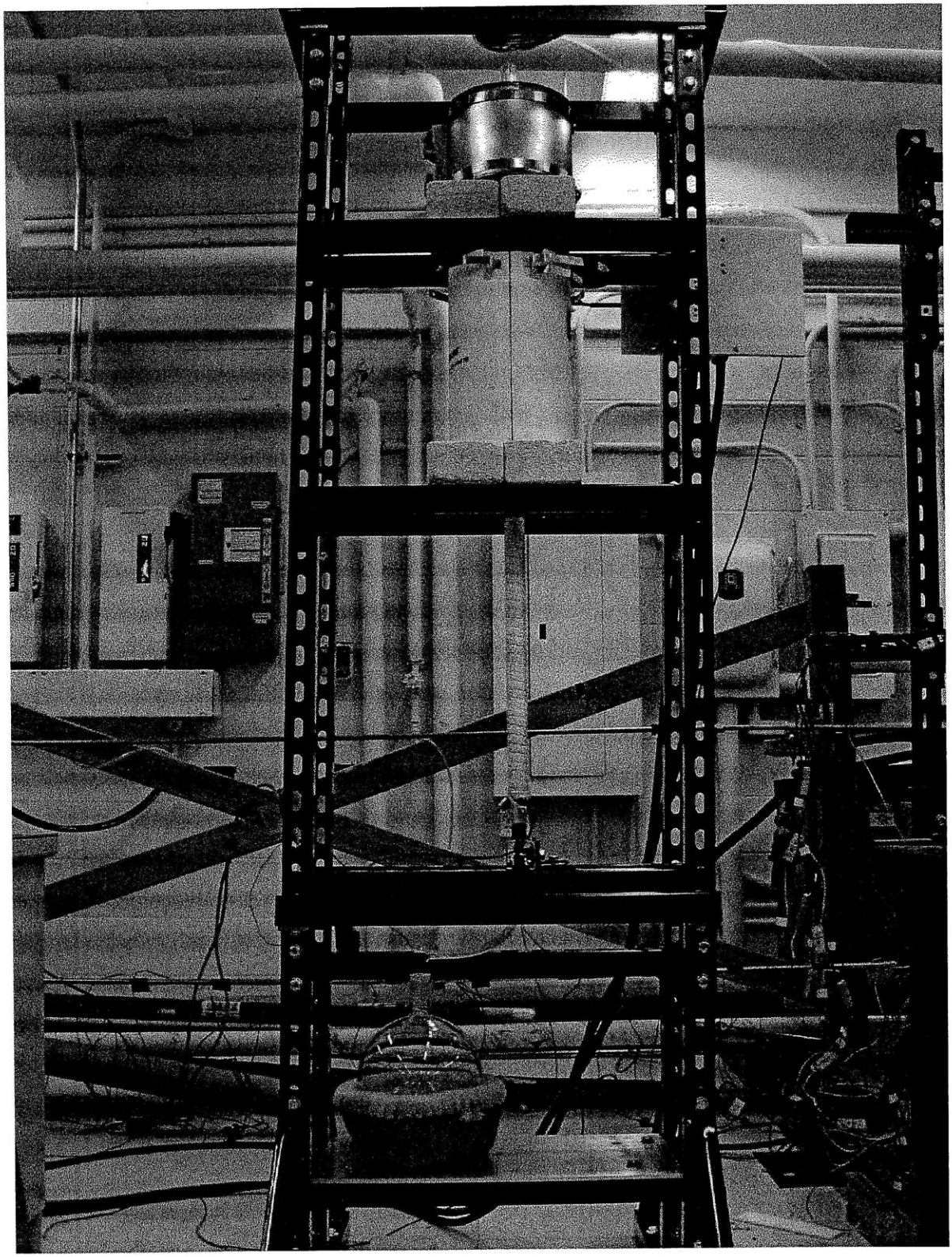

Figure 13 – Picture of oxidation test facility with four heating stages

The first heating stage is the steam generator consisting of a *Glascol #100A-O412* hemispherical mantle and a *KONTES* #KT6010000-0924 spherical flask that fits into the mantle. A variable autotransformer is used to control the heat input of the mantle to the deionized water contained in the flask and the resulting steam generation rate. The boiling inherently takes place at slightly above atmospheric pressure. As discussed in section 3.3.1, steam flow rates were calibrated prior to experimentation by determining the water loss rate in the flask at different power settings on the variable autotransformer. Also, the average flow rate for each experiment is volumetrically calculated by measuring the total water loss. A vertically oriented straight gas adapter directs steam into silicone tubing which is connected to the bottom of the reaction tube by a silicone stopper with a short length of 316 stainless steel tubing going through it. This allows for an airtight seal that will prevent the laboratory atmosphere from entering the reaction tube. Heat tape rated to 760°C is wrapped around the reaction tube beginning approximately 3.8 cm above the top of the silicone stopper to prevent the stopper from melting. This 45.7 cm heated length is the second stage for heating the water which is now in the form of steam. The heat input of the heat tape is controlled by a triac dimmer and will heat the steam to temperatures that approach 760°C.

The steam then passes through the two furnaces which surround the upper section of the reaction tube. The third heating stage is a 30.5 cm long preheater furnace rated to 1,200°C. This furnace is comprised of two *Watlow* #WC-VS403J12S-0001R half-cylindrical ceramic heater shells that use radiant heat transfer to heat the reaction tube and flowing steam inside the reaction tube. The heat input of the preheater furnace is controlled by a triac dimmer and can heat the steam to temperatures that approach 1,200°C. The final heating stage consists of a sample furnace rated to 1,700°C with a 5.1 cm heating length and is discussed in further detail in section 3.3.5. For insulation, there are 7.6 cm vestibules below and above the heating length. The top of the sample will be suspended one quarter of the way down the heated length of the sample furnace by a sample holder. This results in a total sample furnace steam heating length of 10.2 cm prior to the steam reaching the sample. This assumes the sample is approximately 1.3 cm tall and that the bottom vestibule contributes to the heating of the steam. Power is provided to the sample furnace from a linear direct current power supply that rectifies two phase alternating current (AC) to direct current (DC). The heat input of the sample furnace is controlled by a voltage

regulating dial on the DC power supply and will heat the sample and steam to temperatures that approach 1,600°C.

3.1.3 Test Environment

Although the oxidation test facility does not have the ability to perfectly match a LOCA environment, as discussed in section 1.1.2, the effect that atmospheric pressure, high temperature superheated flowing steam has on SiC can be examined. Temperatures of 1,600°C can be safely reached to test SiC well beyond the current NRC peak cladding temperature limit of 1,200°C. Although LOCA events are characterized by pressures greater than one atmosphere, testing was conducted at atmospheric pressure which will still shed light on SiC performance at high temperatures. Also, deionized water chemistry will minimize the amount of impurities that could distort test results. To better understand the concentrations of water and oxygen, two oxidants that have an effect on SiC oxidation, it is important to realize that dissociation of steam at high temperatures does occur. Although no oxygen is added to the system during experimentation, steam dissociation starts around 1,600°C so there is likely a small but measurable amount of it (on the order of parts per billion) during experimentation at 1,600°C [Vasic 1992]. The dissociation of steam as a function of temperature can be seen in Figure 14. As a reference point, at 1,700°C, the molar fractions of water, diatomic hydrogen, diatomic oxygen, hydroxyl, monatomic hydrogen, and monatomic oxygen are 0.991184, 0.005022, 0.00214, 0.001530, 0.000098, and 0.000025, respectively. For the purposes of this study, it can be assumed that all oxidation effects seen at testing temperatures below 1,600°C are due to water because dissociation does not occur at these temperatures while at 1,600°C, it is possible that oxygen may be reacting with the sample on a small scale; however, because there is likely 100 times more water, it can be assumed that the resulting oxidation is almost entirely due to water. The oxidation test facility will produce an atmospheric environment of high temperature superheated flowing steam.

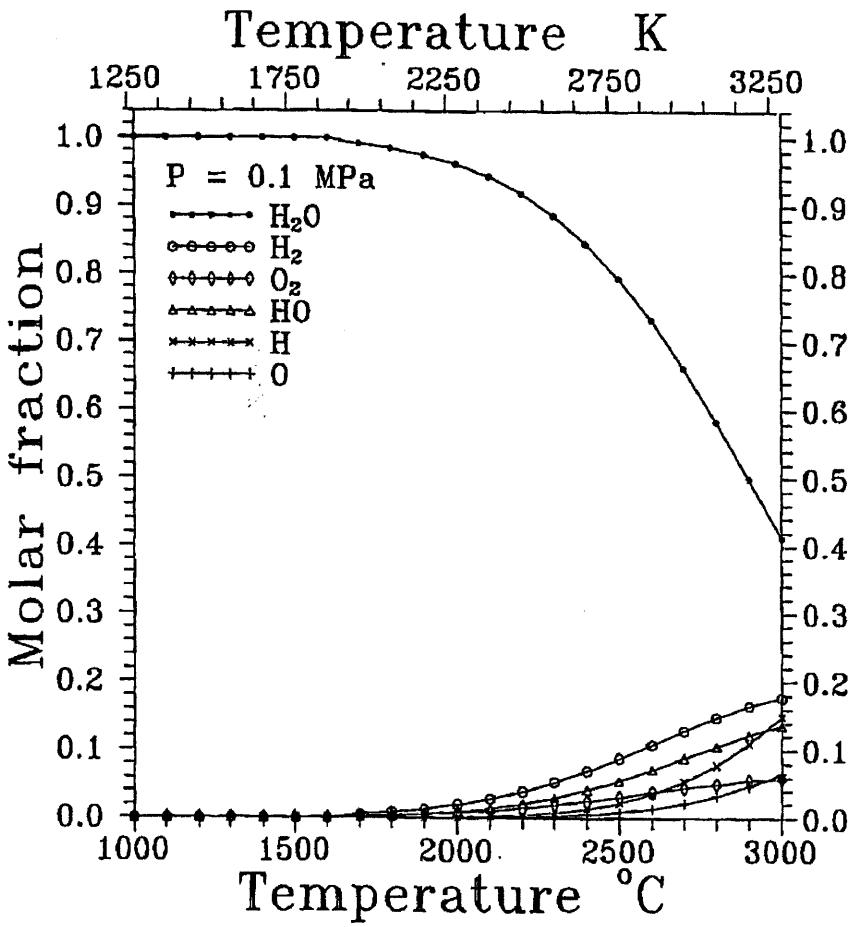

Figure 14 – Molar fraction of dissociated steam as a function of temperature at 0.1 MPa [Vasic 1994]

3.1.4 Experiment Durations

Two different materials were tested during this study – zircaloy-4 and α-SiC. Because of the differences in their resistance to oxidation, zircaloy was tested for durations on the order of minutes while SiC was tested for durations on the order of hours to days. Because of the strong resistance to oxidation of SiC at 1,200°C, it was necessary to operate experiments for durations on the order of days. With only one steam generator, comprised of a mantle and flask, it is only possible to operate until all of the initial water has been vaporized, approximately five to ten hours depending on the steam generation rate. Also, it would not be a good experimental practice to allow the laboratory atmosphere, which is comprised of water vapor and approximately 21 percent oxygen, to enter the reaction tube during steam generator switch-outs

in order to test for longer experiments. With the use a three-way valve and a secondary steam generator operating at an equal steam generation rate as the primary steam generator, it is possible to temporarily switch-out the depleted primary steam generator with the fresh secondary steam generator while the water level of the primary steam generator is replenished in a fairly seamless fashion that does not expose the test sample to the laboratory environment while only briefly stopping steam flow to the experiment. Figure 15 depicts how the switch-out will be possible while sections 3.3.2 and 3.5.4 further discuss the 3-way valve used and the switch-out procedure, respectively. Once researchers practiced the steam generator switch-out procedure, it could be completed in approximately one minute resulting in an effective way to test for an unlimited amount of time.

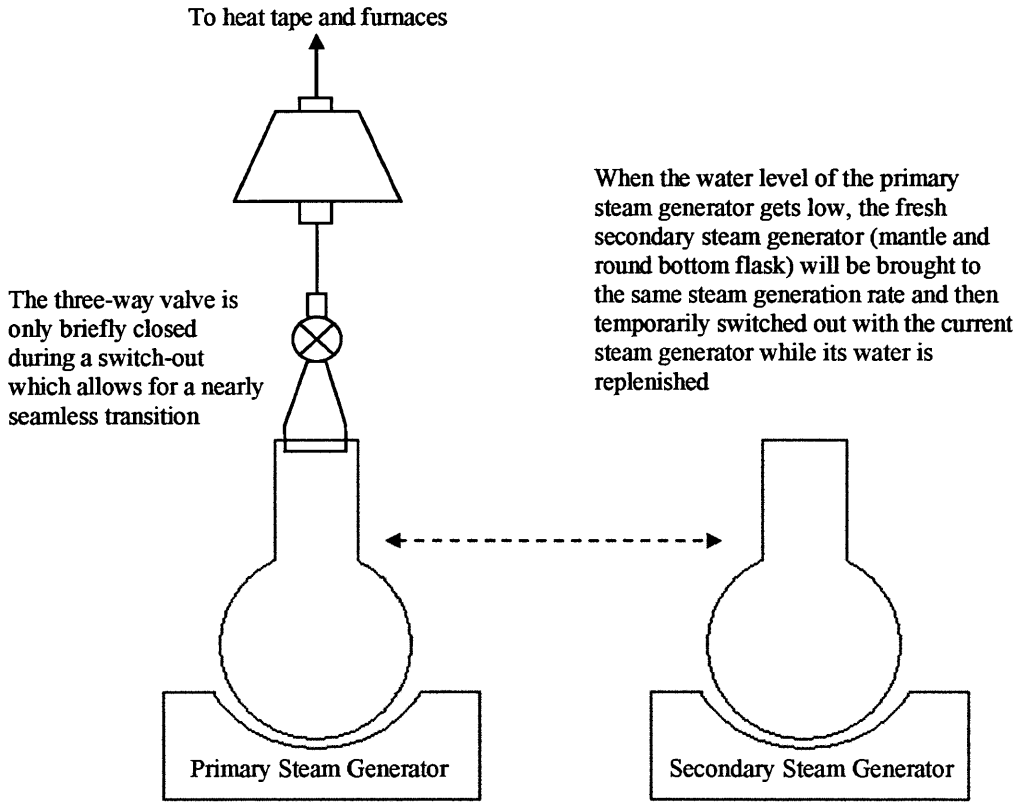

Figure 15 – Long duration experiment switch-out

3.2 Electrical Controls

The oxidation test facility acquires temperatures continuously with a data acquisition system (DAQ) and utilizes an independent electrical control system by way of a temperature deviation

electrical protection circuit. The control system increases the facility's experimentation effectiveness and safety culture by using thermocouples to accurately monitor the real-time temperatures of the different heating zones. The systems also give users the freedom to not have to be continuously monitoring the facility during testing as the system will shut down safely if temperatures rise or fall below designated set points. This allows for longer duration tests to be safely performed.

3.2.1 Thermocouples

In order for either of the electrical control systems to properly function, thermocouples had to be selected for each zone based on the particular operating temperature range and their ability to survive in the environment. Five different zones were chosen for the facility. Zones one and two refer to the two different steam generators, zone three to the heat tape section, zone four to the preheater furnace section, and zone five to the sample furnace section. Zones one through four utilize up to seven K-type thermocouples which use a chromel-alumel alloy combination for each conductor and can operate at temperatures up to 1,250°C when placed into a protective sheath while zone five uses two B-type thermocouples which use a more expensive platinum-rhodium alloy combination but can operate up to temperatures as high as 1,800°C without a sheath.

The highest temperature that the mantles are rated to is 450°C; consequently, for zones one and two, K-type thermocouples were made in-house using K-type thermocouple wire and their placement is between the mantle and the flask. Throughout experimentation when steam is being generated, an average temperature of approximately 160°C was seen which makes the K-type thermocouple selection adequate. Four prefabricated, sheathed K-type thermocouples are utilized in the heat tape and preheater zones to withstand the higher temperature of up to 760°C or 1,200°C. For the heat tape placement, two *Omega* #TJC36-CASS-040U-6 thermocouples are positioned in the middle of the heat tape zone between the reaction tube and the heat tape which allows for an accurate temperature reading of the heat tape and prevents it from burning out. For the preheater furnace placement, two *Omega* #TJ36-CAXL-040U-12 Super OMEGACLAD XL thermocouples are positioned in the middle of the preheater furnace zone between the reaction tube and the preheater furnace as close to the reaction tube as possible without touching it so as not to see any temperature extremes due to a hotspot. *Omega* #TJC36-CASS-040U-6

thermocouples were also temporarily used in the preheater zone; however, due to their less robust sheath, they were seen to burn out substantially faster than the Super OMEGACLAD XL thermocouples. A final K-type thermocouple was fabricated in-house for the purpose of determining the temperature inside the reaction tube during actual testing with flowing steam. The insulation surrounding the K-type thermocouple wire was completely removed so it did not burn when placed up to 25 cm into the flowing steam that is being heated by the preheater furnace inside the reaction tube. This thermocouple was only used to correlate the preheater furnace temperatures when the sample furnace was not integrated into the facility as discussed in section 3.3.5. For all K-type thermocouples, K-type thermocouple wire is used to extend the length of the wires in order to reach the DAQ or the temperature deviation electrical protection circuit.

It was necessary to use B-type thermocouples in the sample furnace zone due to the high testing temperatures of up to 1,600°C. The sample furnace came equipped with a B-type thermocouple already integrated into the center of the furnace to accurately measure the temperature in order to prevent equipment burnout. This thermocouple placement is between the reaction tube and the ceramic heating element positioned as close to the reaction tube as possible without touching it so as not to see any temperature extremes due to a hotspot. An *Omega* #P30R-008-10" butt-welded unsheathed fine gage B-type thermocouple is utilized in a similar fashion as the seventh K-type thermocouple discussed above. A 7.6 cm long alumina sheath partially surrounds the length of this B-type thermocouple while several alumina beads are strung onto the thermocouple to maintain separation between the two conductor wires that are suspended in the flowing steam inside the reaction tube. This thermocouple can be positioned approximately 13 cm into the reaction tube and can be seen in Figure 16. Due to the high cost of B-type thermocouple wire, copper wire is used to extend the length of the B-type thermocouples in order to reach the DAQ or the temperature deviation electrical protection circuit.

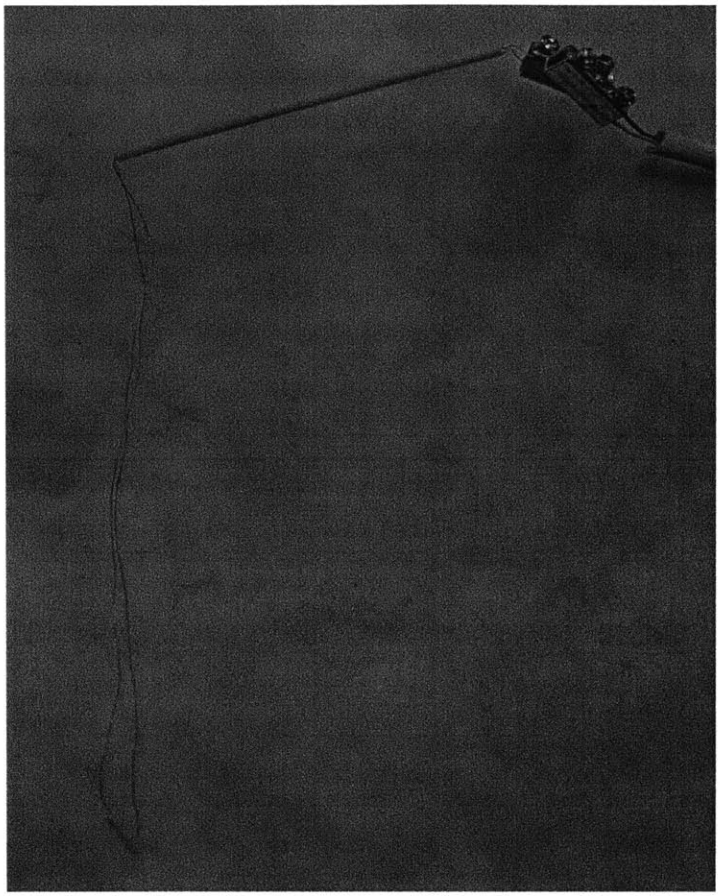

Figure 16 – B-type thermocouple with alumina sheath and beads

3.2.2 Data Acquisition System

The data acquisition system creates an interface that allows users to view and archive real-time temperature and voltage readings from thermocouples and a shunt that are used in the oxidation test facility. Six channels are utilized which take readings at three second intervals from three K-type thermocouples from the heat tape section, the preheater furnace section, and inside the reaction tube, two B-type thermocouples from the sample furnace section and inside the reaction tube, and one DC voltage shunt from the sample furnace. Thermocouple placement is discussed above. The sample furnace shunt was integrated into the power supply circuit between the DC power supply and the sample furnace in order to confirm the operating power of the sample furnace. An *Agilent Technologies* 34980A multifunction switch/measure unit, as seen in Figure 17, converts the electrical readings from the six channels that are used in the *Agilent*

Technologies 34921T armature multiplexer terminal block, as seen in Figure 18, into usable data using the *Agilent Technologies* Benchlink Data Logger for 34980A software suite.

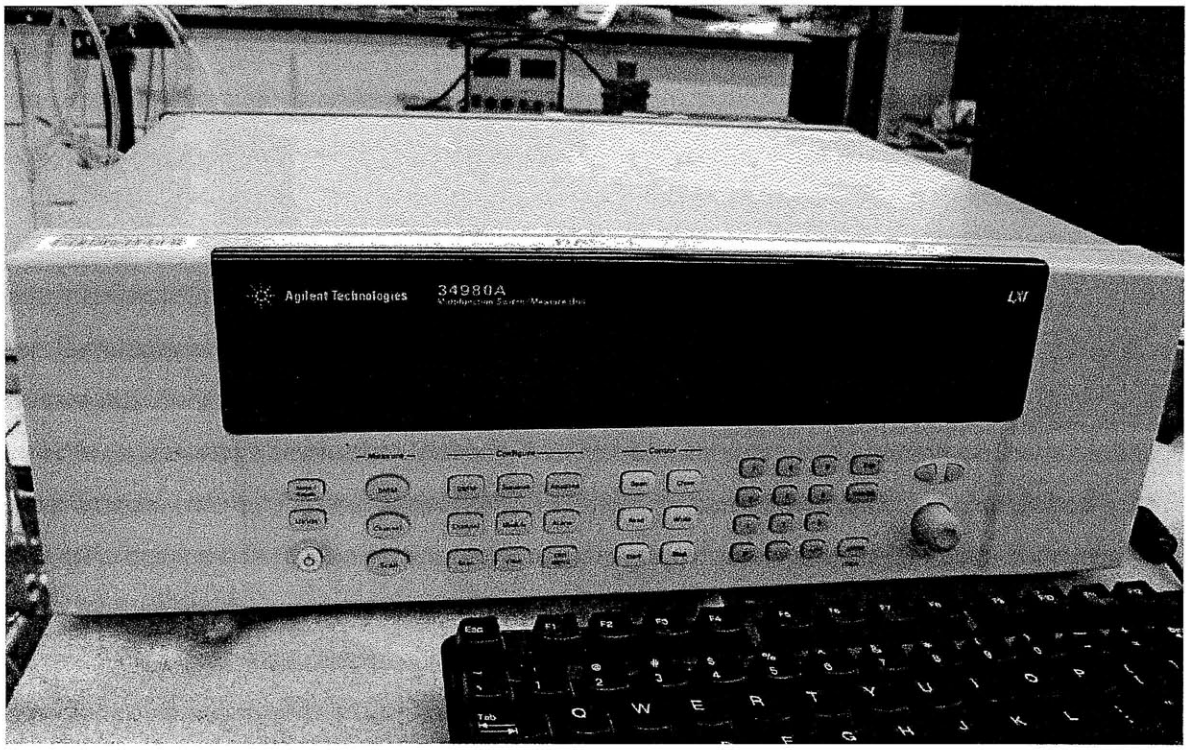

Figure 17 – *Agilent Technologies* multifunction switch/measure unit

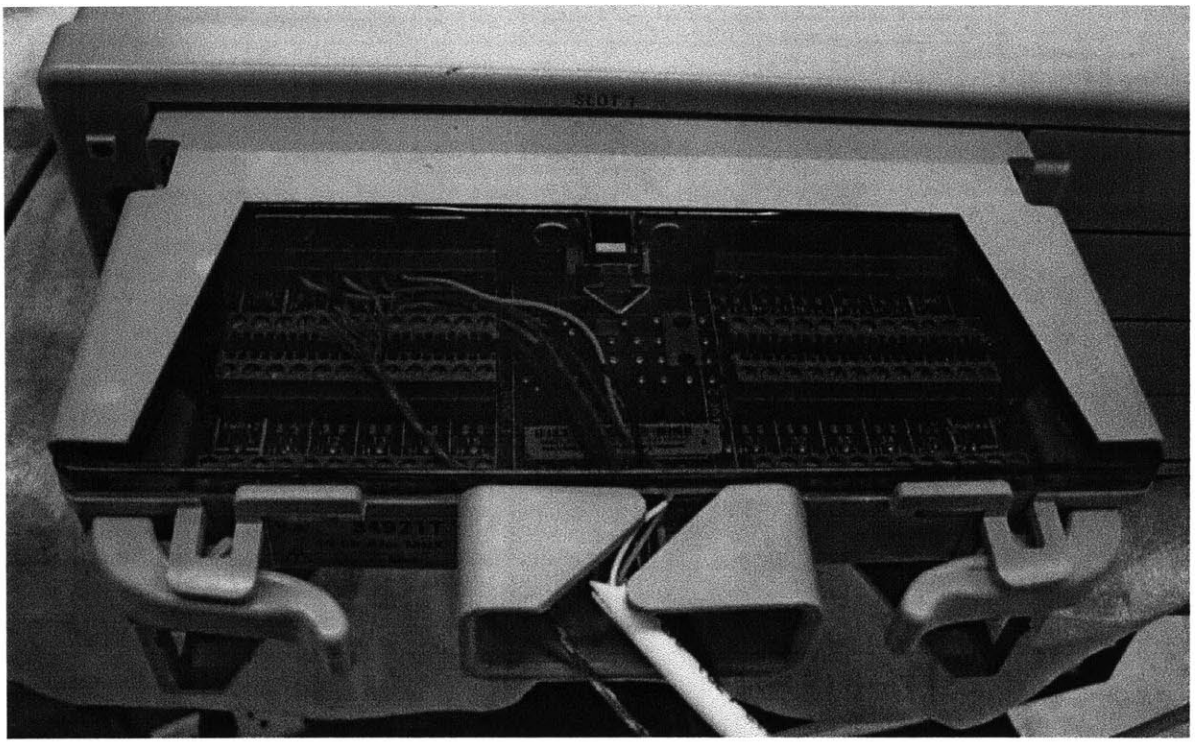

Figure 18 – *Agilent Technologies* armature multiplexer terminal block

3.2.3 Temperature Deviation Electrical Protection Circuit

The temperature deviation electrical protection circuit protects the facility from any unexpected accident such as an over/under temperature situation or an electrical outage and gives researchers the freedom to not have to continuously monitor the facility during testing because the system will shut down into a safe configuration if temperatures rise or fall beyond designated set points. In particular, this allows for overnight operation making longer duration tests possible and further enhancing the capabilities of the oxidation test facility. It is comprised of several pieces of equipment that are contained in a grounded metal box: two controllers in series – an *Omega* CN606TC1 which allows for as many as six programmable zones and an *Omega* CN9121A which has one programmable zone – both of which have one relay inside of them, one DC power supply, two additional high power relays that are controlled by the control signal from the two controllers, and five thermocouples – four K-type's and one B-type – that are integrated into the heating stages of the facility as described in section 3.2.1. Figure 19 shows a diagram of the temperature deviation electrical protection circuit while Figure 20 shows pictures of the closed box and an overhead view of the circuit.

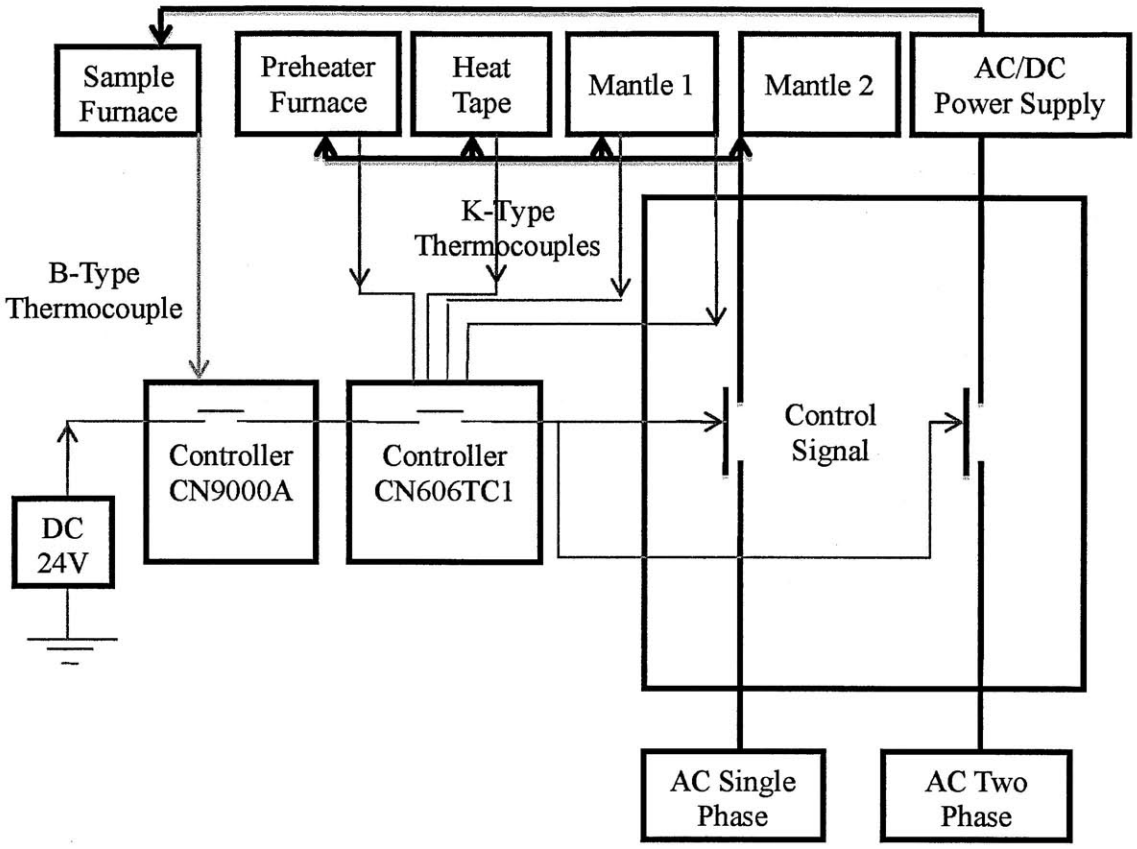

Figure 19 –Diagram of temperature deviation electrical protection circuit

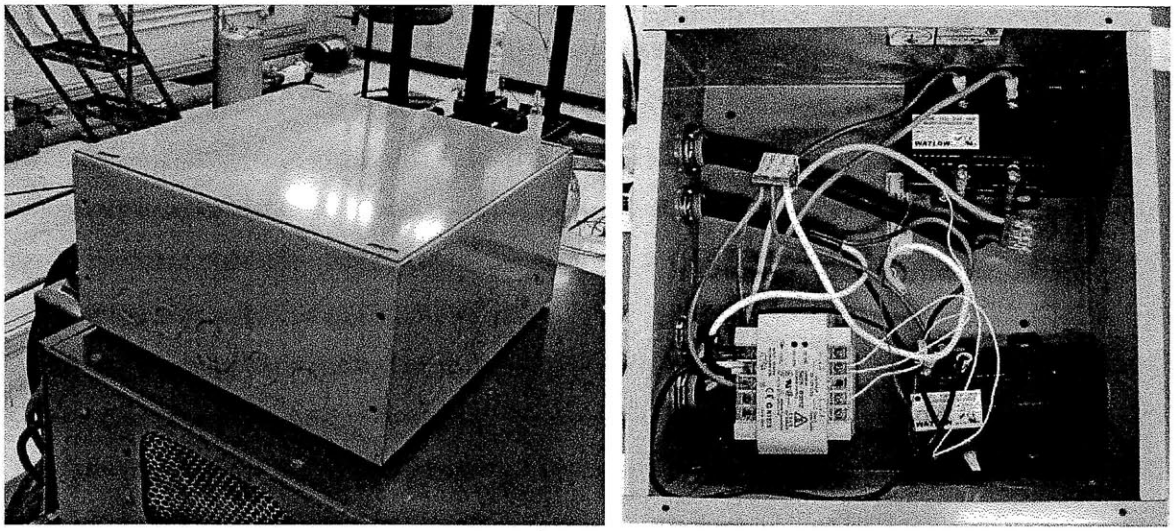

Figure 20 – Pictures of temperature deviation electrical protection circuit

The general idea of the circuit is to monitor the temperature of each heating element – two mantles, the heat tape, the preheater furnace, and the sample furnace – and to shut down the whole system if any of the temperatures rise or fall beyond the prefixed high or low limit set points. Since each controller can only be programmed to read one type of thermocouple, CN606TC1 is used to read the four K-type thermocouples while CN9121A is used to read the B-type thermocouple from the sample furnace. These two controllers, wired in series, monitor the temperatures of the different heating zones in real time. If one of them detects an abnormal temperature, the relay inside this controller will pass from a closed position to an open position resulting in the voltage of the control signal passing to zero which causes the entire system to shut down. For safety reasons, the latching option is chosen on both controllers which means that if the system is shut down by the protection circuit, it will not be able to restart without human involvement. Once the system was properly wired, each thermocouple/zone combination was tested to make sure it could properly trip the system with both its low and high temperature set points. Protection circuit validation tests were first conducted in a low temperature regime and then at temperatures that approached experimental operating conditions. Table 2 presents an example of what the different set points for each zone are for a test that is using the modified setup and operating at 1,200°C.

Table 2 – Low and high temperature set points for a 1,200°C experiment

Zone	Position	Low limit [°C]	High limit [°C]
Zone 1	3,000 mL Mantle	100	400
Zone 2	5,000 mL Mantle	100	400
Zone 3	Heat Tape	700	780
Zone 4	Preheater Furnace	1,150	1,220

3.3 Pre-Analysis and Equipment Parameters

Throughout the entire design process and during times when system upgrades were made to the oxidation test facility, it was necessary to complete calculations to determine an initial understanding of a particular aspect of the design or experiments to determine the required capabilities and make selections of equipment. The pre-analysis design calculations and tests

include calibrating the two steam generators, determining the reaction tube temperature at different points, sizing all electrical components, selecting thermocouples and system materials, and developing an accurate prediction of the temperature profile as the flowing steam rises through the different heating phases. It is also necessary to discuss the more detailed thought process that went into the steam generator adapters and longer duration valve selection and how the system was operated when the sample furnace was inoperable due to a critical repair to its ceramic heating element. By addressing these different concerns, it was possible to effectively size equipment as well as develop and improve the safety features of the facility.

3.3.1 Steam Generators

Prior to testing samples in the oxidation test facility, it was necessary to calibrate the steam generators in order to know what power setting the variable autotransformers should be set to for each test. Because the first tests would look at the oxidation of zircaloy samples in order to validate the capabilities of the facility, a literature review was completed to determine what steam flow rates had been used during previous studies. Several studies listed mass flux ranges that had been proven to not starve the steam-sample oxidation reaction in either that study or another one [Aomi 1999; Aomi 2000; Kawasaki 1978; Nagase 2000; Ozawa 2000; Uetsuka 1989]. Accounting for all reviewed journal articles, the relevant range of steam mass fluxes that were seen to not starve the oxidation reaction was from 0.05 $g/cm^2 \cdot min$ to 1.70 $g/cm^2 \cdot min$. For example, one study determined that the mass flux of steam from 0.05 $g/cm^2 \cdot min$ to 0.47 $g/cm^2 \cdot min$ did not affect the amount of specimen oxidation which can be seen in Figure 21 [Aomi 1999]. For this study's zircaloy testing, it was decided that it would be good practice to be within the first steam mass flux range listed above which for this study's reaction tube with an inner diameter of 1.9 cm correlates to a mass flow rate from 0.14 g/min to 4.85 g/min. To confirm that this would be possible, bench-top calibration experiments were completed with the 3,000 mL steam generator as this setup would be adequate to complete the shorter duration zircaloy tests.

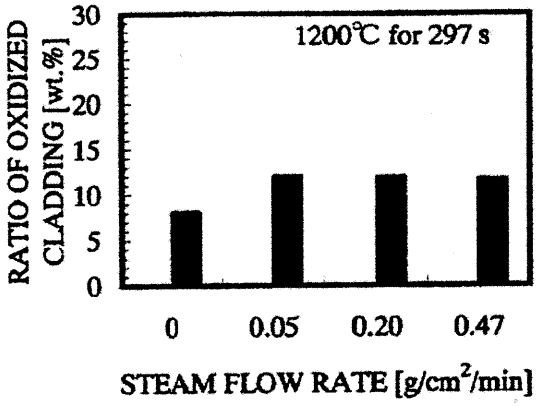

Figure 21 – Example of the effect of steam flow rate on zircaloy oxidation [Aomi 1999]

For the first set of steam generator calibrations, five minute tests were completed at various power settings on the variable autotransformer using the 3,000 mL flask and the 500 W mantle. An L-shaped gas adapter was connected to the mantle which allowed the generated steam to flow down a silicone tube into an Erlenmeyer flask that floated in an ice bath and was partially prefilled with cold water. A picture of a steam generator calibration test using this setup can be seen in Figure 22. This setup allowed the steam to condense in the Erlenmeyer flask which was weighed before and after each experiment to determine the mass flow rate of the steam generator at a given power setting after dividing by the test duration. It was also necessary to determine if there was a dependence on the water level in the steam generator flask to the flow rate, so tests were completed with an initial water volume of approximately 2,000 mL, 1,000 mL, and 500 mL. The results of the first set of calibration tests can be seen in Figure 23.

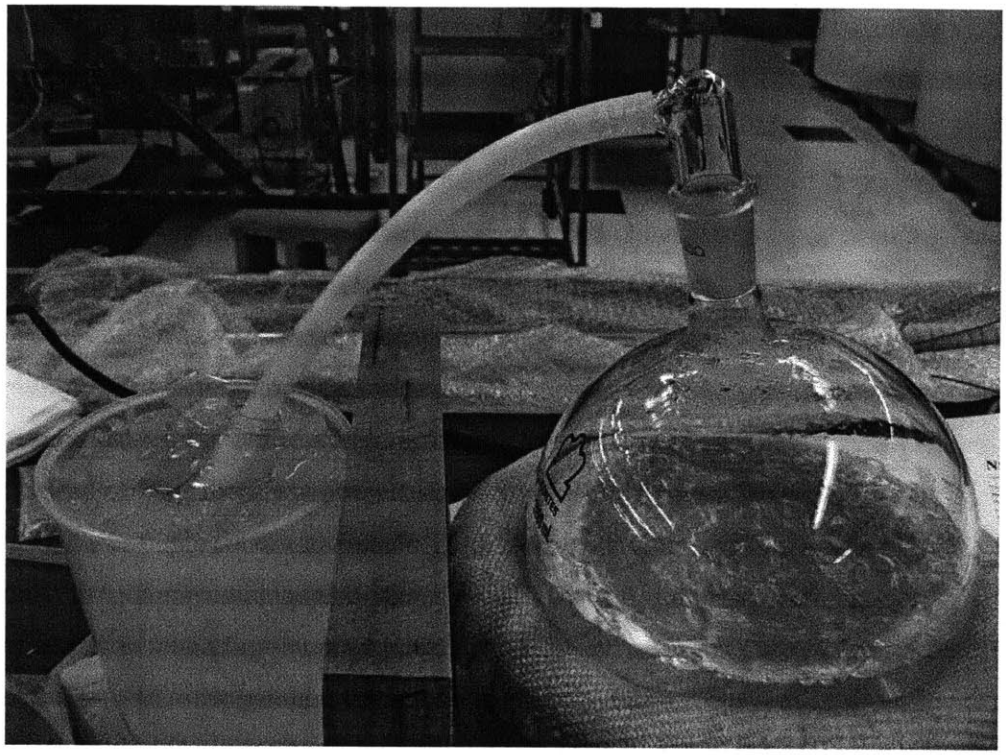

Figure 22 – Setup of first steam generator calibration tests

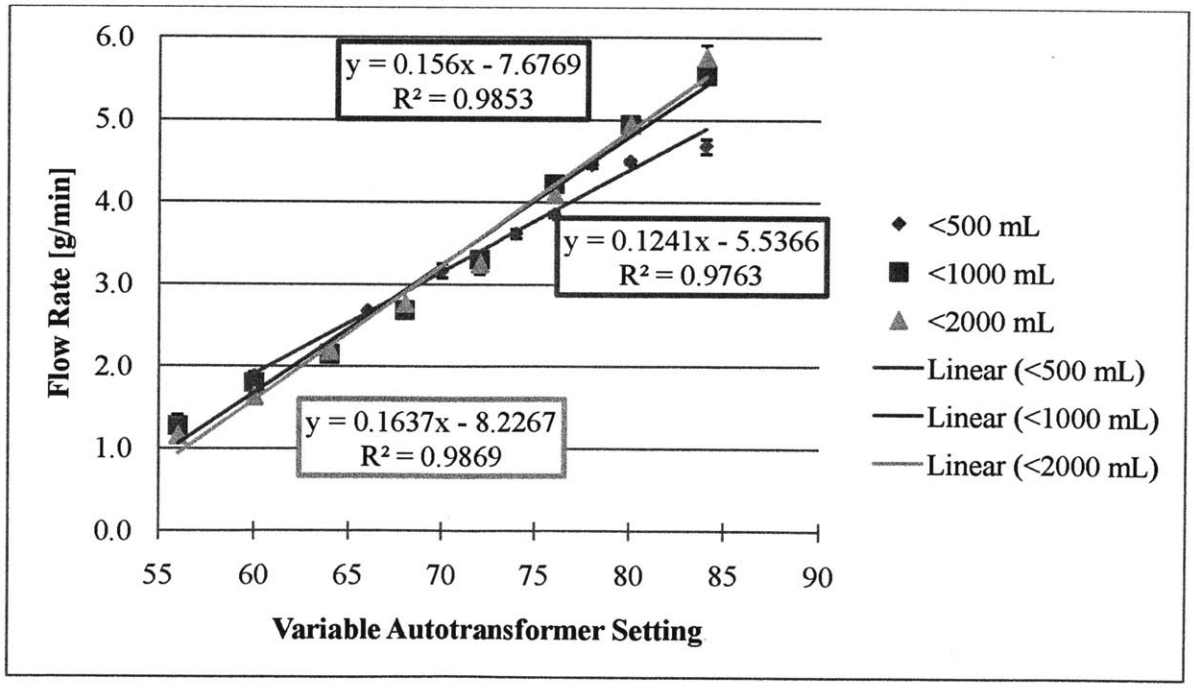

Figure 23 – Steam generator calibration results of first bench-top tests

With the calibration curves, it is important to note that each data point represents the average of at least two tests that were completed at that power setting and has a range bar that indicates the high and low data point of that test. It can be seen that there is little deviation in redundant tests. On the maximum power setting of 100, it was observed that steam generation rates approaching 10 g/min were attainable; however, in order to know more precisely what this upper limit is, it would be necessary to develop an improved calibration method because during these tests, the ice bath quickly melted and was not able to fully condense all of the steam as it was generated at such a fast flow rate. Also, there is a minor dependence on the water level in the flask to the flow rate, but there is a range of settings where the measured flow rates are fairly close. For this reason, a power setting of 71, which results in a measured flow rate of approximately 3.40 g/min using this bench-top calibration setup, was chosen for the initial zircaloy oxidation tests to be completed. This mass flow rate can be converted to a steam mass flux of 1.19 $g/cm^2 \cdot min$ which is within the acceptable range that will not starve the steam-sample reaction. During the oxidation experimentation, averaged mass flow rates were calculated for each day of testing by measuring the volume of water in the flask before and after the tests at room temperature. Table 3 shows a summary of this data as well as the duration of steam generation and a description of the testing completed. Of the six days that the averaged experiment steam flow rate was calculated effectively while operating at a power setting of 71, from May 3, 2011 to June 15, 2011, a range was seen from 2.90 g/min to 3.66 g/min which is fairly close to the 3.40 g/min flow rate that was determined from the first bench-top calibration. It is important to note that during the first three days of experimenting, this calculation was not completed accurately or measured at all and therefore not included in the range listed above.

Table 3 – Summary of shorter duration experiments operated at power setting 71

Date	Approximate Duration of Steam Production [hrs]	Averaged Steam Flow Rate [g/min]	Description of Testing
4/14/11	2	4.00	Temperature correlation
4/21/11	unknown	unknown	1,000°C Zry-4 tests
4/22/11	4	4.45	Temperature correlation
5/3/11	4.5	3.11	1,200°C Zry-4 tests
5/10/11	8.5	2.90	1,200°C SiC test
5/12/11	8.5	3.01	1,200°C SiC test
6/14/11	3	3.66	800°C Zry-4 tests
6/15/11	3	3.12	800°C and 1,000°C Zry-4 tests

The first set of steam generator calibrations was adequate to complete all testing that required less than 2,750 mL of water – the maximum volume that the 3,000 mL flask was filled. However, for longer duration tests that used the steam generator switch-out method discussed in section 3.1.4, it was necessary to complete a second set of calibrations. It was decided to utilize a 5,000 mL capacity flask and a 600 W mantle for the second steam generator to decrease the number of switch-outs required for longer duration tests, therefore, it was necessary to calibrate this larger mantle-flask combination. To do so, a new setup was devised for the bench-top calibrations as seen in Figure 24. For the second set of calibration tests, steam was generated at a given power setting for at least one hour. Then, the averaged mass flow rates were calculated for each test by measuring the volume of water in the flask before and after the tests as done during the oxidation testing, multiplying by the density of water, and then dividing this by the test duration. The goals of these tests were to determine the mass flow rate ranges that could be attained with each steam generator and the respective power settings that resulted in the same flow rate between steam generators. This would allow for modifying the flow rate at which tests were completed and have no noticeable difference in the flow rate between the two steam generators when a switch-out was required. In total, 19 valid tests were completed, each with a duration of at least one hour. Figure 25 presents the results of the valid tests. It can be seen that

the trendline is not linear; rather, it is parabolic as it was noticed after further examination that the power setting on the variable autotransformers is directly proportional to the voltage. Therefore, the power setting (dial position) is directly proportional to the $(\text{power})^{1/2}$ and a quadratic fit is necessary. By utilizing the extrapolated calibration curve equations, it is possible to match a given flow rate between the two steam generators when a switch-out is required. For example to attain the standard flow rate of approximately 3 g/min, a power setting of 54 is used with the 5,000 mL steam generator. Recall, that a power setting of 71 is used to attain this with the 3,000 mL steam generator.

Figure 24 – Setup of second steam generator calibration tests

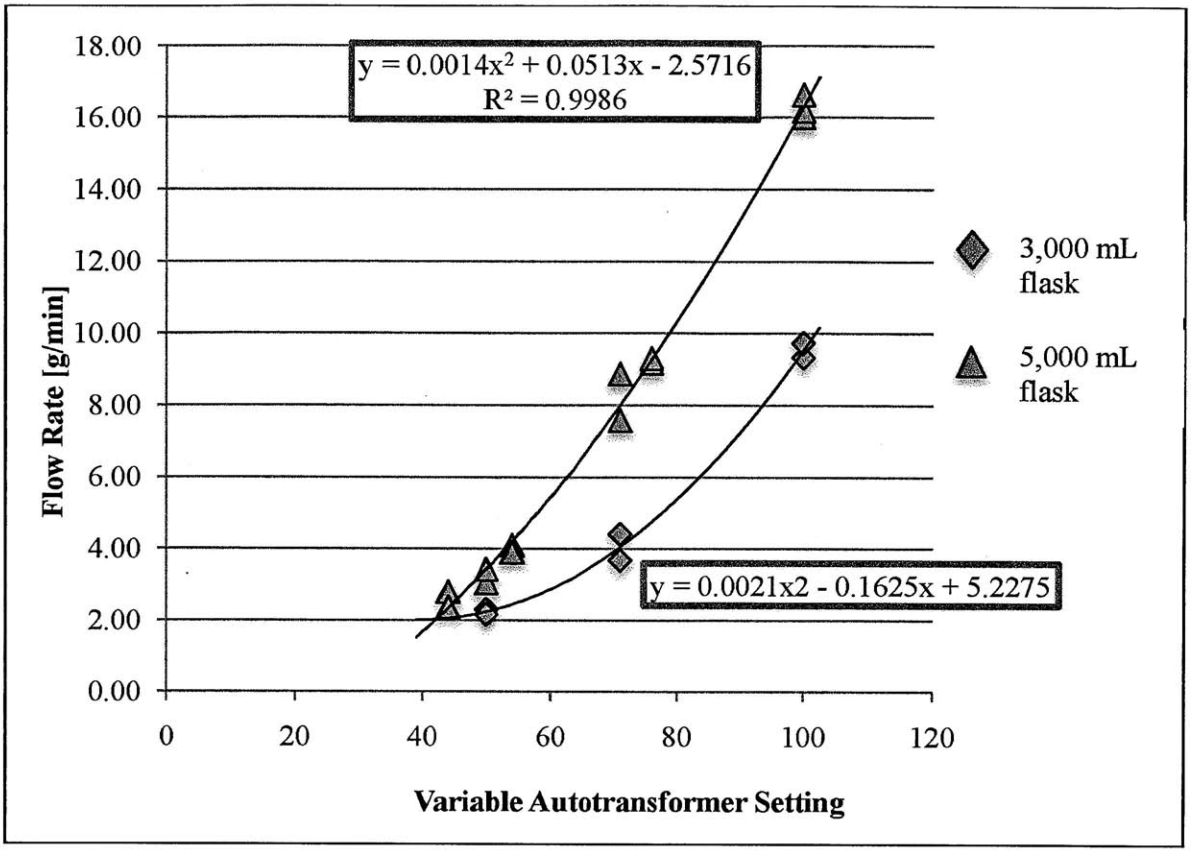

Figure 25 – Steam generator calibration results of second bench-top test

3.3.2 Steam Adapter and Longer Duration Valve

As discussed briefly in section 3.1.2, during the shorter duration tests that are summarized in Table 3, a vertically oriented straight gas adapter was used to direct steam into a short length of silicone tubing. However, throughout the experimental process, two other gas adapters were considered for use in the facility. Figure 26 and Figure 27 show pictures of the three different gas adapters that were evaluated – the L-shaped adapter, the straight adapter, and the stopcock valve adapter – and the 3-way valve that is used during longer duration experiments. Initially, the L-shaped adapter was considered for directing steam into the silicone tubing; however, after testing it in the facility, it was noticed that too much steam was condensing in the curved silicone tubing and therefore never reaching the reaction tube. This was not an optimal choice for the gas adapter so a completely vertical orientation of the steam flow was chosen which utilized a straight adapter. With this equipment change, minimal steam condensation occurs prior to reaching the reaction tube. Of the steam that does condense once in the reaction tube, it is seen

to boil off due to the heat of the heat tape and the flowing steam at a rate that prevents accumulation of water in the stopper at bottom of the reaction tube.

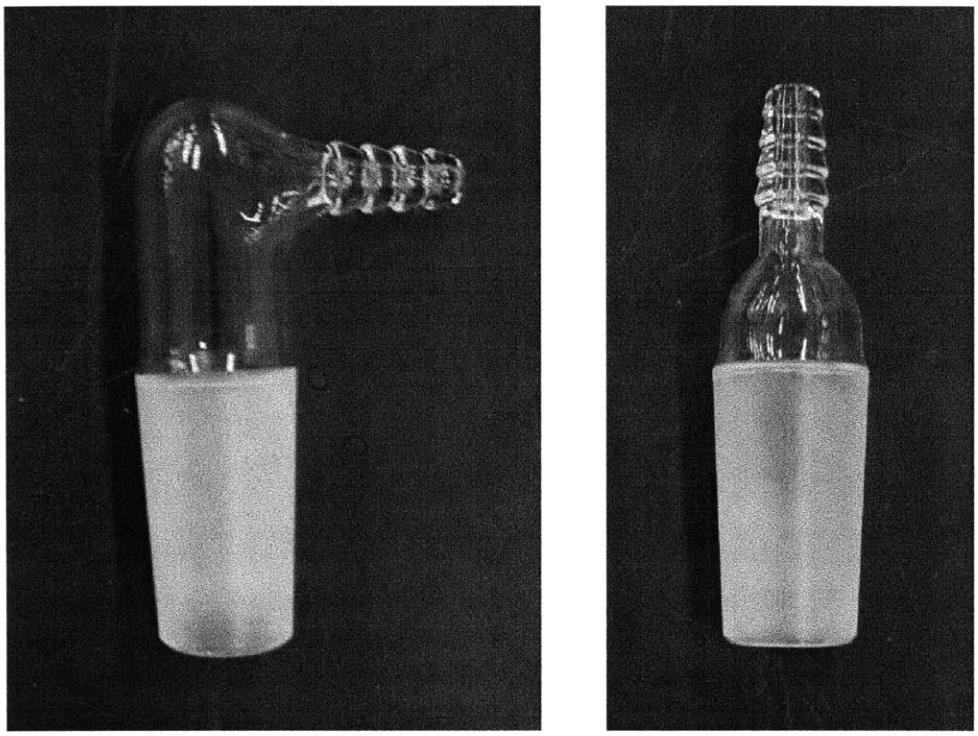

Figure 26 – L-shaped and straight gas adapters

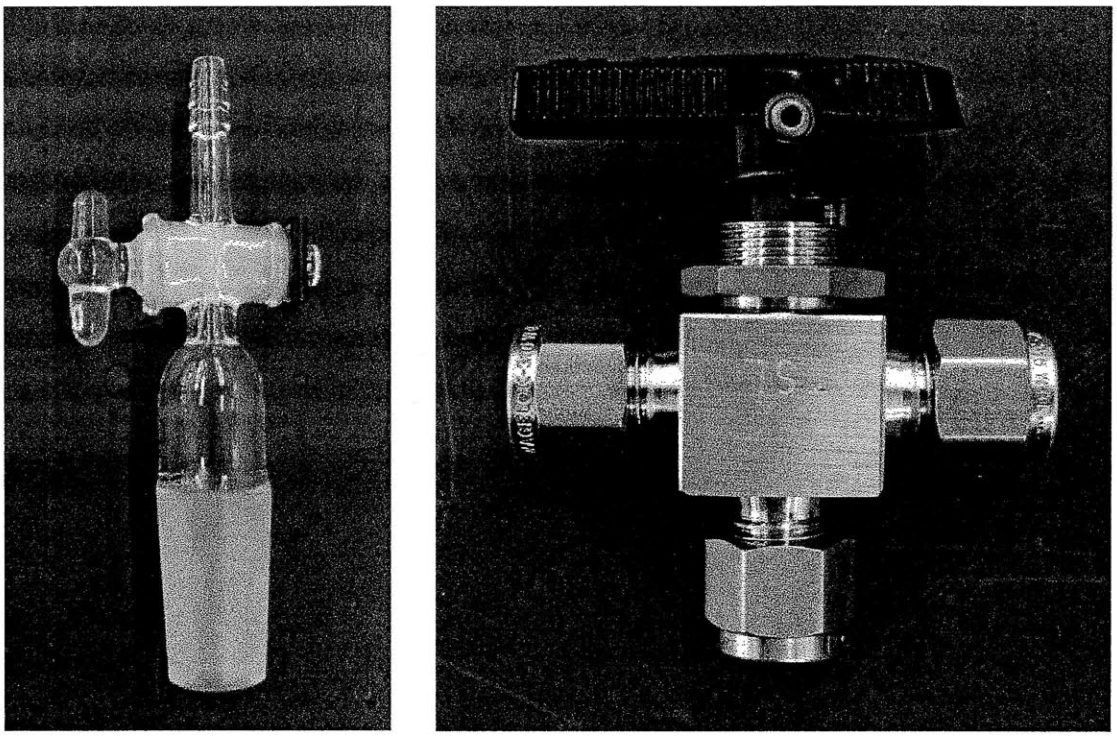

Figure 27 – Stopcock valve gas adapter and 3-way valve

For longer duration experiments that require a steam generator switch-out, a modified connection between the flask and the reaction tube is needed to prevent any of the laboratory atmosphere from entering the reaction tube. It was first considered to use the stopcock valve adapter shown above, however, after further thought it was realized that there would still be no way to prevent a small pocket of natural atmosphere from entering the reaction tube after each switch-out. Because there was an approximate volume of 15 mL below the actual valve in the stopcock adapter, a pocket of air containing approximately 21 percent oxygen would be able to enter the reaction tube and possibly alter the ongoing oxidation test, approximately $1.75 \cdot 10^{-4}$ mol O_2. A calculation was completed to determine what effect this amount of oxygen could have on a SiC sample. To do this, it was first assumed that the same percentage of this flowing pocket of oxygen would react with the SiC as does flowing steam as determined from experimental results. It is important to note that this is a conservative approximation because water is a more effective oxidant of SiC than oxygen is, as discussed in section 2.3. As discussed in chapter five, approximately $1.4 \cdot 10^{-4}$ percent of the flowing steam during a 1,200°C, eight hour test reacts with the SiC. Taking this percentage into account, it was calculated that an approximate mass of

$4.73 \cdot 10^{-9}$ g SiC would react with the postulated flowing pocket of air, approximately five orders of magnitude less than the actual reaction that was seen to occur with flowing steam. Although this calculation shows that the oxygen contained in the air pocket would not have any measurable effect on the sample oxidation due to the mechanisms discussed in chapter two, it was still decided to improve the setup to guarantee that an ongoing test would not be disturbed by a brief change in the flowing gas composition. In order to effectively switch-out the steam generators in a seamless fashion, a *Swagelok* 42GXHLS4 3-way valve wrapped with insulation tape is used. This valve allows the flowing steam to either flow through it into the reaction tube in the 'experimentation' position, or by turning it to the 'closed off reaction tube/flow into the laboratory' position, the steam flow is diverted into the laboratory. Section 3.5.4 discusses the steam generator switch-out procedure in further detail.

3.3.3 Reaction Tube Temperature

It was necessary to determine the temperature of the reaction tube beyond the heating zones, i.e., below the heat tape and above the sample furnace, to make sure that the ends wouldn't melt or burn anything such as the silicone stopper. To do so, it was necessary to perform a heat transfer calculation [Welty 2001]. Equation 3.1 represents the heat, Q, that is conducted through the cross-sectional area of the reaction tube away from the heat tape or sample furnace. The thermal conductivity of fused quartz, k, is 1.38 W/m·K while dT is assumed to be the difference between the operating temperature of the heating element, either 760°C or 1,600°C, and the desired reaction tube end temperature of 100°C. Equation 3.2 represents the heat that is lost from the reaction tube to the laboratory atmosphere. The heat transfer coefficient, h, was conservatively assumed to be 5 W/ m^2·K, T_{avg} was taken to be the average temperature between the operating temperature of the heating element and 100°C, while T_{air} was assumed to be 25°C.

$$Q = \pi \cdot \left[\frac{D_o{}^2 - D_i{}^2}{4}\right] \cdot \frac{k}{L} \cdot dT \qquad \text{Equation 3.1}$$

$$Q = h \cdot \pi \cdot D_o \cdot L \cdot \left(T_{avg} - T_{air}\right) \qquad \text{Equation 3.2}$$

By setting these two equations equal to each other, the safe distances needed between the bottom of the heat tape and the stopper, to prevent melting at the top of the sample furnace and the end of the reaction tube for extra safety, were calculated to be 3.4 cm and 3.6 cm, respectively.

To confirm the validity of this calculation, a bench-top experiment was performed. Heat tape was wrapped around the reaction tube for a length of 33 cm and insulation wool was wrapped around the heat tape, both in the same fashion as done in the facility setup. The heat tape was heated until the thermocouple at the centerline of the heated length between the heat tape and reaction tube measured 760°C. The experimental setup can be seen in Figure 28. Temperatures inside the reaction tube were taken at various distances from the edge of the heat tape and can be seen in Figure 29. Negative distances represent temperature readings that were taken beyond the edge of the wrapped reaction tube while positive distances represent those that were taken at locations inside the wrapped reaction tube. This experiment confirms the validity of the calculation discussed previously and an approximate distance of 3.8 cm was chosen to prevent the silicone stopper from melting.

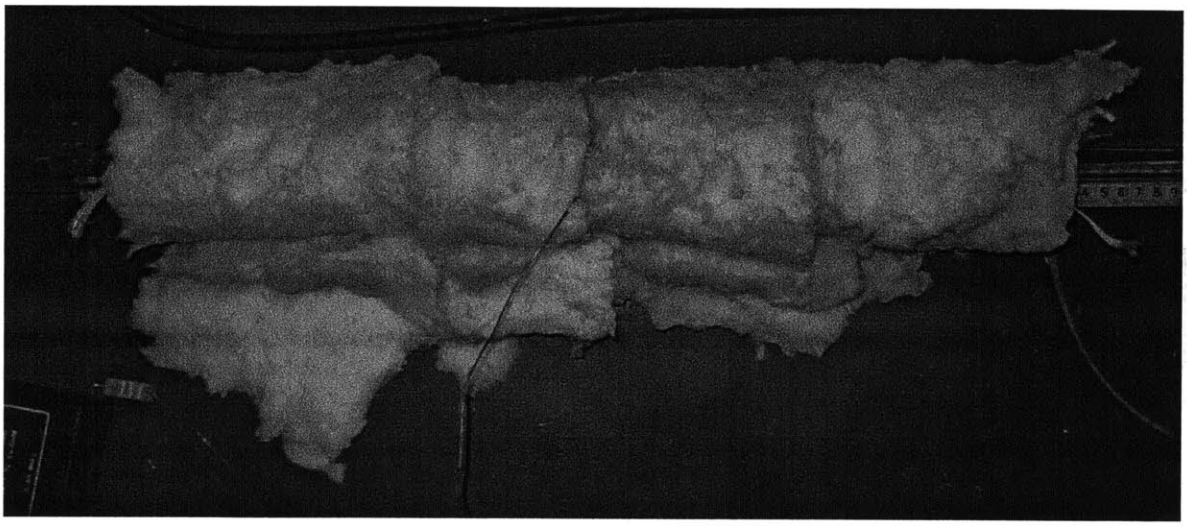

Figure 28 – Setup of reaction tube/heat tape temperature test

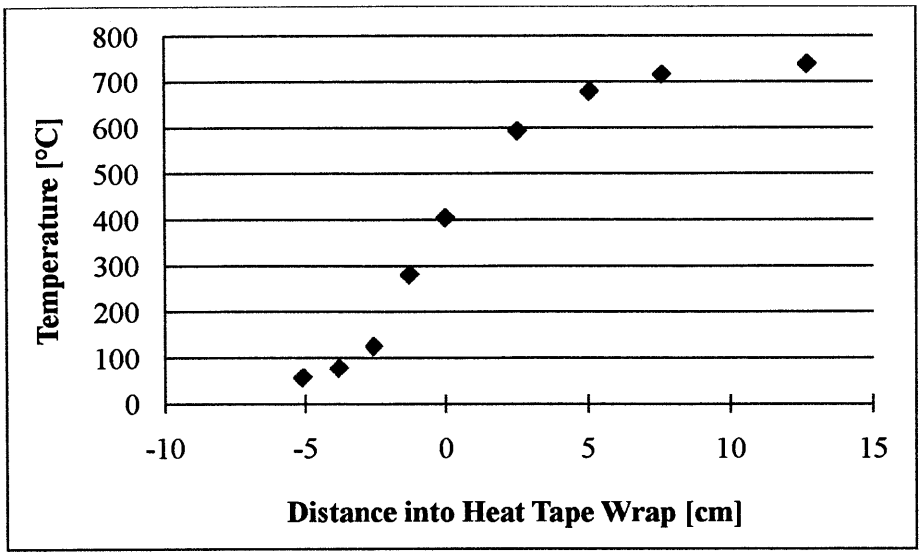

Figure 29 – Temperature of reaction tube with respect to the edge of heat tape

3.3.4 Temperature Profile of Flowing Steam

When designing the different heating stages, it was necessary to develop an accurate prediction of the temperature profile as the flowing steam rises through the facility so that the heating elements could be properly sized. To do so, it was necessary to perform a heat transfer calculation. Equation 3.3 shows Newton's law for heat transfer where the $q"$ is the heat flux, h is the heat transfer coefficient, T_w is the temperature of the reaction tube wall, either 760°C, 1,200°C, or 1,600°C depending on which heating stage is being evaluated, and T_z is the temperature of the flowing steam as a function of position. Equation 3.4 shows the relationship between heat added to the steam, $\dot{Q}$, and the mass flow rate, $\dot{m}$, the specific heat capacity of steam, C_p, and the temperature gradient between the flowing steam and the reaction tube wall, ΔT.

$$q" = h \cdot (T_w - T_z) \qquad \text{Equation 3.3}$$

$$\dot{Q} = \dot{m} \cdot C_p \cdot \Delta T \qquad \text{Equation 3.4}$$

By setting the two equations equal to one another, making the appropriate unit conversions, and integrating as seen in Equation 3.5, where T_{in} is the steam temperature as it enters the respective heating stage, L is the length of the tube or the position of the steam at a particular point, and D is the diameter of the reaction tube, one is able to get a result of Equation 3.6 which can be used

to show the temperature profile of the steam in the reaction tube once a final manipulation is completed.

$$\int_{T_{in}}^{T_z} \frac{1}{(T_w - T)} dT = \int_0^L \frac{h \cdot \pi \cdot D}{\dot{m} \cdot C_p} dz \qquad \text{Equation 3.5}$$

$$\ln\left(\frac{T_w - T_{in}}{T_w - T_z}\right) = \frac{h \cdot \pi \cdot D}{\dot{m} \cdot C_p} L \qquad \text{Equation 3.6}$$

Equation 3.6 has three unknowns, T_z, L, and h. By using the proper heat transfer correlations, it is possible to solve for h which then allows one to solve for the temperature profile as a function of position in the reaction tube, L. Equation 3.7 gives a relationship between the Nusselt number and the heat transfer coefficient, where k represents the thermal conductivity of the flowing steam, while Equation 3.8 allows one to solve for the Nusselt number for laminar fluid flows that are not fully developed which is the case for this study, where Re is the Reynolds number and Pr is the Prandtl number [Mills 1999].

$$Nu = \frac{h \cdot D}{k} \qquad \text{Equation 3.7}$$

$$Nu = 3.66 + \frac{0.065(D/L)Re \cdot Pr}{1 + 0.04[(D/L)Re \cdot Pr]^{2/3}} \qquad \text{Equation 3.8}$$

With the heat transfer coefficient known, Equation 3.6 was used to determine the necessary temperature of the flowing steam as it progresses through the reaction tube for a given flow rate and the temperature that could be reached when changing the steam flow rate. Figure 30, Figure 32, and Figure 34 show the temperature profile of flowing steam through the heat tape stage, the preheater furnace stage, and the sample furnace stage, respectively. It is important to note that for this calculation, a steam flow rate of 3.36 g/min was used. It can be seen that for the heat tape and preheater furnace stages, outlet temperatures are able to approach the heating element's temperature adequately. However, for the sample furnace, a conservative estimate for the temperature of the steam as it reaches the bottom of the sample is seen. Figure 31 and Figure 33 show the outlet temperature of the flowing steam as a function of the flow rate for the heat tape stage and the preheater furnace stage, respectively. It can be seen that with faster flow rates, a lower outlet temperature from the preheater furnace stage will occur. However, it is expected

that by doubling the flow rate, adequate heating of the steam will still occur. These calculations are also conservative because they ignore radiative heat transfer.

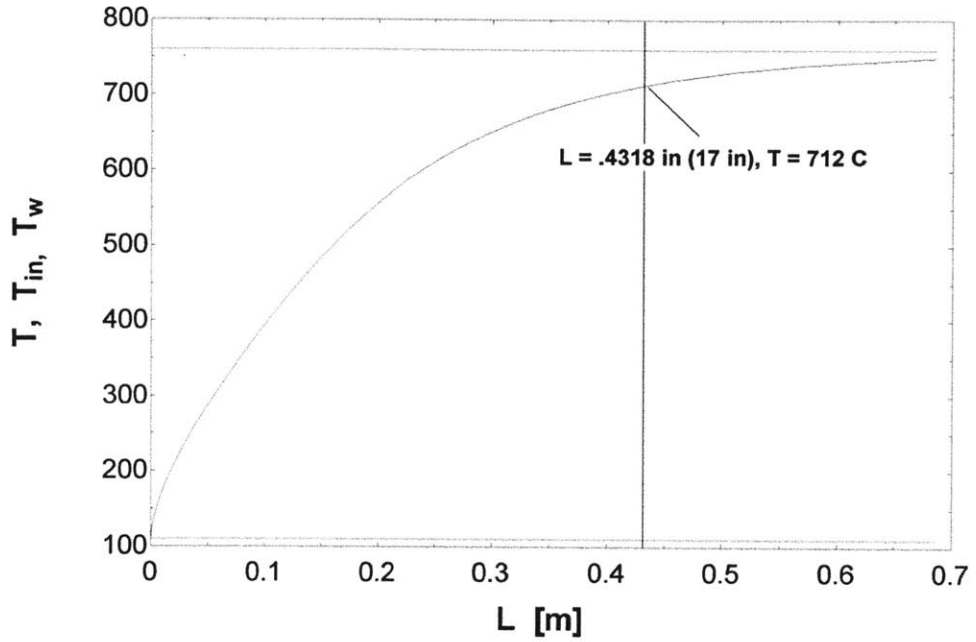

Figure 30 – Temperature profile of flowing steam through the heat tape stage (vertical line indicates end of heated length)

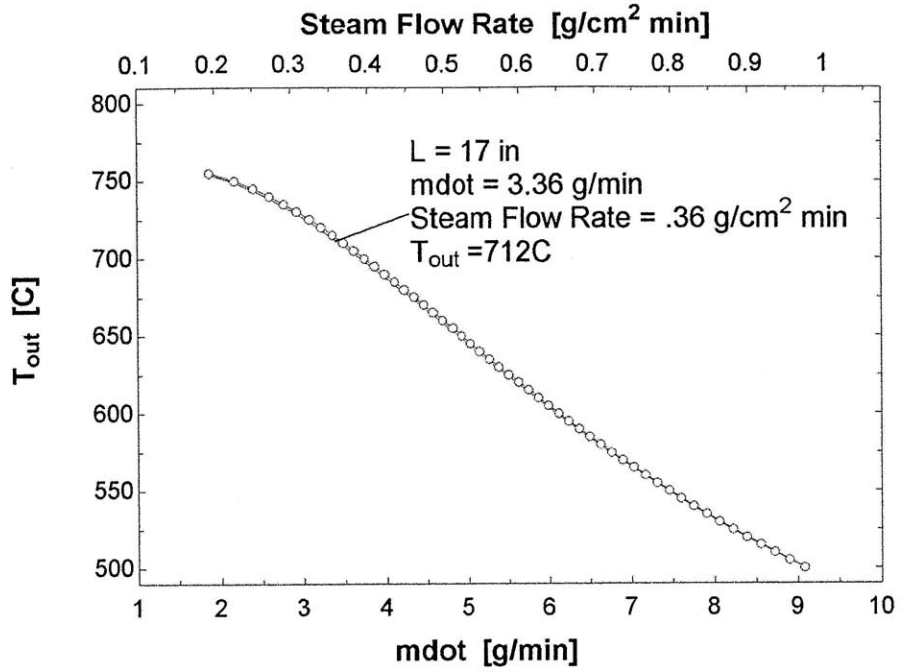

Figure 31 – Outlet temperature of flowing steam as a function of flow rate for the heat tape stage

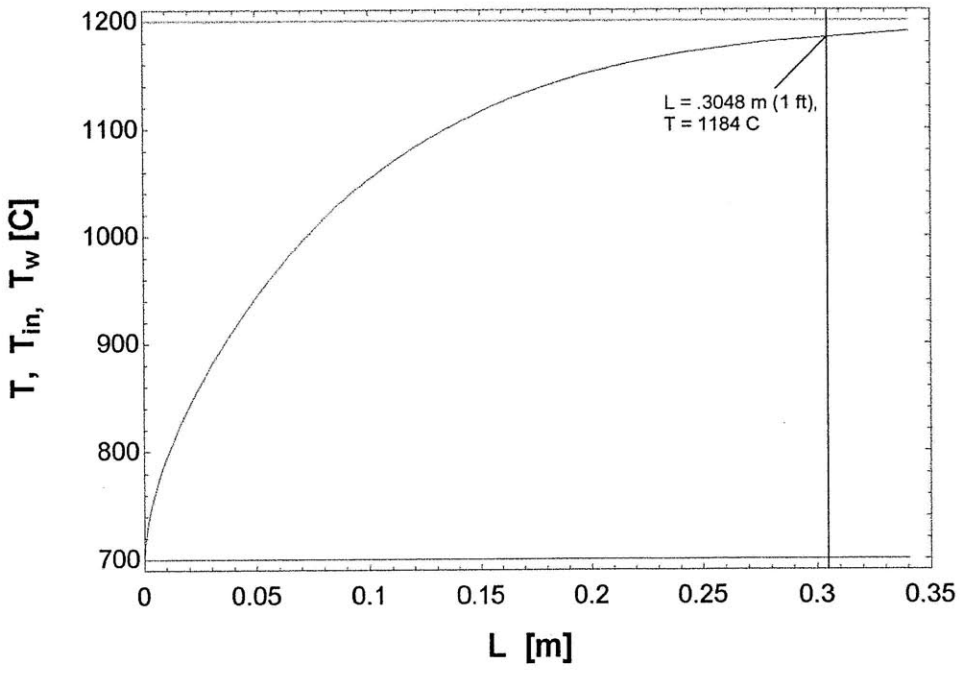

Figure 32 – Temperature profile of flowing steam through the preheater furnace stage (vertical line indicates end of heated length)

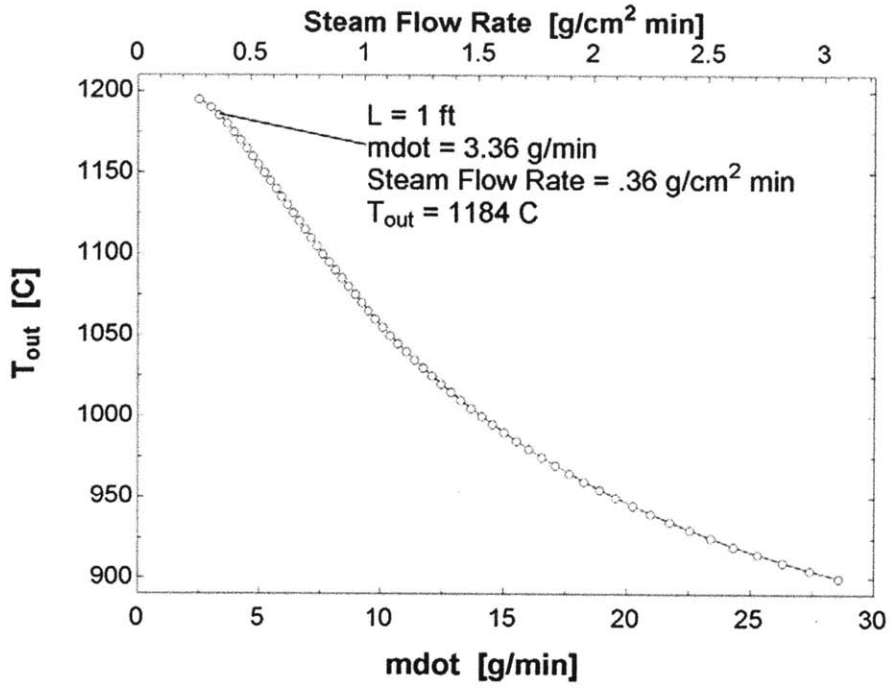

Figure 33 – Outlet temperature of flowing steam as a function of flow rate for the preheater furnace stage

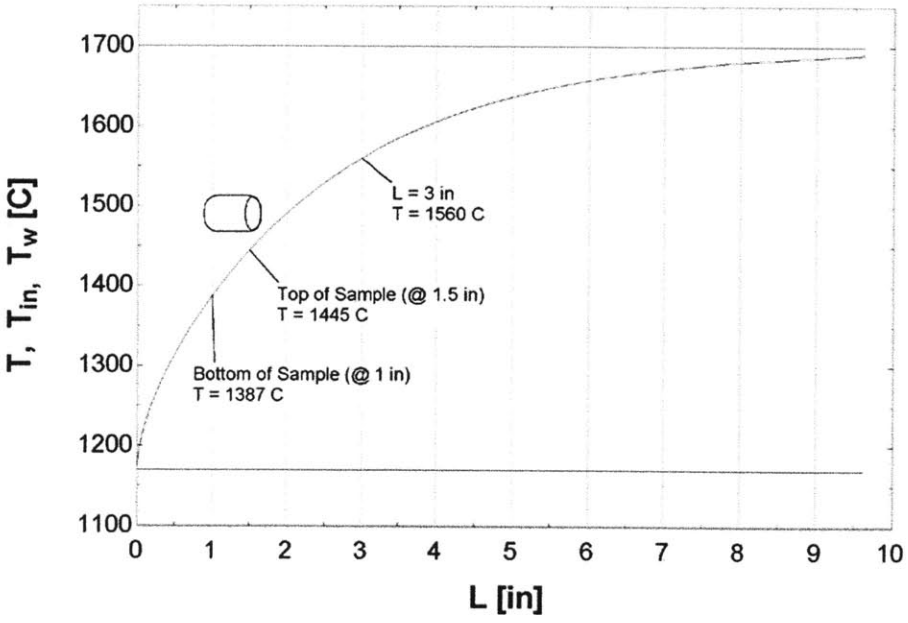

Figure 34 - Temperature profile of flowing steam through the sample furnace stage (end of heated length is 2 in)

Another safety concern that came up when developing the facility involves the thermal power of the steam as it exits the reaction tube and is pulled into the laboratory ventilation system. It was necessary to confirm that this would not be a fire hazard. By knowing the enthalpy of steam at 1,600°C and conservatively assuming a mass flow rate of 5 g/min, the thermal power was calculated to be approximately 542 W. To put this number into perspective, a Bunsen burner has an average heat output from 235 to 352 W while the more powerful Tirrill burner has an average heat output from 587 to 938 W [Cole-Parmer 2011]. With this analysis, it was determined that the thermal power of the steam does not create a fire safety hazard for the ventilation system of the laboratory.

3.3.5 Sample Furnace

The sample furnace is a RHUL-MP2125-3 UltraCoil Robust Radiator purchased from *Micropyretics Heaters International Inc.*, located in Cincinnati, Ohio, on February 6, 2008. The heating element of the sample furnace has a spiral shape with a heating length of 5.1 cm with the two ends acting as electrical leads that extend outside the shell of the furnace. While proofing the oxidation test facility, it was discovered that one of the leads of the heating element was broken, hence making the furnace inoperable. A picture of the broken lead and the inoperable furnace can be seen in Figure 35. Because the heating element is fabricated from a molybdenum disilicide ceramic, $MoSi_2$, it becomes fragile and brittle after being exposed to the extreme temperatures that it produces. Even a small force could break one of the leads which would effectively sever the circuit, making it impossible to produce a steady current through the element or effectively operate it. This presumably occurred at some point with the furnace used in this study. To make use of the downtime while the sample furnace was being repaired, experiments were completed at temperatures of up to 1,200°C with a modified setup, which is shown in Figure 36 and Figure 37. The major difference between the two setups is that the modified one has a reaction tube length of 0.95 m and only three heating stages. Recall that the four heating stages setup has a reaction tube length of 1.18 m. It is also important to note that samples were suspended 7.6 cm into the preheater furnace in this setup which is approximately a quarter of the way into the furnace. At this level, it was expected that the flowing steam temperature would be adequately close enough to the operation temperature measured by the preheater furnace thermocouple and verification of this assumption is given in section 4.1. A

summary of the experiments that used the modified test facility setup can be seen in Table 3 of section 3.3.1.

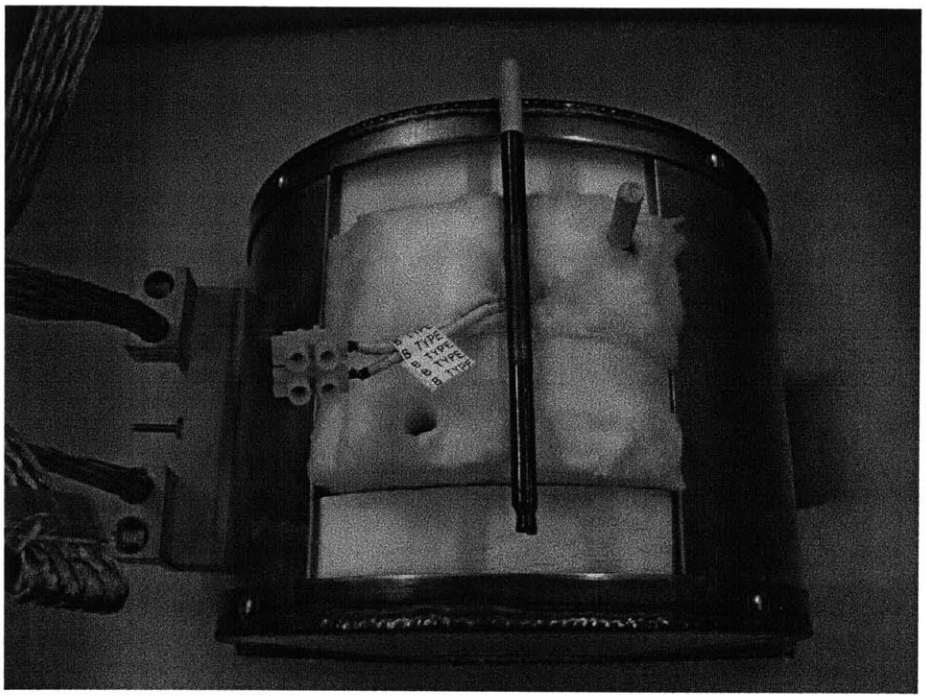

Figure 35 – Inoperable sample furnace with a broken lead

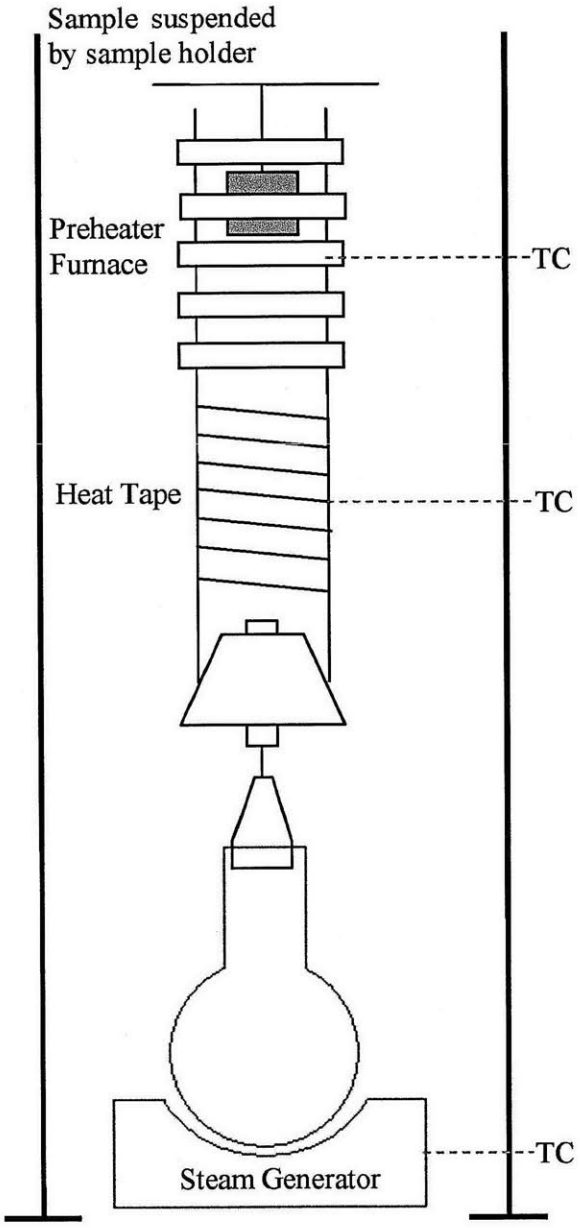

Figure 36 – Modified experimental setup of oxidation test facility with three heating stages

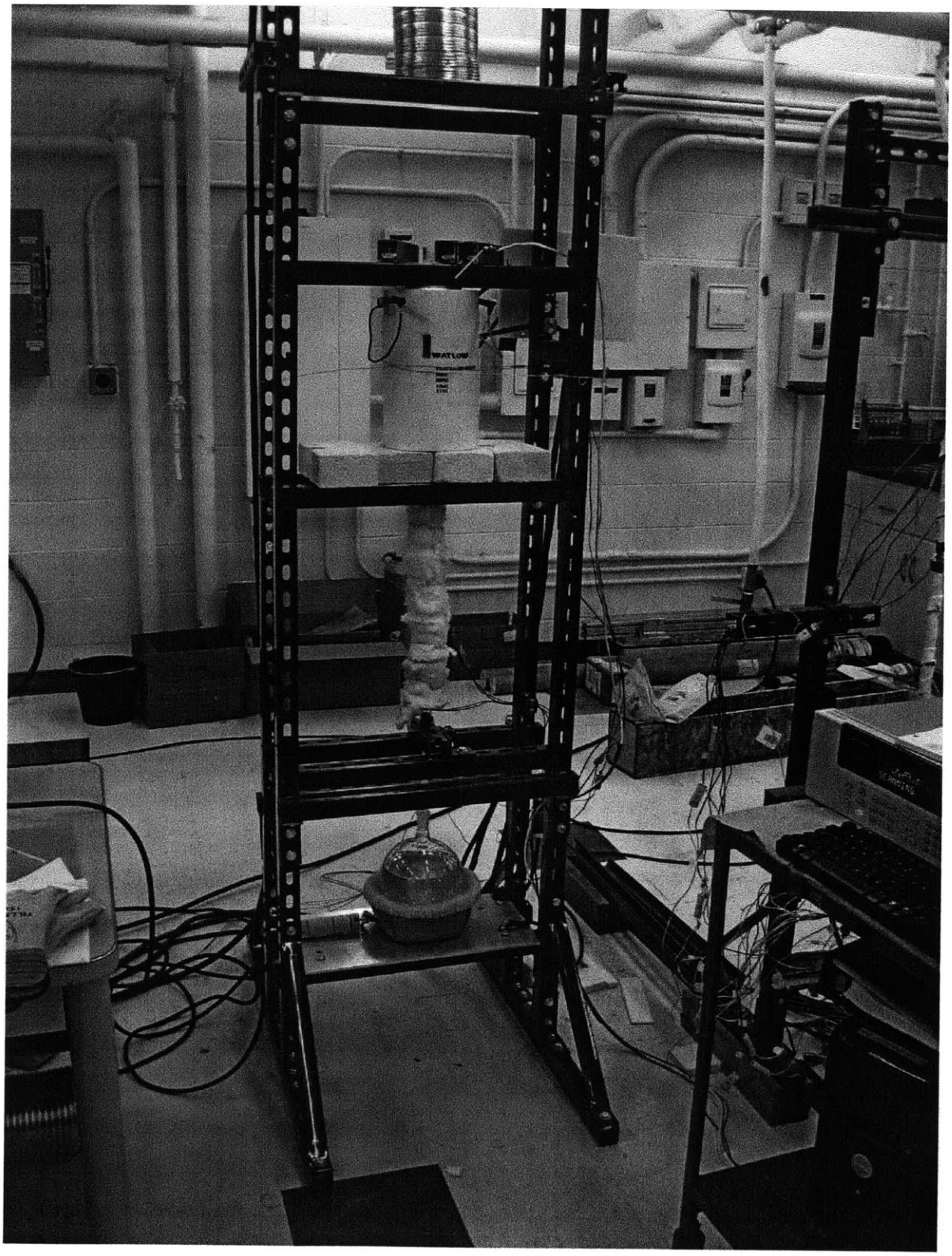

Figure 37 – Picture of the modified oxidation test facility

3.4 Sample Holder

A crucial piece of equipment for the oxidation test facility is the sample holder which had to be designed to survive the oxidation environment at the high temperatures required during testing for durations on the order of magnitude of days without breaking under the load of the sample and the sample holder itself. If this were to happen, there could be a significant loss of time as the test would need to be restarted and the sample holder and sample would need to be retrieved from the bottom of the reaction tube which would require the shutdown and cooling of the facility to allow access into the reaction tube. Also, a loss of materials would result as the sample would no longer be useful and the reaction tube could break due to the hot sample contacting it. Because of the two different facility setups, as discussed in sections 3.1.2 and 3.3.5, two different sample holder styles were utilized. For low temperature testing which only went up to 1,200°C, a much simpler design for the sample holder was used with K-type thermocouple wire acting as the vertical support piece. A more thorough sample holder design and analysis process was necessary to complete for the high temperature testing which went up to 1,600°C.

3.4.1 Low Temperature Approach

For experiments that operate at 1,200°C or lower, a simple sample holder design is utilized. The three components of the sample holder are the vertical support wire made of K-type thermocouple wire rated to 1,250°C and the lower and upper horizontal support rods made of an alumina rod. Pictures of the sample holder can be seen in Figure 38 and Figure 39. The lower horizontal support rod is cylindrical with a diameter of 1.6 mm allowing it to fit through the holes that were machined into the samples. This rod is also notched in three places with small grooves which allow the sample to sit in the notches and the K-type thermocouple wire to be wrapped in the center notch. The vertical support wire consists of two K-type thermocouple wires which are wrapped around the top and bottom horizontal support rods. For the top horizontal support rod, either a cylindrical rod with the same dimensions as the bottom rod or a square rod with 3.2 mm sides is used. While performing the shorter duration experiments, it is more efficient to utilize two sample holders – one sample holder would suspend a sample in the facility while a second sample holder was setup with the next sample to be tested. This allowed for only a short amount of time to be lost between experiments. Throughout the 36 shorter

duration zircaloy tests that were performed and the six longer duration SiC tests, no sample holders broke while being used in the facility. However, several sample holders broke at the bottom most part of the K-type thermocouple wire right above where it wraps around the bottom horizontal support rod after being removed from the test and setting them down. Low temperature sample holders were made in the same fashion as the original one to replace broken sample holders when necessary.

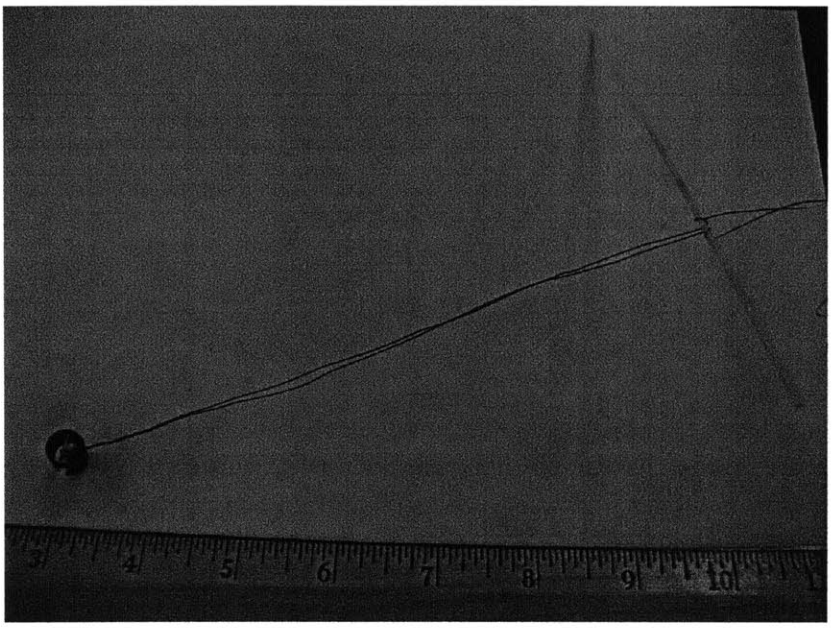

Figure 38 – Low temperature sample holder

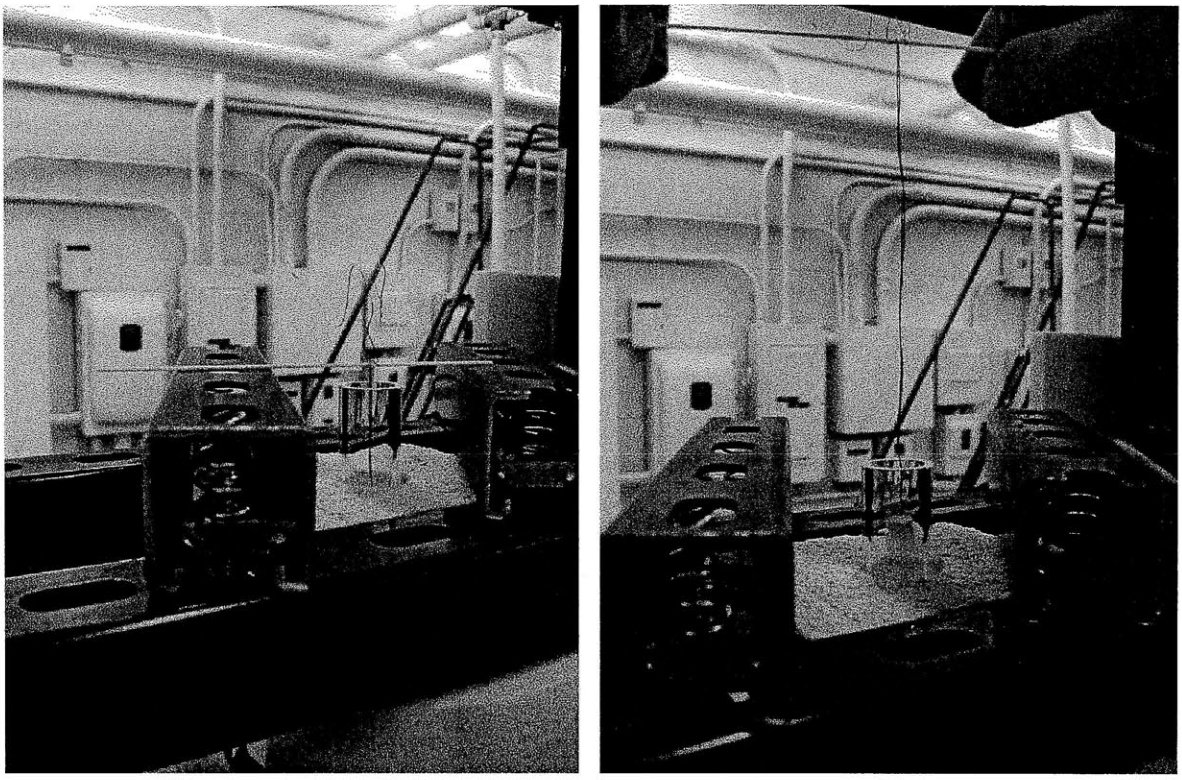

Figure 39 – Low temperature sample holder being used in the modified setup

3.4.2 High Temperature Approach

For high temperature experiments that operate at temperatures up to 1,600°C, it was necessary to complete a more thorough sample holder design and analysis process. As discussed in the following sections, the design geometry was first decided, and then material selection of the sample holder was completed. Finally, a structural analysis was performed and in-house fabrication was attempted unsuccessfully. It was then decided that the sample holder will be fabricated at *Ferro-Ceramic Grinding Inc.*, a specialty machine shop located in Wakefield, Massachusetts, when it is needed.

3.4.2.1 Design

For the design geometry of the high temperature sample holder, two main issues had to be considered – how the samples would be held and suspended by the sample holder and how to size the vertical support rod. For the first concern, four different design iterations were evaluated before a fifth design was decided on to be the best choice. All five design iterations can be seen in Figure 40. A common concern with the first four designs was that there would be significant

steam flow restriction due to the samples inner void being blocked by the lower horizontal support. This issue was lessened with each consecutive sample holder iteration until Design E was determined to not inhibit the steam flow to an acceptable level. With Design A, the sample tube would sit inside a larger tube with a lower rod supporting the sample, however, it was determined that steam flow restriction was too great and the tolerances of this design were too tight to comfortably position it in the reaction tube as the largest sample that was expected to be tested had an outer diameter of approximately 13 mm while the reaction tube has an inner diameter of 19 mm. With Design B, a star-shaped base plate would be suspended from the vertical rod, but steam flow restriction was too significant with this design. Design C, used the same base plate concept as Design B but with a cross shape, however, once again the steam flow restriction would be too great due to the necessary widths of the cross to support itself and a sample in an oxidizing environment at 1,600°C. With Design D, the cross base plate was kept while adding raiser blocks onto the ends of the cross tips to raise the sample off of the base plate and reduce the steam flow restriction to an acceptable level. However, it was decided that this base plate would be too flimsy, too expensive to fabricate, and due to the raiser blocks, it would be necessary to fabricate one for each sample size rendering this design undesirable. With Design E, a much simpler approach was taken. The fabrication process would only require two holes to be drilled into the vertical support rod so two cylindrical horizontal rods could be positioned through the vertical rod. One disadvantage of this design is that two holes would have to be machined into each sample so that the lower horizontal support rod could fit through and suspend the sample. This would expose more end surface (faces that are perpendicular to the axial direction) and could be more susceptible to oxidation; however, it was decided that since the samples are sintered, their end surfaces are not expected to react at an accelerated rate.

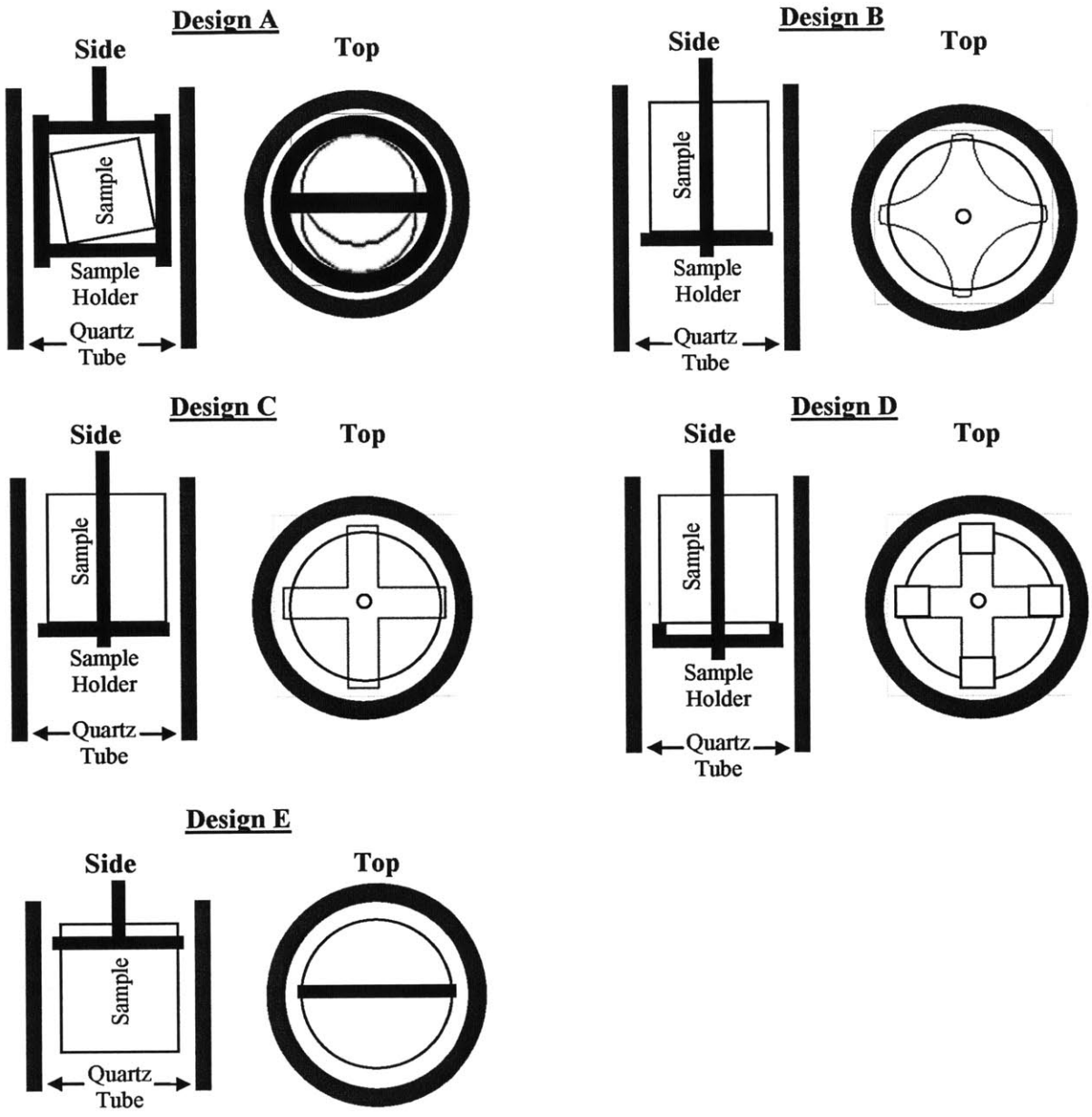

Figure 40 – Sample holder design iterations

The second design geometry issue that had to be addressed involved the sizing of the vertical support rod. Once again, steam flow restriction was the primary concern. Accordingly, the rod needed to be as small as possible yet still able to support the operating load at temperature. It was expected that SiC tube samples with an inner diameter of approximately 11 mm would be tested so square rods with 3.2 or 6.4 mm sides were considered. For the 6.4 mm side rod, steam

flow restriction would be approximately 45 percent and the diagonal of this rod of 9 mm would make for tight tolerances. On the other hand, the 3.2 mm side rod would create a flow restriction of approximately 11 percent and not have tolerance issues making this the ideal choice. However, in the end a 6.4 mm side rod has been chosen for reasons to be discussed in section 3.4.2.4.

3.4.2.2 Material Selection

Once the design geometry was decided upon, material selection occurred. Although many materials were considered in this process including ceramics, metals, glass, and composites, only three candidates seemed to be potentially viable options that would be investigated further – tungsten, SiC, and alumina. Tungsten was considered due to its ability to maintain its strength at high temperatures. It has also been seen to survive in a flowing steam environment at 1,350°C [Greene 2001]. For this reason, several tungsten stock rods and wires were purchased in an attempt to form them into the necessary geometry; however, these attempts were unsuccessful. At room temperature, tungsten is extremely brittle making it impossible to bend or cut it successfully. Tungsten wire with a diameter of 1.6 mm was heated to 1,000°C with a *Thermo Scientific* Thermolyne F6018 furnace in an attempt to soften the metal and bend it into the necessary geometry. Upon removing the tungsten wire from the furnace, it was flexible for only a matter of seconds before quickly cooling and then snapping due to its brittleness from the force applied in the bending process. It was also seen that it quickly oxidized with a yellowish oxidation layer in the laboratory atmosphere when heated to 1,000°C even for only ten minutes which can be seen in Figure 41. With these two observations made, the work with tungsten was suspended and SiC and alumina were further evaluated.

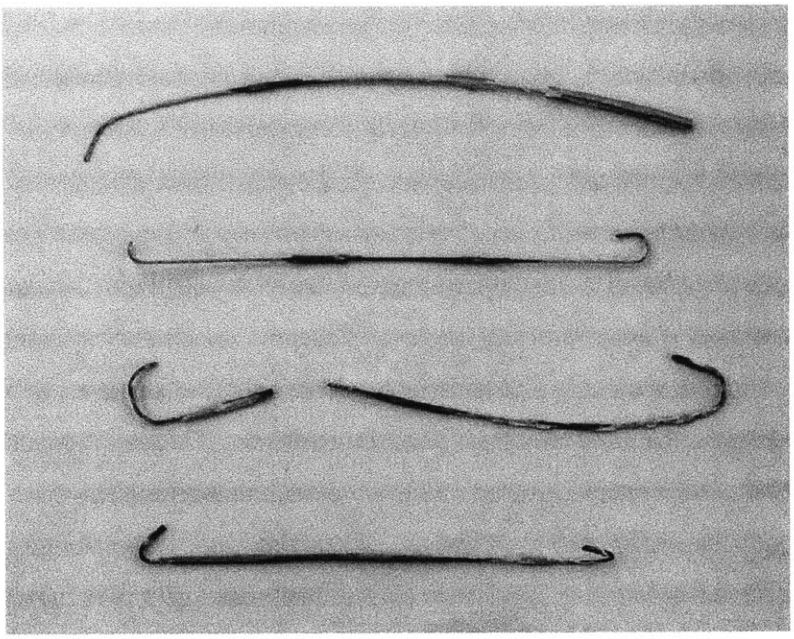

Figure 41 – Tungsten wire that was oxidized after being heated to 1,000°C

SiC and alumina are both ceramics that have high melting points, 2,545°C and 2,054°C, respectively [Bauccio 1994; Snead 2007]. They also have been seen to have strong performances in high temperature steam environments [Horn 1979]. Figure 42 shows the oxidation of four ceramics in a flowing steam environment. Although, these experiments only went up to temperatures of 1,395°C, the oxidation rates can be extrapolated and it can be seen that alumina has the best performance in this particular study. One argument that favors SiC is that the samples to be tested are made of SiC. By using a sample holder made of the same material, no impurities would be added into the system. Also, because the samples contact the sample holder, there would not be any potential weight changes due to atoms of a material other than SiC reacting with the SiC sample. Even when this last point is taken into account, it was decided that alumina would make for the best material to fabricate the high temperature sample holder. It is also important to note that even with an extensive search, it was not possible to purchase any stock SiC rods in small quantities that could be used in an attempt to fabricate the sample holder in-house, whereas, very high temperature nonporous high-alumina ceramic rods could be ordered and received the following day from *McMaster-Carr* which is located in Robbinsville, New Jersey.

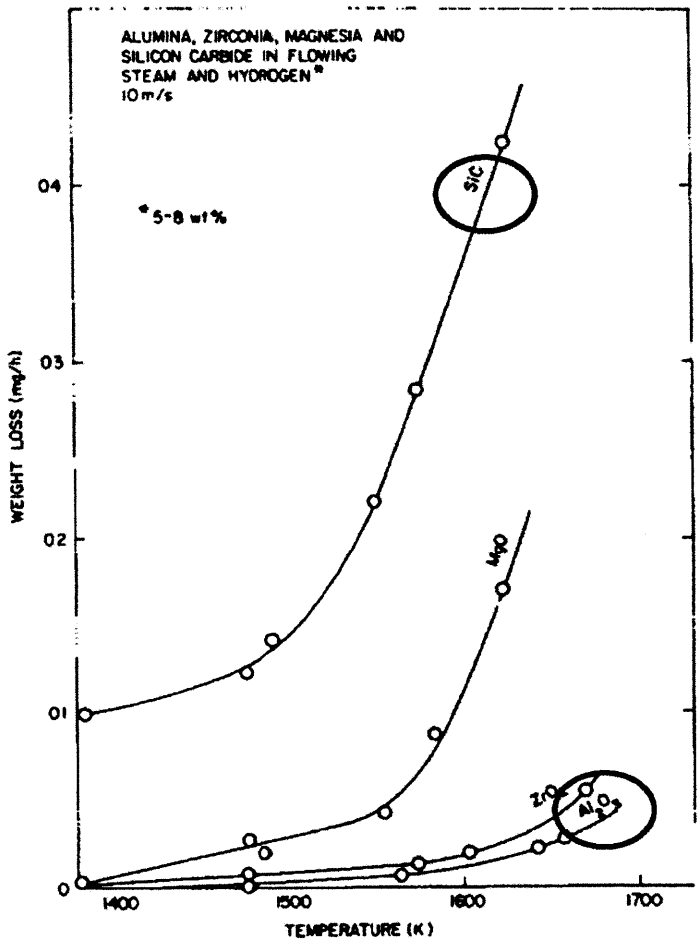

Figure 42 – Oxidation of four ceramics: SiC, MgO, ZrO_2, and Al_2O_3 [Horn 1979]

3.4.2.3 Structural Analysis

A preliminary structural analysis of the alumina high temperature sample holder was completed that looked at and evaluated several properties – tensile strength, shear strength, and creep rate. For the analysis, a vertical support rod with a height of 15.2 cm and square sides of 3.2 mm was conservatively assumed. For the tensile strength, σ_{TS}, calculation, the weakest point that was evaluated was at the cross-sectional face at the midpoint of the top hole in the vertical support rod. This point has the lowest surface area and must support the force of the majority of the vertical support rod and the entirety of the lower horizontal support rod and the sample. The total stress at the evaluated point was calculated to be 15.4 kPa while the tensile strength of alumina at 1,600°C is 11.2 MPa, approximately three orders of magnitude larger than the maximum load making the alumina sample holder adequately sized in terms of this property

[Munro 1997]. For the shear strength, τ_S, calculation, the relationship shown in Equation 3.9 was applied between shear strength and tensile strength. The top horizontal support rod was seen to have the greatest shear stress at the point where it contacted the vertical support rod. The total shear stress at this point was calculated to be 39.1 kPa while the shear strength of alumina at 1,600°C is 7.49 MPa, approximately 2.5 orders of magnitude larger than the maximum shear load making the sample holder adequately sized in terms of this property. For the creep rate, $d\epsilon/dt$, calculation, Equation 3.10 was evaluated using the parameter values of $3.6 \cdot 10^{11}$ s^{-1} for A, 1.08 for n, and 323 kJ/mol for E_{act} [Munro 1997]. This resulted in a creep rate of approximately $1.11 \cdot 10^{-8}$ s^{-1}. Assuming the vertical support rod is 15.2 cm and an experiment time of 48 hours, the maximum lengthening of the support rod would be 0.029 cm making the sample holder adequately sized in terms of this property.

$$\tau_S = \frac{2}{3} \cdot \sigma_{TS} \qquad \text{Equation 3.9}$$

$$\frac{d\epsilon}{dt} = A \cdot \sigma^n \cdot exp(-E_{act}/RT) \qquad \text{Equation 3.10}$$

If a sample holder were to be fabricated out-of-house at a significant expense or if an already used sample holder broke, it would be recommended to complete a more thorough structural analysis to potentially improve any weak points of the sample holder; however, it was decided that this analysis was adequate to proceed with attempting in-house fabrication.

3.4.2.4 Fabrication

Once the sample holder design geometry and material selection was completed, it was possible to attempt in-house fabrication of the alumina sample holder. Two machining techniques were used to make the necessary cuts – a wet saw with a diamond bonded blade and a drill press with a diamond bonded drill hole bit. First, the wet saw was used to cut the stock rods down to the necessary length. Although this technique worked fairly well, it was noticed that the shortened vertical support rods would occasionally have a permanent twist warped into them which led to problems when using the drill press. The drill press was used to machine the two holes into the top and bottom of the already cut vertical support rod. For this cut, 1.6 mm diamond bonded drill hole bits were purchased from *Discount Diamond Bits* located in Stone Mountain, Georgia and deionized water was continuously sprayed into the hole at a slow flow rate in an attempt to

dissipate heat from the drill bit. Although more than ten hole drilling attempts were made into 3.2 mm rods, the team was never successful in making two holes on the same rod. Several times, one hole was made successfully but when attempting the second hole, the rod would always break. It was also noticed that the diamond powder that was glued onto the drill bits would quickly fall off due to the epoxy melting if too much pressure was applied to the drill press. The team also attempted several times to drill into the 6.4 mm rods in the hope that the rod would not break due to its larger dimensions. However, these attempts were also unsuccessful as the drill bit would be completely dulled before making it through the longer drill length. Because of these unsuccessful attempts, it was decided to outsource the machining of the sample holder to *Ferro-Ceramic Grinding Inc.*, a specialty machine shop located in Wakefield, Massachusetts. Although the official order has not been placed yet because the high temperature sample holder is not required at this point due to the sample furnace being inoperable, the order can be made with a fairly short lead time when the team decides the alumina sample holder is needed. A 6.4 mm side rod will be used as it is more likely to result in a successful fabrication, it will have a lower chance of failure during the required tests, and it does not inhibit steam flow to an acceptable level as was discussed in section 3.4.2.1.

3.5 Facility Operation

When operating the oxidation test facility, it is necessary to follow several procedures in order to keep the system in a safe condition and to obtain valid experimental results. The different procedures that are regularly followed can be divided into four groups – system heat-up, testing, steam generator switch-out, and system cool-down. It is also useful to understand how the temperature of a sample changes as it is put into the facility with a sample holder.

3.5.1 System Heat-Up Procedures

In order to protect the functionality and structural integrity of the three heating stages that are used to heat the steam, it is necessary to heat the system in a methodical fashion at a temperature change rate of no greater than approximately 10°C per minute. To do this, each of the three heating stages has to be regularly checked while slowly increasing the power level with the appropriate controller until each heating element reaches their necessary temperature for the experiment that is going to be run. For example, to run a 1,200°C experiment, the system heat-up would take at least two hours while the heat tape is brought up to approximately 750°C and

the furnace is brought up to approximately 1,200°C. Once the three stages are at the appropriate temperatures, steam flow from the steam generator is added into the system which is then given time to reach a steady state temperature. Then, final adjustments are made with the appropriate controllers to attain the necessary temperatures more precisely as the addition of the flowing steam into the system changes the temperatures. Once the steady state experimental temperature is reached, the lower temperature set points of the temperature deviation electrical protection circuit are raised to the appropriate operating set points. While starting up the oxidation test facility, several issues occurred including tripping the fuse for the circuit that the heating stages are connected to and also not having a functioning data acquisition system. To best prevent tripping a circuit, it was necessary to make sure the triac dimmers and variable autotransformers were turned to their lowest setting before turning them on. By doing this, a spike in the current demand can be avoided preventing a tripped circuit and loss of time. When starting up the data acquisition system, it is necessary to properly connect the terminal block to the *Agilent* multifunction unit and turn it on prior to turning on the computer that is connected to the system. This has been seen to minimize software issues with the data acquisition user interface.

3.5.2 General Test Procedures

Two main procedures are followed to help in obtaining valid experimental results – sample loading and unloading into the system and water handling. It is important to be consistent with the procedures so the results are repeatable. Prior to positioning a previously cleaned sample into the sample holder, several tasks are completed. Measurements of the outer diameter, inner diameter, thickness, and height are taken at multiple points on the sample. Also, the mass of the sample is weighed on a *Sartorius CP224S* balance with a resolution of 0.0001 g at least twice until two measurements are the same. Also, a nickel was used to confirm the balance accuracy for longer duration tests. Then, the sample is positioned into the sample holder which is done on a thermally insulated aluminum work surface that is cleaned with acetone, methanol, and deionized water before daily experimentation begins. Once a sample has been cleaned, all handling of it is done with a fresh pair of nitrile gloves so that no grease or debris on the operator's hands rubs off onto the sample. Once the facility has come to a steady state, including the steam flow rate and the temperature, and the sample has been positioned onto the sample holder, the sample holder is lowered into the facility, set into place for the experiment, and the

time is recorded. A picture of this process using the low temperature sample holder and the modified facility setup can be seen in section 3.4.1. Thermal resistant gloves are used when adding or removing the sample holder from the system as there is a burn hazard from the flowing steam as it exits the reaction tube before it is pulled into the ventilation system of the laboratory. When the experiment is complete, the sample holder is carefully removed from the facility while trying not to bump or drag it up the reaction tube. It is allowed to air cool for approximately 30 seconds before setting it back down onto the insulated work surface and allowed to cool further. After at least three minutes, the sample is removed from the sample holder and if necessary, the next sample is loaded. Before the end of the day, the tested sample will be reweighed on the same scale in the same fashion as done before the experiment.

Another experimental procedure that is important to be consistent with is the handling of the water that is used to generate steam. In order to calculate the averaged experiment steam flow rate for the day, precise volume measurements are required. First, the necessary amount of deionized water is added to the appropriate volumetric flask(s) and then transferred with a funnel into the spherical test flask. To decrease the time it takes the water to boil, the volume of water is then microwaved until boiling inception. While it is being microwaved, the mantle is heated to the necessary level for the experiments that will be run. Once boiling occurs in the microwaving flask, it is immediately transferred to the hot mantle. Although it has been seen that the boiling sometimes stops due to the heat losses to the environment, boiling will eventually restart and reach an approximately constant mass flow rate. Once continuous boiling is observed, the time is recorded. When all experiments are completed for the day, the spherical flask, now with a lower volume of water, is removed from the mantle and the time recorded. The water is allowed to cool over night as the thermal expansion of water would otherwise make for an inaccurate post-experiment volume measurement. Then, the water volume is accurately measured using the appropriate volumetric flask(s) and a graduated cylinder. With the recorded data – the times of the start and ending of the boiling, and the difference in pre- and post-experimentation deionized water volumes – an averaged steam flow rate for the day of experimenting is calculated. It is important to note that the instantaneous flow rate or even the averaged flow rate for each sample test is not known, but only the averaged flow rate for the entire day of experimenting. This is a limitation of the current oxidation test facility; however,

with the appropriate amount of funding it could be possible to improve the accuracy of the flow rate measurements.

3.5.3 Sample Temperature

It is important to understand how the temperature of a sample changes as it is put into the facility with the sample holder. In particular, it is necessary to know how quickly the sample heats up after being placed into the high temperature flowing steam environment as experimental results would need to reflect the actual temperature of the sample if it did not come to the experiment temperature quickly. To do this, a calculation was completed using the lumped capacitance method which reduces a thermal system to a number of discrete 'lumps' and assumes that the temperature difference inside each lump is negligible. In the case of this study, it could be assumed that there is only one lump, that of the entire sample as it is thermally heated by the flowing steam. To determine that this was a suitable assumption, the Biot number, *Bi*, of the system had to be calculated using Equation 3.11 where the characteristic length, L_c, is equal to the volume of the sample divided by the surface area of the sample, the heat transfer coefficient, *h*, is calculated in the same way as done in section 3.3.4, and the thermal conductivity of the sample, *k*, is conservatively assumed to be 21.5 W/m-K and 77.5 W/m-K for zircaloy-4 and α-phase SiC, respectively [ATI Wah Chang 2003; Saint-Gobain 2003]. The Biot number is a dimensionless parameter of the system that is defined as the ratio of the conductive heat resistance within the object to the convective heat transfer resistance across the object's boundary. When the thermal resistance to heat transferred into the object is larger than the resistance to heat being diffused completely within the object, the Biot number is less than one. The Biot number must be less than 0.1 in order to have a usefully accurate approximation of the heat transfer using the lumped capacitance model. In the case of both zircaloy-4 and α-phase SiC, the Biot numbers are several orders of magnitude less than 0.1 making the lumped capacitance model acceptable. [Welty 2001]

$$Bi = L_c \cdot \frac{h}{k} \qquad \text{Equation 3.11}$$

Once it was determined that the lumped capacitance model could be used, a heat transfer energy balance was set up between the flowing steam and the sample. This can be seen in Equation 3.12 where T_∞ is the temperature of the flowing steam, T is the unknown temperature of the sample

that will be solved for, and A_s, ρ, C_p, and V are the surface area, density, specific heat capacity, and volume of the sample, respectively. After integrating and solving the new equation in terms of time, t, the temperatures at different times, T_f, can be calculated using Equation 3.13. The calculated temperature of a zircaloy-4 sample as a function of time can be seen in Figure 43. Different temperatures and the times that they are reached have been marked accordingly. It is important to note that this is a conservative approximation as radiative heat transfer from the furnace is not taken into account; only convective heat transfer of the steam to the sample is assumed. Because of this, it was determined that the sample was heated fast enough to neglect the heat-up time and just assume it is at the steady state temperature for the entirety of the test. This assumption is fitting as the majority of the tests are much longer than one minute – the time it would take the sample to reach 1,150°C if it was only heated by convective heat transfer.

$$h(T_\infty - T)A_s = \rho\, C_p\, \frac{\partial T}{\partial t}\, V \qquad \text{Equation 3.12}$$

$$t = \frac{\rho\, C_p}{h}\, \frac{V}{A_s}\, \ln\left(\frac{T_\infty - T_o}{T_\infty - T_f}\right) \qquad \text{Equation 3.13}$$

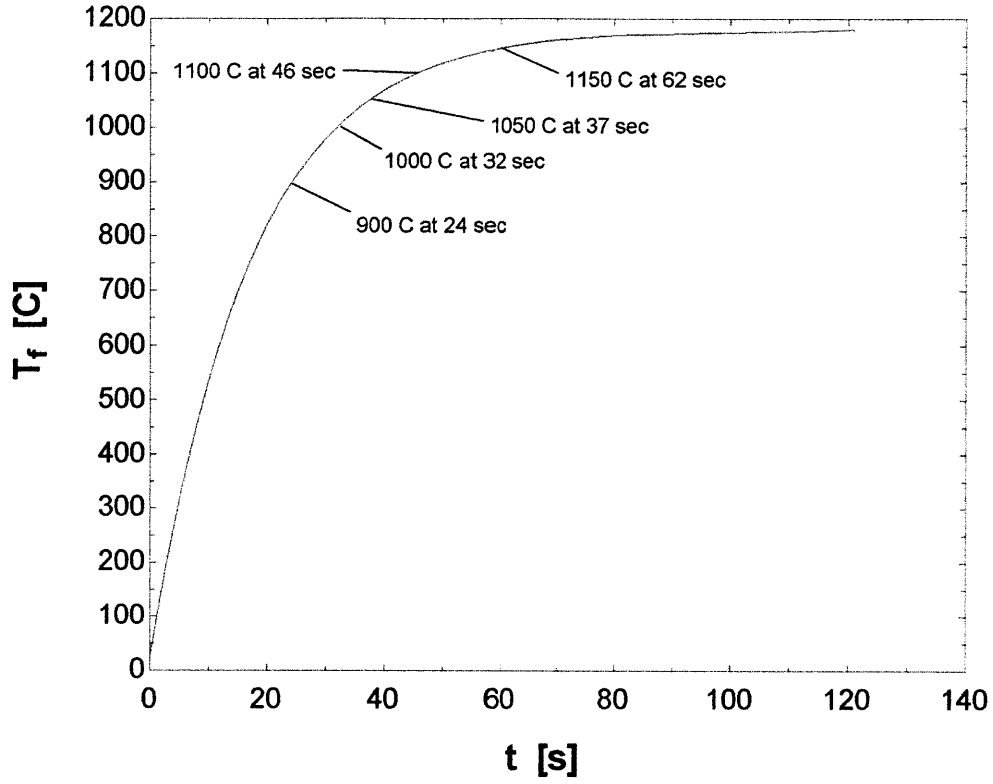

Figure 43 – Temperature as of function of time of a sample as it is convectively heated in the facility

3.5.4 Steam Generator Switch-out

As discussed in section 3.1.4, it is necessary to temporarily switch-out the depleted primary 5,000 mL steam generator with the fresh secondary 3,000 mL steam generator during longer duration experiments. It is important for the procedure of a switch-out to be completed quickly and precisely as any problems that occur such as taking too long or allowing the laboratory environment to enter the reaction tube could reflect in the experiment results making the data unsuitable for analysis. Prior to the switch-out, it is necessary to heat the secondary flask up to a level that will be equivalent to the in-experiment flask's steam flow rate. Also, the necessary amount of water needed to replenish the primary steam generator is brought to a boil. As discussed in section 3.3.1, steam generator calibrations were completed to make the transitions as seamless as possible. Once the fresh secondary steam generator has reached the necessary steady state steam flow rate, it is placed next to the depleted primary steam generator. Then, the 3-way valve is placed into the 'closed off reaction tube/flow into the laboratory' position and the

gas adapter is switched to the fresh steam generator as it is positioned under the facility. Once a steady flow of steam is seen to be exiting the 3-way valve into the laboratory, it is placed back into the 'experimentation' position to once again allow steam flow into the reaction tube. After being trained properly, researchers were able to complete the switch-out in less than one minute which is assumed to be adequate for testing procedures. Once the switch-out has occurred, the depleted primary steam generator is emptied and its volume recorded before being refilled to the necessary level with the pre-boiled water. Finally, after allowing the primary steam generator to reattain its steady state flow rate, the switch-out process is completed again to get the system back into its original state with the primary steam generator. During longer duration experimentation, switch-outs were completed approximately every ten hours. The secondary steam generator was used for approximately five minutes during each switch-out.

3.5.5 System Cool-Down Procedures

Once all testing has been completed for a particular day, it is necessary to shut down the system in a methodical fashion which will once again protect the functionality and structural integrity of the three heating stages. To do so, it is first necessary to decrease the lower temperature set points of the temperature deviation electrical protection circuit back to room temperature so that the system isn't shutdown inappropriately by a set point being tripped. Once the spherical flask of the steam generator has been removed from the mantle, the system cool-down process can be started which is done in an analogous fashion to the system heat-up process in that it is necessary to cool-down the system methodically at a temperature change rate of no greater than approximately 10°C per minute. While the system is cooling down, the data acquisition system is left on until the furnaces reach approximately 600°C. At this point, it is possible to completely shut off all power sources to the heating stages as it has been seen that they will cool by natural air convection at a rate slower than 10°C per minute. The data acquisition system and computer are turned off after the collected data from the experiments has been saved.

This Page Left Intentionally Blank

4. Oxidation Test Facility Benchmarking and Validation

4.1 Experimental Temperature Testing

While operating the modified experimental setup, temperature readings of the heating elements are taken every three seconds; however, as discussed in section 3.2.1, the thermocouple placement is at the middle of the furnace while samples are suspended approximately a quarter of the way into the furnace. This means that the temperature at the position of the sample is likely not identical to the thermocouple temperature reading. The furnace thermocouple is located at the center of the furnace because this is the hottest point of the furnace while it is operating and the equipment must be protected from burnout. It was also decided that having a thermocouple inside the reaction tube, at the level of the sample, during experimentation could introduce impurities into the experiment and make for a more challenging experimental setup. For these reasons, it was necessary to run several benchmark tests to determine the difference in temperatures between a quarter of the way down the furnace heated length (where a sample is suspended) and the middle of the furnace (where the furnace thermocouple is located). Two different tests were completed with the modified setup: one with the in-house fabricated K-type thermocouple suspended in the reaction tube at the appropriate height without a sample in place and one with a sample in place. These two tests were completed to determine if the sample's presence had an effect on the temperature of that location. A third test with the butt-welded B-type thermocouple was completed; however, because it can only extend 3.8 cm into the preheater furnace heating zone while a sample is suspended at approximately 7.6 cm, the results were not useful.

4.1.1 Correlation – Modified Setup/No Sample

The first temperature correlation was between the temperature in the middle of the preheater furnace, outside of the reaction tube (referred to as the furnace temperature) and inside the reaction tube a quarter of the way into the furnace with no sample (referred to as the sample temperature). Thermocouple placement and selection for this test is discussed in section 3.2.1. During the test, steam was generated with the variable autotransformer set to the standard operating power setting of 71 which resulted in an averaged steam flow rate of 4.45 g/min. Five readings were taken from 800°C to 1,200°C at increments of approximately 100°C. For each reading, the system was allowed ample time to reach a steady state. Then, the time was noted

and the system was left alone for several minutes so an average temperature for both thermocouples could be calculated. Equation 4.1 presents the resulting temperature correlation while Figure 44 shows the different data points that were taken. It is interesting to note that below 900°C, the furnace temperature is lower than the sample temperature while above the 900°C, it is the opposite. This is likely due to the fact that the flowing steam, which is heated by the preheater furnace, gets hotter as it moves up through the furnace, however, at a certain temperature, approximately 900°C in this case, the heat losses to the environment outweigh the heating of the steam and result in a higher temperature reading in the center of the furnace.

$$T_{sample} = (0.9591 \cdot T_{furnace}) + 36.818 \qquad \text{Equation 4.1}$$

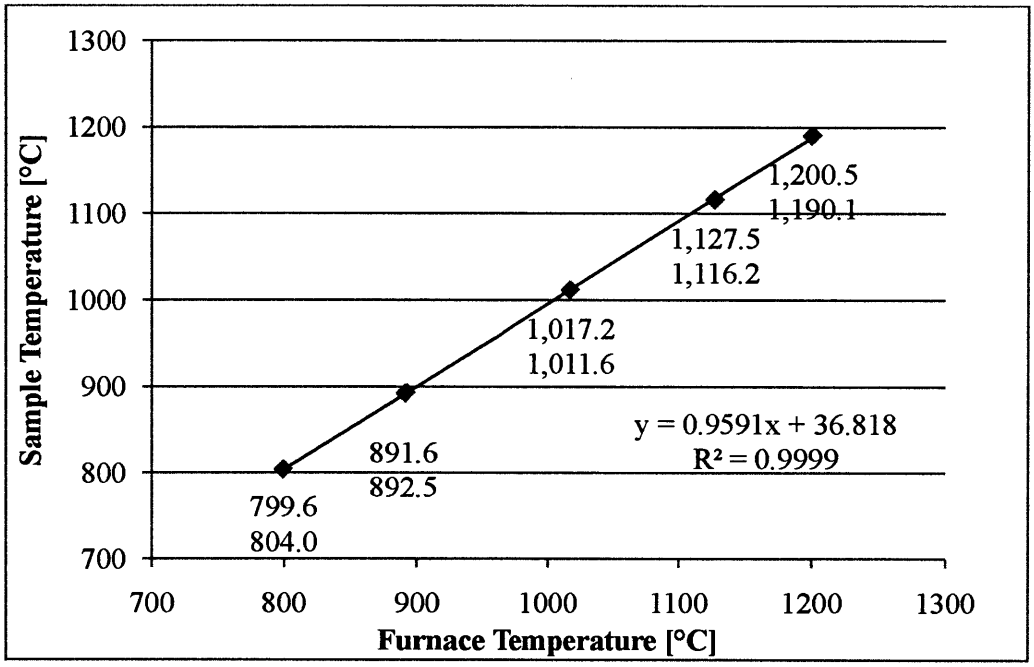

Figure 44 – Temperature correlation between preheater furnace K-type thermocouple and sample level K-type thermocouple without a sample

Table 4 presents the correlated temperatures using the first correlation for each zircaloy-4 experiment that was completed using the modified setup and with a steam generator power setting of 71. It is important to note that although tests are grouped together by the approximate temperature that they were completed at throughout this study, e.g., 800°C, 1,000°C, and 1,200°C, the actual preheater furnace test temperature that was measured is not necessarily the

grouping temperature. Also, the temperature that the sample was exposed to is likely neither the grouping temperature nor the recorded furnace temperature as will be shown with the next correlation.

Table 4 – Temperature correlation of zircaloy-4 experiments completed with the modified setup and a steam generator power setting of 71

Date	Sample	Time [min]	Grouping Temperature [°C]	Furnace Temperature [°C]	Correlated Sample Temperature [°C]
4/21/2011	Zry001	10	1,000	1,000.2	996.2
	Zry002	20	1,000	998.9	994.9
	Zry003	30	1,000	1,003.1	998.9
	Zry004	Void	Void	Void	Void
	Zry005	5	1,000	1,005.4	1,001.1
5/3/2011	Zry006	2	1,000	998.0	994.0
	Zry007	2	1,200	1,203.0	1,190.6
	Zry008	2	1,200	1,203.6	1,191.2
	Zry009	5	1,200	1,200.1	1,187.8
	Zry010	5	1,200	1,200.0	1,187.7
	Zry011	10	1,200	1,201.1	1,188.8
	Zry012	10	1,200	1,201.7	1,189.4
	Zry013	20	1,200	1,202.2	1,189.9
	Zry014	20	1,200	1,201.5	1,189.2
	Zry015	30	1,200	1,198.6	1,186.4
	Zry016	30	1,200	1,198.1	1,185.9
6/14/2011	Zry017	30	800	801.4	805.4
	Zry018	20	800	804.4	808.3
	Zry019	10	800	798.2	802.4

Date	Sample	Time [min]	Grouping Temperature [°C]	Furnace Temperature [°C]	Correlated Sample Temperature [°C]
	Zry020	5	800	804.8	808.7
	Zry021	2	800	805.3	809.2
	Zry022	30	800	800.7	804.7
6/15/2011	Zry023	20	800	801.0	805.1
	Zry024	10	800	801.9	805.9
	Zry025	5	800	801.1	805.2
	Zry026	2	800	800.6	804.7
	Zry027	30	1,000	997.6	993.7
	Zry028	20	1,000	1,002.0	997.8
	Zry029	10	1,000	996.4	992.5
	Zry030	5	1,000	999.9	995.8
	Zry031	2	1,000	1,002.4	998.2

4.1.2 Correlation – Modified Setup/With Sample

A second correlation was completed to determine if the sample's presence has an effect on the temperature. For this test, a thermocouple was placed inside a small hole that was drilled into a zircaloy sample. To hold the thermocouple in place, a refractory cement was used. Then, the sample suspended with the thermocouple was placed into the reaction tube. Because the cement begins to melt at temperatures above 1,100°C, temperature readings were not taken beyond this temperature; however, because there is a strong fit to the linear trend, temperatures up to 1,200°C can be extrapolated. Four readings were taken from 800°C to 1,100°C. For each reading, the system was allowed ample time to reach a steady state. Then, the time was noted and the system was left alone for several minutes so that an average temperature for both thermocouples could be calculated. Equation 4.2 presents the resulting temperature correlation while Figure 45 shows the different data points that were taken. For this correlation, the centerline temperature is lower

than the sample level temperature at temperatures below 1,094°C while above this temperature, it is the opposite. This is a similar trend as observed in the calibration performed in section 4.1.1.

$$T_{sample} = (0.982 \cdot T_{furnace}) + 19.699 \qquad \text{Equation 4.2}$$

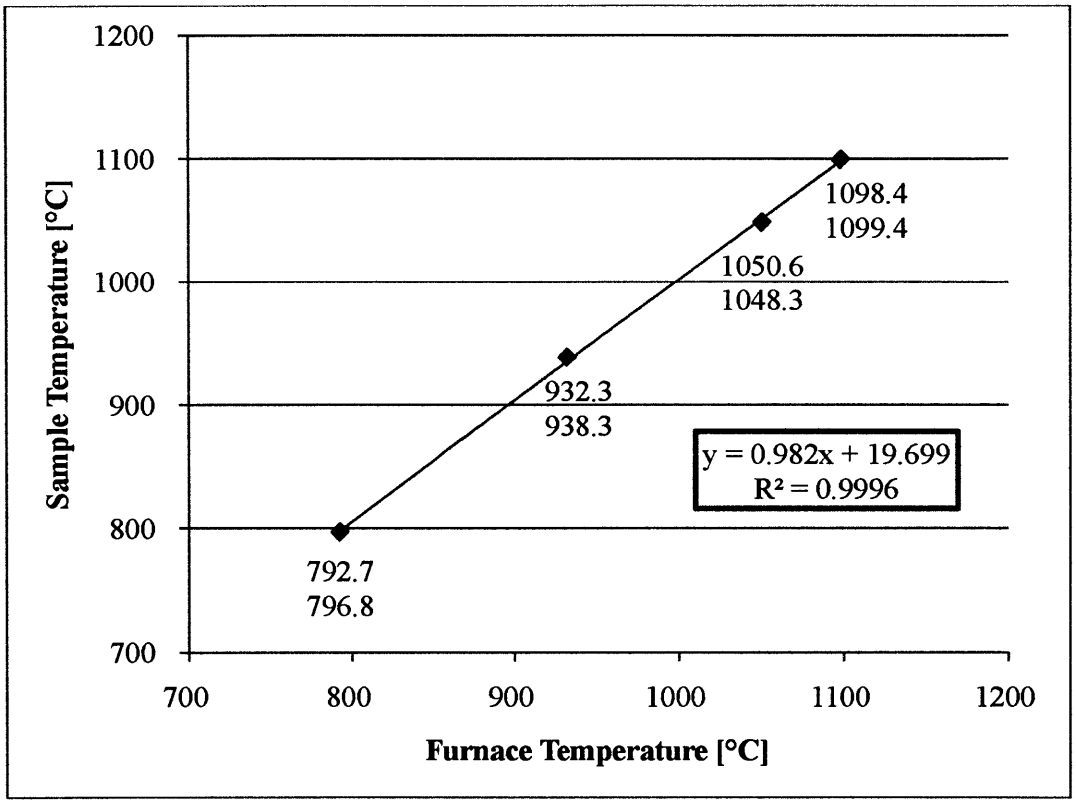

Figure 45 – Temperature correlation between preheater furnace K-type thermocouple and sample level K-type thermocouple cemented to a sample

When comparing the two correlations, it can be seen in Table 5 that when the sample is present, the correlation has a temperature that is closer to the temperature outside of the reaction tube and is likely more accurate. At lower temperatures, there is little difference between the two correlations; however, as the temperature increases beyond 900°C, the second correlation with the sample present maintains a very small difference between the two temperature readings. This is likely due to the increased radiative heat transfer that occurs when a sample is present and it can therefore be concluded that the presence of the sample does have a small effect on the temperature.

Table 5 – Temperature correlation comparison

Grouping Temperature [°C]	Correlated Sample Temperature – No Sample [°C]	Correlated Sample Temperature - With Sample [°C]
800.0	804.1	805.3
900.0	900.0	903.5
1,000.0	995.9	1,001.7
1,100.0	1,091.8	1,099.9
1,200.0	1,187.7	1,198.1

4.2 Zircaloy-4 Experimentation

Zircaloy oxidation rates have been studied by the nuclear community dating as far back as the 1960's and the results of oxidation experiments are understood and well documented [Baker 1962; Ballinger 1976; Leistikow 1987]. It has been shown that when subjected to high temperature steam, zircaloy forms a zirconium dioxide (ZrO_2) layer in a similar fashion to the Deal-Grove model, as discussed in section 2.1. For this reason, zircaloy testing is an excellent way to validate the MIT oxidation test facility setups and the procedures used during SiC oxidation testing. 30 oxidation tests were completed using a flow rate of approximately 3 g/min. For these tests, 10 tests were run at each temperature, 800°C, 1,000°C, and 1,200°C, and for each temperature, five experiment durations were tested twice each for redundancy: 2, 5, 10, 20, and 30 minutes. Also, six tests were completed at variable flow rates to determine if there was a dependence of the zircaloy oxidation on the steam flow velocity.

Zircaloy stock tubes received in January of 2005 from *Westinghouse Electric Company* were used for the validation tests that were conducted. The receiver of these tubes stated that they were Zircaloy-4; however, this was never verified via chemical analysis. Two stock tubes were used to cut the needed zircaloy-4 cladding samples to a height of approximately 1.26 cm. Although both tubes are from the same order and have the same outer diameter and thickness, 0.950 cm and 0.058 cm, respectively, the stock tube that each sample was machined from was recorded; Zircaloy-4 samples 1 through 21, denoted Zry001 to Zry021, were machined from

stock tube #1, while samples numbered 22 and higher were machined from stock tube #2. To machine the samples properly, a drill press with a heavy duty tin coated high speed twist drill bit is first used to drill two holes each with a diameter of 1.6 mm on opposite faces of the tube so the bottom horizontal support rod of the sample holder can fit through both holes and suspend the sample in the reaction tube. The holes are drilled approximately 3.2 mm from the top of the sample. Once the two holes are successfully drilled, a tube cutter is used to cut the sample from the tube stock while being careful not to permanently deform either the sample or the tube stock out of its cylindrical shape. The edges of the sample are then smoothed down first using a de-burrer and then aluminum oxide waterproof sandpaper. Once the sample is properly machined, the sample is cleaned with acetone, methanol, and deionized water and allowed to air dry. Finally, measurements of the outer diameter, inner diameter, thickness, and height are taken at multiple points on the sample and the mass of the sample is weighed on a *Sartorius CP224S* balance with a resolution of 0.0001 g at least twice until the two measurements are the same. Also, a nickel was used to confirm the balance accuracy for longer duration tests. Because the mass was not properly recorded before testing, the test that was completed with Zry004 was not used in the analysis.

4.2.1 Weight Change Data Analysis

Thirty zircaloy oxidation tests were completed using the modified setup in order to effectively validate the oxidation test facility. The results of these tests can be seen in Table 6. Testing was completed at 800°C, 1,000°C, and 1,200°C. For each temperature, five experiment durations were tested twice each for redundancy: 2, 5, 10, 20, and 30 minutes. The standard operating power setting of 71 was used for all of these tests and the averaged steam flow rates can be seen in Table 3 of section 3.3.1. For the weight gain, in units of mg/cm^2, the inner diameter was calculated using the density of zircaloy-4, 6.55 g/cm^3, because there is some variability when measuring the inner diameter depending on exactly where the caliper tips are positioned. Figure 46 shows a picture of an unoxidized zircaloy-4 sample and one that was oxidized at the highest intensity of all tests – 30 minutes at 1,200°C. A definite difference in the colors can be seen as the expected ZrO_2 is much darker and duller than the shiny, unoxidized, metallic zircaloy-4. Also, with a closer examination, a white overly oxidized layer can be seen to have formed on most of the intergranular boundary surfaces due to the fact that the tubes are extruded, producing

a needle-like texture of the grains making the zircaloy tube more susceptible to oxidation at surfaces that are perpendicular to the extrusion direction. Although this increased oxidation cannot be taken into account by a calculation or correlation, the intergranular boundary surfaces only account for approximately 4.4 percent of the total surface area of a sample which is deemed to be acceptable.

Table 6 – Results of zircaloy-4 validation tests

Sample	Temp. [°C]	Test Duration [min]	Initial Weight [g]	Weight Gain [g]	Weight Gain [%]	Weight Gain [mg/cm^2]	Equivalent Oxide Thickness [μm]	ECR [%]
Zry021	800	2	1.2415	0.0044	0.35%	0.62	2.71	0.5%
Zry026	800	2	1.2889	0.0043	0.33%	0.59	2.57	0.4%
Zry020	800	5	1.2840	0.0069	0.54%	0.95	4.12	0.7%
Zry025	800	5	1.3098	0.0068	0.52%	0.93	4.02	0.7%
Zry019	800	10	1.3233	0.0083	0.63%	1.11	4.83	0.8%
Zry024	800	10	1.3294	0.0088	0.66%	1.18	5.12	0.9%
Zry018	800	20	1.2871	0.0113	0.87%	1.54	6.68	1.2%
Zry023	800	20	1.3358	0.0111	0.83%	1.47	6.38	1.1%
Zry017	800	30	1.2631	0.0124	0.98%	1.72	7.48	1.3%
Zry022	800	30	1.2808	0.0123	0.96%	1.71	7.40	1.3%
Zry006	1000	2	1.2320	0.0176	1.43%	2.53	10.96	1.9%
Zry031	1000	2	1.2848	0.0176	1.37%	2.44	10.58	1.8%
Zry005	1000	5	1.2942	0.0271	2.09%	3.70	16.03	2.8%
Zry030	1000	5	1.3406	0.0273	2.04%	3.61	15.64	2.7%
Zry001	1000	10	1.2738	0.0353	2.77%	4.87	21.13	3.7%
Zry029	1000	10	1.2540	0.0330	2.63%	4.66	20.18	3.5%

Sample	Temp. [°C]	Test Duration [min]	Initial Weight [g]	Weight Gain [g]	Weight Gain [%]	Weight Gain [mg/cm^2]	Equivalent Oxide Thickness [μm]	ECR [%]
Zry002	1000	20	1.2833	0.0442	3.44%	6.11	26.47	4.6%
Zry028	1000	20	1.2992	0.0456	3.51%	6.25	27.08	4.7%
Zry003	1000	30	1.3186	0.0547	4.15%	7.34	31.80	5.5%
Zry027	1000	30	1.3237	0.0516	3.90%	6.88	29.83	5.2%
Zry007	1200	2	1.2968	0.0536	4.13%	7.32	31.75	5.5%
Zry008	1200	2	1.3017	0.0539	4.14%	7.34	31.82	5.5%
Zry009	1200	5	1.2997	0.0812	6.25%	11.08	48.01	8.3%
Zry010	1200	5	1.2948	0.0810	6.26%	11.12	48.19	8.3%
Zry011	1200	10	1.2984	0.1141	8.78%	15.54	67.35	11.7%
Zry012	1200	10	1.2967	0.1162	8.96%	15.90	68.94	12.0%
Zry013	1200	20	1.2468	0.1566	12.56%	22.20	96.24	16.7%
Zry014	1200	20	1.2854	0.1642	12.77%	22.64	98.14	17.0%
Zry015	1200	30	1.3185	0.2061	15.63%	27.69	120.04	20.9%
Zry016	1200	30	1.2873	0.2004	15.57%	27.54	119.40	20.8%

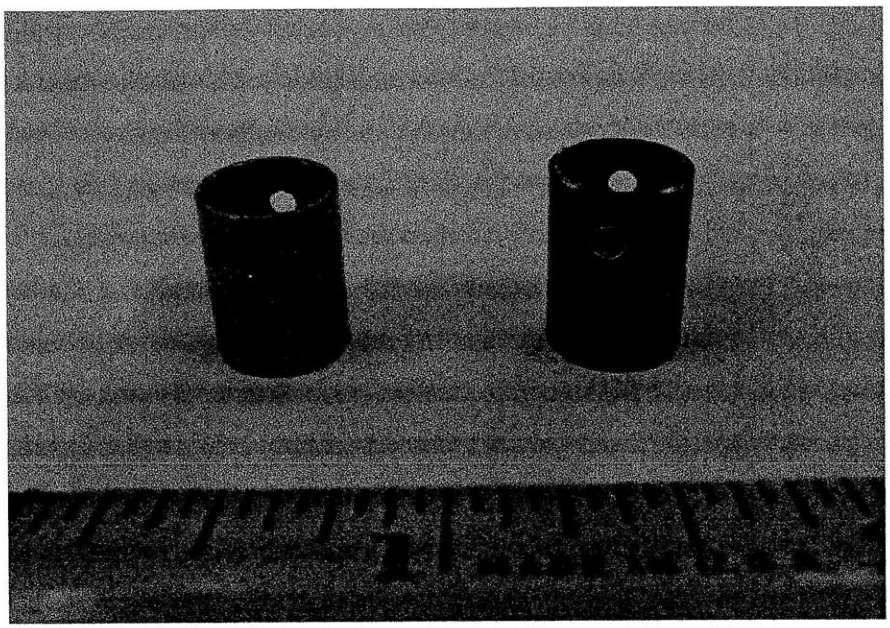

Figure 46 – Picture of unoxidized and oxidized sample

Figure 47 shows the experimentally determined oxidation rates as a function of time. Each point represents the average of two tests that were completed at a given experiment duration and temperature. A parabolic trend can be seen with each temperature curve with the lines having a steeper initial slope and more curvature as the temperature increases. This is due to the fact that zircaloy oxidation increases significantly with temperature. Figure 48 shows the experimentally determined oxidation rates of this study and two correlations – Baker-Just and Leistikow [Baker 1962; Leistikow 1987]. In this figure, the x-axis is in units of $min^{1/2}$ which allows for a linear trendline to be fitted for this study and shows the trend of the other two presented studies. The Baker-Just correlation is important as it was one of the first correlations completed to investigate the zirconium-water reaction, and remains widely used today. It is inherently conservative because it heats a zirconium sample with the condenser-discharge method to a temperature between 1,100°C to 4,000°C that is then submerged in water at a temperature from 20°C to 315°C; therefore, it is logical that this study's reaction rates and that of the Leistikow study are well below that of the Baker-Just results. Selected results of the Leistikow study, which tested at a range of temperatures from 600°C to 1,600°C with a procedure similar to this study, are plotted as an example of a more recent study that is not necessarily overly conservative. However, it is accepted and often referenced in other studies making it useful to compare to the results of this

study which has a relatively close fit to it. Because of these two successful comparisons, the oxidation test facility should be considered a viable tool to test oxidation rates of SiC in high temperature flowing steam.

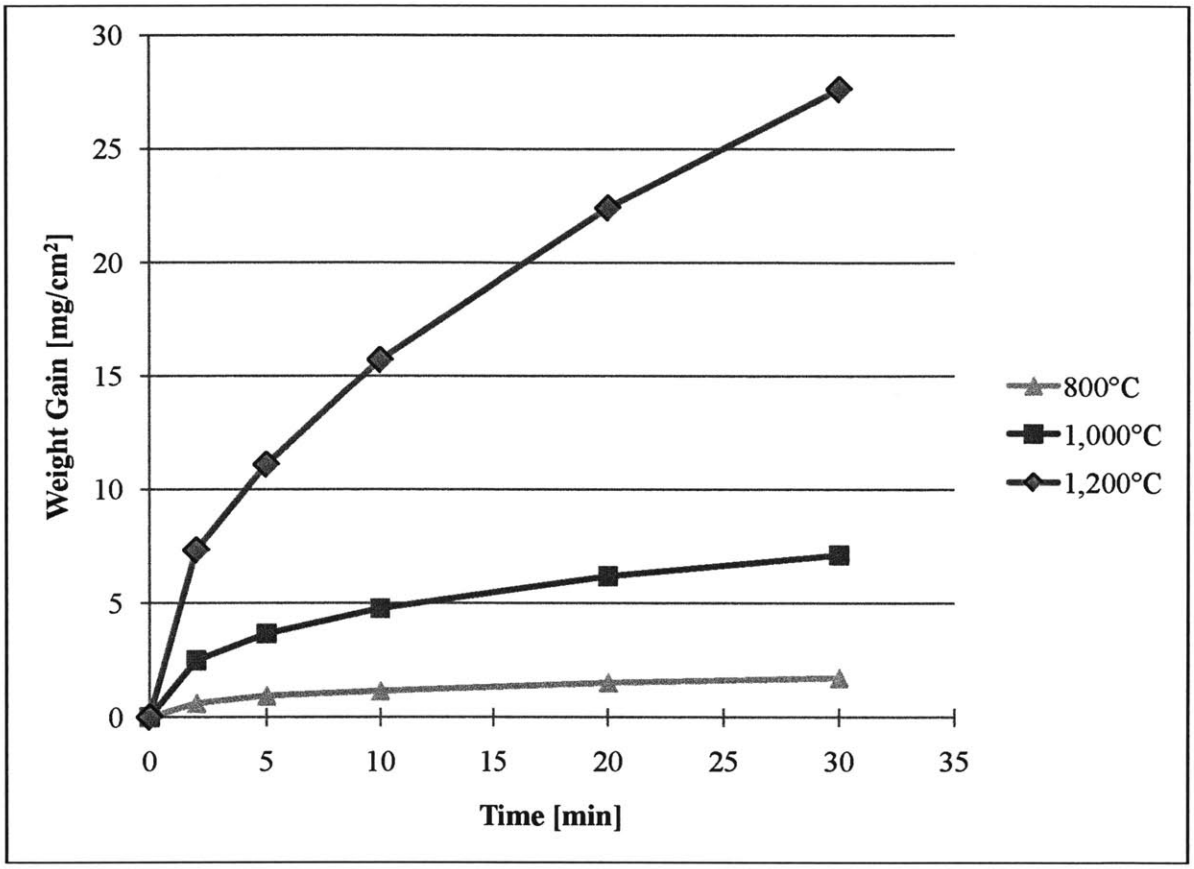

Figure 47 – Zircaloy-4 oxidation as a function of time

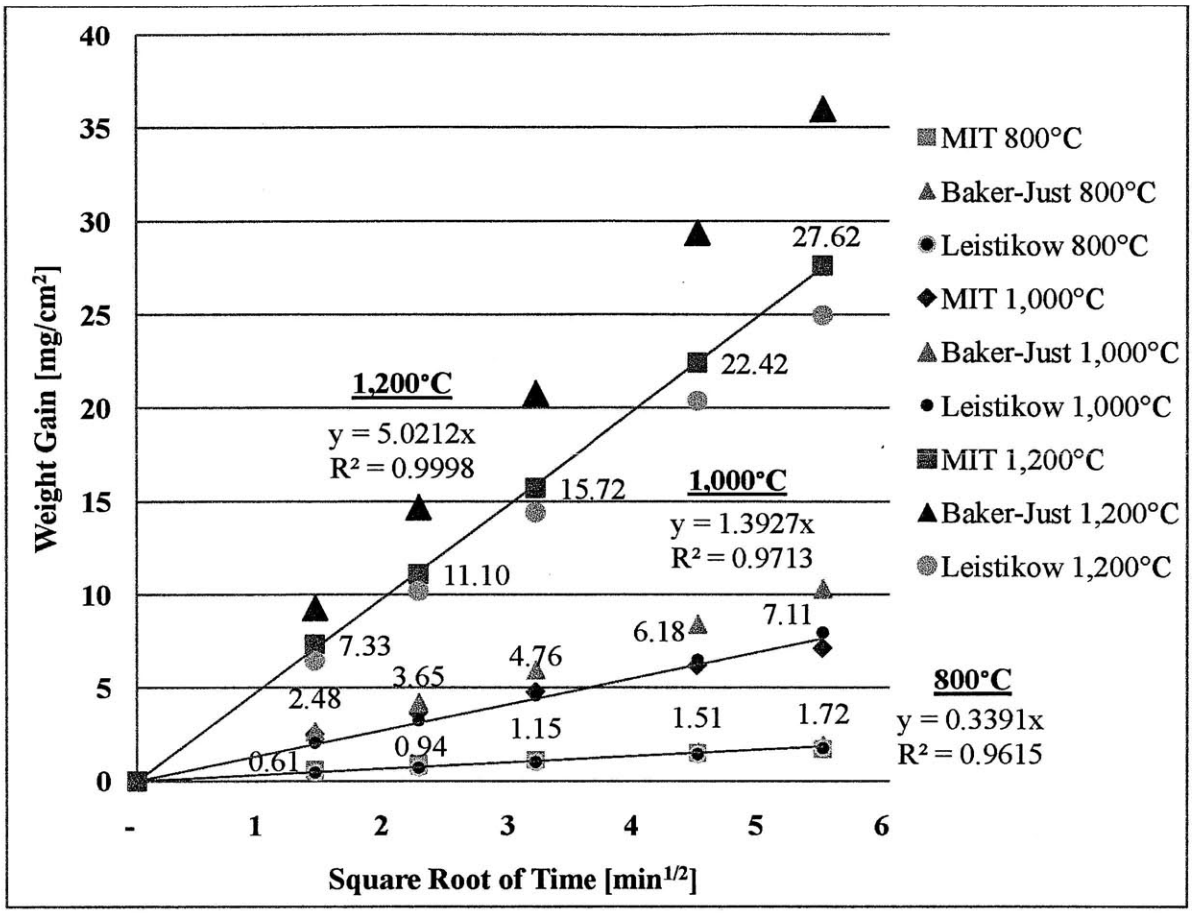

Figure 48 – Comparison of zircaloy oxidation results [Baker 1962; Leistikow 1987]

4.2.2 Zircaloy-4 Correlation

With the results of the previous section, it is possible to determine the activation energy, E_a, of the oxidation reaction and make a correlation very similar to those seen in other zircaloy oxidation studies. As seen in Figure 48, the weight gain has a linear dependence on $(\text{time})^{1/2}$. From the data, a parabolic rate model in the form of Equation 4.3 can be set up and evaluated for each temperature regime that was tested, where w is the weight gain, t is the experiment time, and k is the parabolic rate constant. Once this is completed, three temperature-rate constant combinations are known. Equation 4.4, known as the Arrhenius equation, gives the dependence of the parabolic rate constant of chemical reactions on the temperature, T, and the activation energy, E_a, where A is a pre-exponential factor and R is the gas constant (1.986 cal/K·mol). By manipulating this equation with the natural logarithm function as seen in Equation 4.5, a linear regression Arrhenius plot of $ln(k)$ versus T^{-1}, as seen in Figure 49, can be used to calculate the

activation energy of the chemical reaction from the slope of the trendline in the plot. From the results of this study, the activation energy of zircaloy was calculated to be 42.1 kcal/mol while the pre-exponential factor was determined to be $39.5 \cdot 10^6$ $mg^2/cm^4 \cdot s$ from the y-axis intercept. As seen in Table 7, the calculated activation energy of this study falls nicely within the group of activation energies of the other studies. These results continue to reinforce that the oxidation test facility should be considered a viable tool to test oxidation rates of SiC in high temperature flowing steam.

$$w^2 = k \cdot t \qquad \text{Equation 4.3}$$

$$k = A \cdot e^{-E_a/R \cdot T} \qquad \text{Equation 4.4}$$

$$\ln k = -\frac{E_a}{R \cdot T} + \ln A \qquad \text{Equation 4.5}$$

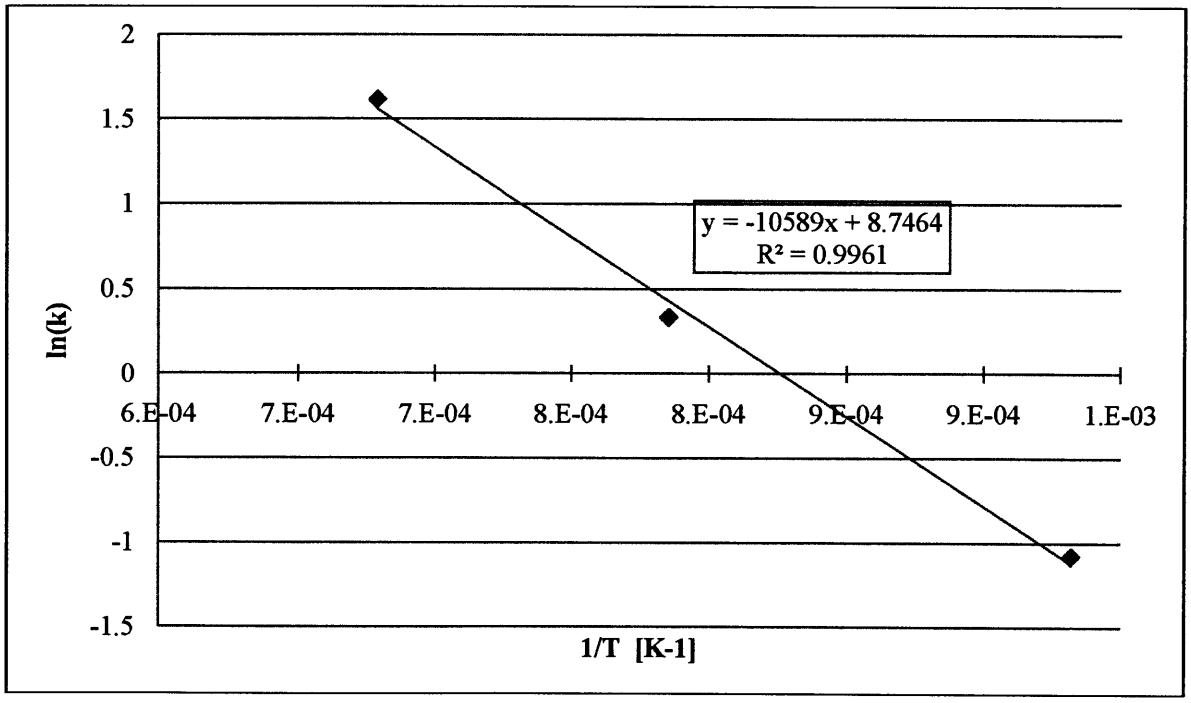

Figure 49 – Arrhenius equation plot

Table 7 – Arrhenius plot of zircaloy-4 rate constant [Baker 1962; Kawasaki 1978; Leistikow 1987]

	E_a [kcal/mol]
MIT Study	42.1
Baker-Just	45.5
Leistikow	41.7
Kawasaki	40.7
Cathcart	39.9

4.2.3 Equivalent Cladding Reacted

Another way to measure the amount of oxidation that has occurred in zircaloy cladding, which is also used in the NRC ECCS safety regulations, as discussed in section 1.1.3, is to calculate the equivalent cladding reacted (ECR). Recall that 10 CFR § 50.46 requires that no calculated total cladding oxidation shall exceed 0.17 times the total cladding thickness before oxidation. To calculate this piece of data, also referred to as ECR, it is assumed that all cladding metal is totally converted to stoichiometric ZrO_2 as can be seen in Equation 1.1 [Waeckel 2000]. For the purpose of this study, this means that the total weight gain represents the chemical reaction of zirconium to form ZrO_2. The total weight gain of a tested sample, in units of mg/cm^2, can be converted to equivalent oxide thickness, in units of μm, using the appropriate molar masses, the density of zircaloy, and the stoichiometry of the chemical reaction. Finally, to get the ECR, the calculated equivalent oxide thickness is divided by the initial thickness of the cladding. Figure 50 shows the oxidation results of this study in terms of equivalent oxide thickness. This plot has the same shape as the lines in Figure 48 since the only difference between the two are the units of the y-axis. Both show the linear relationship between $(time)^{1/2}$ and oxidation rate. Figure 51 shows the oxidation results of this study in terms of ECR and with units of minutes for the x-axis. It can be seen that after approximately 20 minutes of exposure to 1,200°C flowing steam, the zircaloy-4 samples will oxidize beyond the NRC ECCS limit. This information and the rest of the weight gain results will be used in chapter five to compare with those of SiC. Because other researchers have seen this same order of magnitude of time to reach the ECR limit in their experiments, the ECR results further strengthen the viability

of the oxidation test facility as a tool to test oxidation rates of SiC in high temperature flowing steam [.

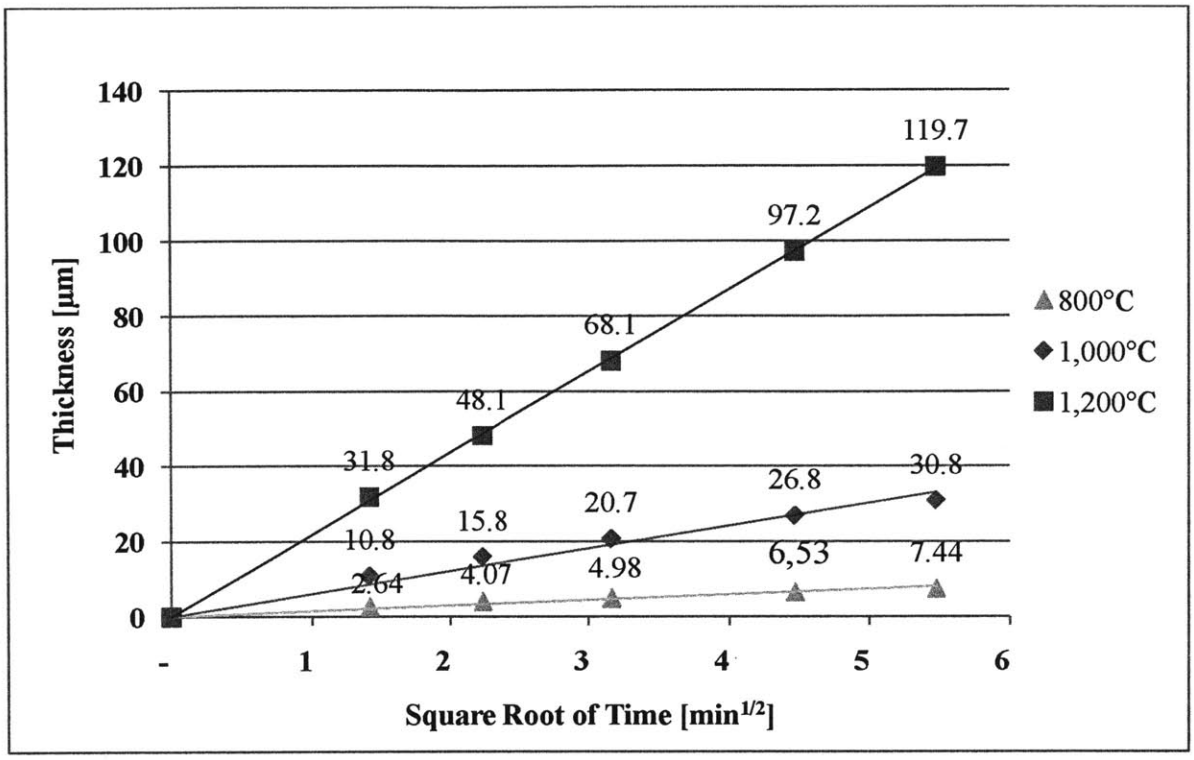

Figure 50 – Equivalent oxide thickness of zircaloy oxidation

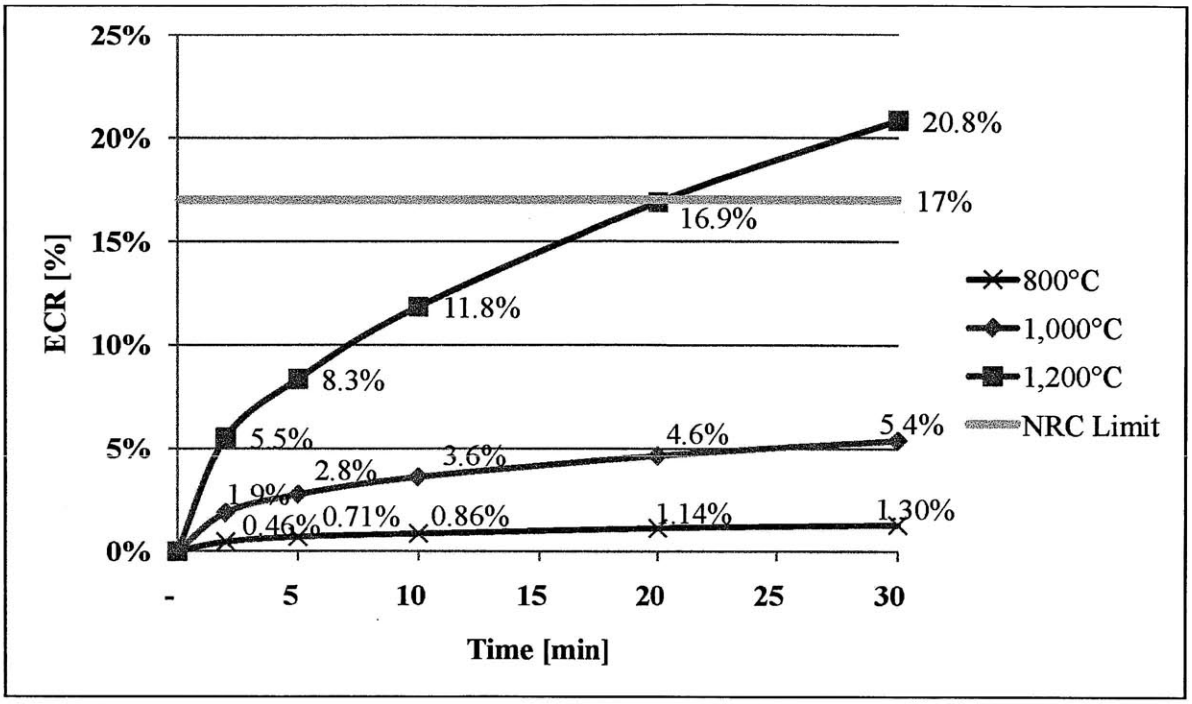

Figure 51 – Equivalent cladding reacted as a function of time

4.2.4 Variable Flow Rate Results

Variable steam flow rate tests were completed with zircaloy-4 samples to confirm that the measured oxidation rates are not dependent on steam velocity, as was expected and has been seen in past studies [Aomi 1999; Aomi 2000; Kawasaki 1978; Nagase 2000; Ozawa 2000; Uetsuka 1989]. High and low flow rate testing was completed at the most intense temperature and time combination of 1,200°C for 30 minutes. Six additional tests – two tests each at three different combinations of steam generator setups and power settings – were completed as summarized in Table 8. Conditions during the Zry034 test were not at a steady state throughout the duration of the experiment as seen by the wide temperature range; therefore, this test was not considered in the analysis or shown on the accompanying plot. When combined with the first two tests completed in the zircaloy oxidation analysis, it can be seen in Figure 52 that there is no obvious trend between the flow rate and the resulting ECR. It does appear that a flow rate below a approximately 3.0 g/min leads to slower zircaloy oxidation likely due to a lower concentration of the oxidant; however, because the 30 zircaloy tests discussed in section 4.2.1 were completed at a high enough steam flow rate, it is assumed that steam flow rate did not have an effect on the zircaloy oxidation.

It can also be seen that there is a large difference in the calculated steam flow rates between the two different test setups that were completed at a power setting of 42 - one without the 3-way valve and one with the 3-way valve but without insulation. This is due to the significant amount of condensation that occurs with the uninsulated 3-way valve. Because of this recognition, insulation tape and insulation wool were wrapped around the valve for all future testing.

Table 8 – Zircaloy variable flow rate tests

Sample	Temp. [°C]	Steam Generator Setup & Setting	Steam Flow Rate [g/min]	Weight Gain [mg/cm^2]	Equivalent Oxide Thickness [μm]	ECR [%]
Zry036	1200	3000 mL with 3-way valve, 42%	0.64	20.96	90.84	15.7%
Zry037	1200	3000 mL with 3-way valve, 42%	0.64	18.06	78.27	13.6%
Zry034	*1185 - 1236*	*3000 mL, 42%*	*2.24*	*31.76*	*137.69*	*23.9%*
Zry035	1200	3000 mL, 42%	2.24	19.65	85.16	14.7%
Zry015	1200	3000 mL, 71%	3.11	27.69	120.04	20.9%
Zry016	1200	3000 mL, 71%	3.11	27.54	119.40	20.8%
Zry032	1200	3000 mL, 88%	8.32	24.94	108.11	18.7%
Zry033	1200	3000 mL, 88%	8.32	26.16	113.41	19.7%

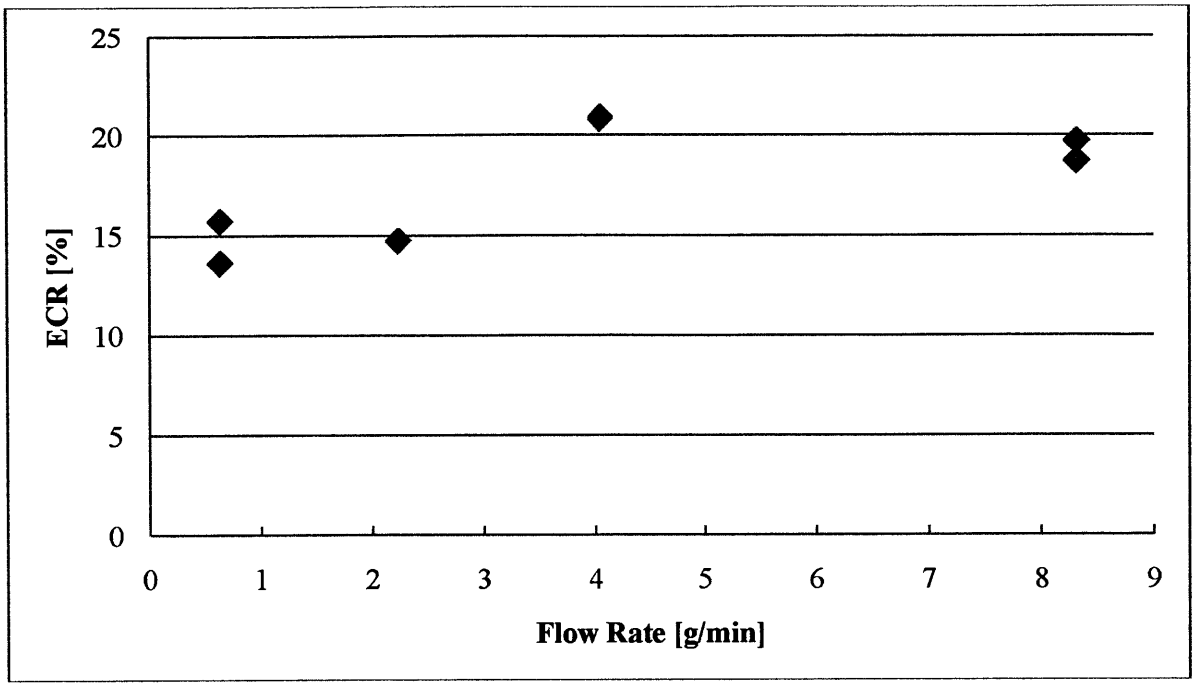

Figure 52 – Equivalent cladding reacted as a function of flow rate

5. Silicon Carbide Experimentation

5.1 Test Samples

A primary testing material of Hexoloy tubes, made of α-phase SiC and manufactured by *Saint-Gobain Ceramics* located in Niagara Falls, New York, was chosen due to its availability, relevancy, and suitability for benchmarking with similar *CTP* data. These primary test samples were to be tested at a minimum of three furnace temperatures – 1,200°C, 1,400°C, 1,600°C. Also, for each test temperature, samples will be run at several different time durations. Finally, variable flow rate tests will be completed at no less than one of the temperatures to determine the effect that steam velocity has on the oxidation rate of SiC. Due to the limited amount of time available for this study and equipment availability, testing at 1,200°C and 1,140°C was completed. A 0.91 m Hexoloy α-phase SiC tube with an outer diameter and thickness of 1.28 cm and 0.11 cm, respectively, was provided by *CTP* for the purpose of this study as seen in Figure 53. Because SiC is a brittle ceramic, the machining of the samples was completed by *Ferro-Ceramic Grinding Inc.* Samples were machined to a height of 1.27 cm with 0.19 cm holes drilled 0.32 cm from the top of the sample so the bottom horizontal support rod of the sample holder can fit through both holes and suspend the sample in the reaction tube. With the α-phase SiC tube, *Ferro-Ceramic Grinding Inc.* was able to successfully machine 49 samples. During the machining process, they estimated that approximately 10 samples were broken.

Figure 53 – Primary SiC testing stock material

Secondary testing materials – four α-phase SiC rectangular blocks and a 4.8 cm long β-phase SiC tube as seen in Figure 54 – were also provided by *CTP* with the expectation that comparisons between the MIT experimental setup and that of *CTP* and between α- and β-phase SiC could be made. Although the α-phase SiC blocks are not all the same dimensions, they are approximately 2.24 cm by 1.15 cm by 0.94 cm and are adequate for four tests. The β-phase SiC tube has an outer diameter and thickness of 1.05 cm and 0.076 cm and can be carefully machined to make three samples. Although neither of these testing materials has been machined to be able to

suspend them using the sample holder, a quote to complete the necessary machining was received from *Ferro-Ceramic Grinding Inc.* for $753.00. This quote is based on the drawings that are in the Appendix. Prior to machining, it should be thoroughly considered as to how the samples will be suspended and at what testing conditions they will be subjected.

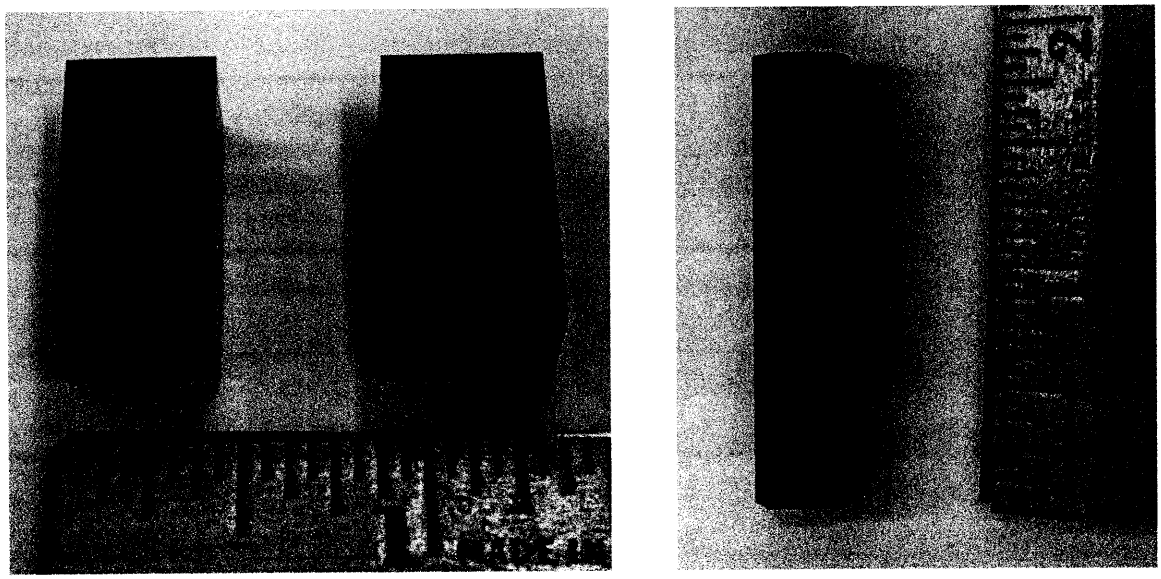

Figure 54 – Secondary SiC test stock material

5.2 Sample Preparation

Because SiC is a ceramic and because particular cleaning techniques were seen to be effective in past studies, a more rigorous sample preparation was chosen compared to the zircaloy-4 samples [Opila 1999]. SiC samples were ultrasonically cleaned for three minutes in each of the following solutions: deionized water with detergent, deionized water only, acetone, ethanol, and then deionized water again. Careful precautions were also taken to not cross-contaminate cleaning beakers. Also, four different combinations of weighing, cleaning, and baking at 150°C were completed to determine which combinations should be used for sample preparation so as not to affect the weight measurements. Table 9 summarizes the different combinations that were tried. It should be noted that after baking, samples were removed and immediately placed in a desiccator so as to prevent any postulated moisture from being reabsorbed into the SiC samples; however, it was seen that baking the samples had no effect on the weight and was therefore not

necessary. After reviewing all of the weight change results, it was determined that the best approach was to clean the samples and then weigh them in the same fashion that zircaloy-4 samples are weighed. It was seen that cleaning the samples removed a noticeable amount of impurities from the samples – a darker cloud of contaminants could be seen in the different cleaning beakers and there was a noticeable weight loss of some samples after being cleaned. Once properly prepared for experimentation, the SiC samples were ready to be subjected to the superheated flowing steam LOCA environments to test for different oxidation rates.

Table 9 – Sample preparation combinations

Samples	Description of Sample Preparation
SiC001/002	weigh, no clean, bake at 150°C for approximately two hours, weigh
SiC003/004	weigh, no clean, bake at 150°C for approximately four hours, weigh
SiC005/006	weigh, clean, weigh, bake at 150°C for approximately two hours, weigh
SiC007/008	weigh, clean, weigh, bake at 150°C for approximately four hours, weigh

5.3 Silicon Carbide Test Results

Six α-phase SiC oxidation tests have been completed using the modified setup of the oxidation test facility – two tests at 1,200°C for eight hours, two tests at 1,140°C for 24 hours, and two tests at 1,140°C for 48 hours. The standard operating power setting of 71 was used for both tests and the averaged steam flow rates were approximately 3 g/min or 1 m/s. The results of the tests are summarized in Table 10. It can be seen that very little oxidation occurred with the samples over the duration of the tests. Compared to the average weight change from the two zircaloy-4 1,200°C/30 minute tests, a 15.6 percent weight gain, SiC had a very insignificant weight change of more than two orders of magnitude less, a 0.077 percent weight loss. With a visual inspection, the tested samples look slightly darker than the untested samples, likely due to the formation of a silica layer which can be confirmed with an SEM analysis. It was initially planned to also complete several tests at shorter durations such as two and four hours, however, because the weight loss of the first two tests was so small, it was decided against this as no significant results would be gained from these tests. Instead, two 24 tests and two 48 hour tests were completed at 1,140°C. This lower temperature was chosen in order to protect the integrity

of the preheater furnace for these longer duration experiments. Future testing plans are discussed in the following section.

Table 10 – Results of initial SiC tests

Date	Sample	Temp. [°C]	Test Duration [hr]	Velocity [m/s]	Initial Weight [g]	Weight Loss [g]	Weight Loss [%]	Weight Loss [mg/cm^2]
5/10/11	SiC005	1,200	8	1.14	1.2623	0.0004	0.034	0.043
5/12/11	SiC006	1,200	8	1.19	1.2565	0.0015	0.119	0.148
7/21/11 – 7/22/11	SiC007	1,140	24	0.98	1.2576	.0039	0.310	0.388
8/1/11 – 8/2/11	SiC008	1,140	24	0.89	1.2602	.0032	0.254	0.319
8/2/11 – 8/4/11	SiC001	1,140	48	1.01	1.2558	.0054	0.434	0.547
8/4/11 – 8/6/11	SiC002	1,140	48	0.95	1.2662	.0056	0.442	0.559

Figure 55 shows the results of the six longer duration SiC tests. A linear trend, as seen in Equation 5.1 where w is the weight loss in units of mg/cm^2 and t is the time in units of hours, can be seen from the 1,140°C tests which is consistent with existing models and the results of past studies. Recall that the linear rate constant is predicted to be dominant over the parabolic rate constant at the high steam flow rates in this study due to the SiO_2 volatilization reaction, as discussed in section 2.3. Although the linear trendline was calculated from two different experiment duration times, it can be more strongly proven once two eight hour tests are completed at 1,140°C.

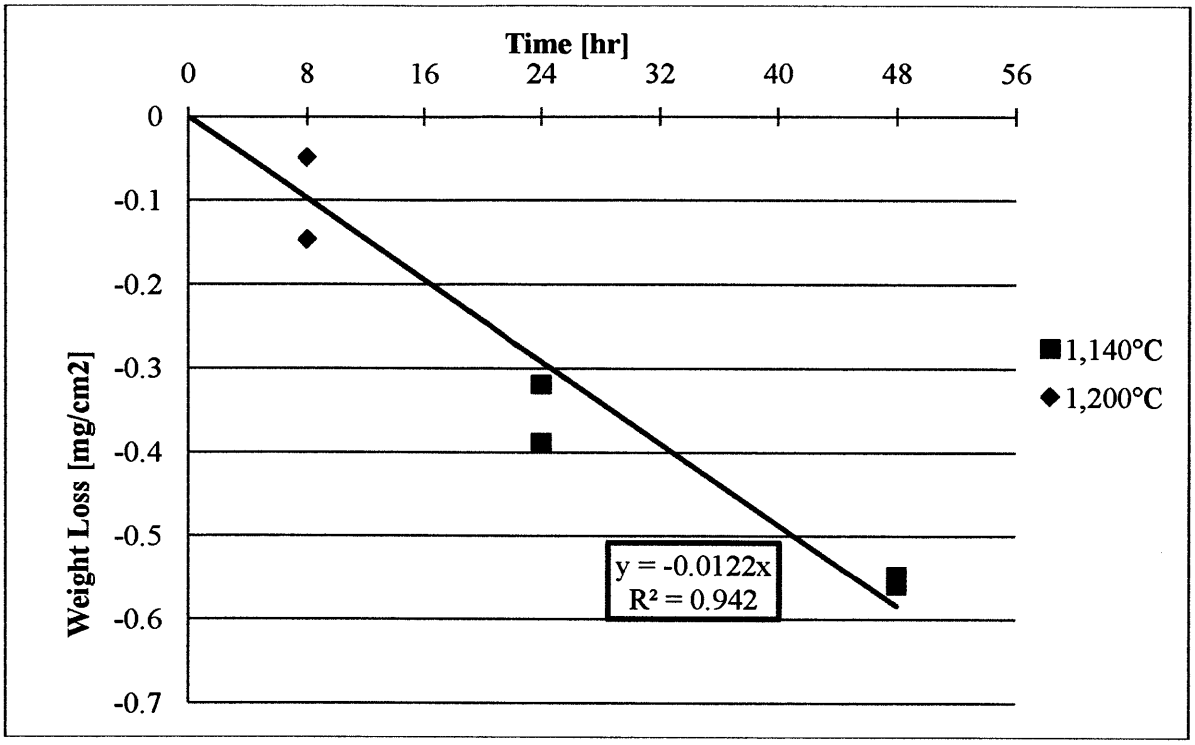

Figure 55 – SiC oxidation as a function of time

$$w = -0.0122 \cdot t$$ Equation 5.1

When compared to the tests completed by *CTP*, as seen in Figure 56, this study's results match up well and follow the same trend [Feinroth 2011]. Weight loss of the nine α-phase SiC tests appears to be minimal for the 1,200°C tests. Although *CTP* only completed these tests up to six hours, a fairly linear trendline can be extrapolated to run horizontally across the plot which would intercept with this study's two data points. For *CTP*'s 1,400°C tests, it can be seen that oxidation rates begin to increase which is expected although this is still not on the same order of magnitude of weight change of the zircaloy-4 testing at 1,200°C. One β-phase SiC test was completed by *CTP* and the results do not show there to be a significant measurable difference between the 1,400°C/8 hr α-phase SiC tests.

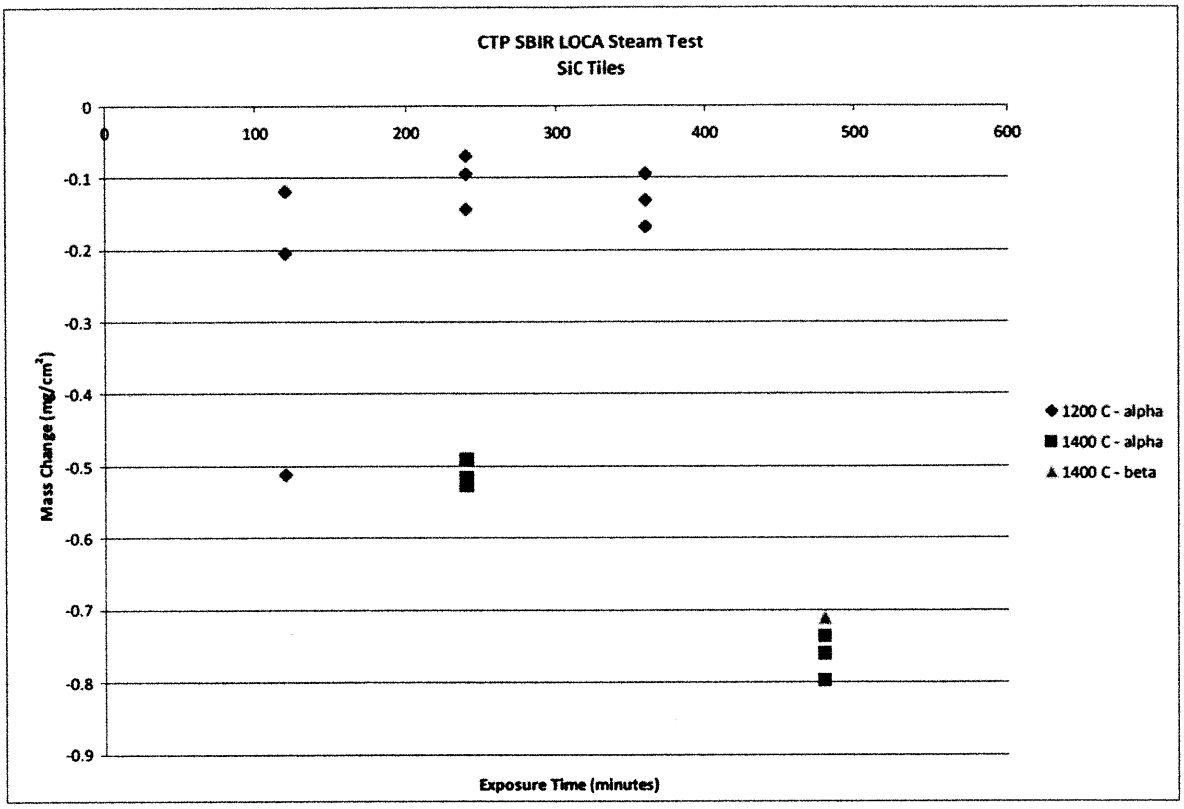

Figure 56 – Results of initial *CTP* SiC LOCA tests [Feinroth 2011]

5.4 Ongoing and Future Tests

Two main issues have prevented more SiC tests from being completed to date. Most significantly, the sample furnace was inoperable as it was sent to the manufacturer for repairs when experimenting begun on this study. Further, the facility has needed system modifications in order to allow for longer duration testing. The sample furnace has been repaired, safely delivered back to MIT, and will soon be reintegrated into the facility making higher temperature testing an option. Also, with the recent system integration of the temperature deviation electrical protection circuit and the 3-way valve, longer duration testing and higher flow rate testing can also be completed. Upcoming variable flow rate tests at 1,140°C have been planned to further investigate the effect that steam velocity has on SiC oxidation and SiO_2 volatilization.

Once the 1,700°C sample furnace is integrated back into the facility, high temperature SiC tests can commence. Initially, eight hour tests will be completed at 1,400°C and then at 1,600°C. Then, depending on the weight loss results, longer and/or shorter duration tests will be

completed. The effect that steam flow rate has on the SiC oxidation rate will also be looked at with one or more temperatures. Finally, the secondary samples will also be tested. Throughout the testing program, an SEM materials analysis will be completed to shed further light on the different reaction mechanisms that occur during the LOCA testing.

This Page Left Intentionally Blank

6. Summary, Conclusions, and Recommendations for Future Work

Thirty six short duration zircaloy tests and six long duration SiC tests have been successfully completed at the MIT oxidation test facility. Although this study is part of a continuing program of SiC testing at higher temperatures, significant conclusions can be drawn from the testing completed to data.

- The oxidation test facility has been successfully designed and fabricated to eventually have the ability to run high-flowing steam tests at atmospheric pressure, at temperatures up to 1,600°C.
- Extensive zircaloy-4 oxidation testing at a range of temperatures from 800°C to 1,200°C was performed. Comparison of the test results to existing models and data from past studies validates the oxidation test facility as a viable tool to examine oxidation rates of SiC in high temperature flowing steam.
- The zircaloy-4 activation energy, 42.1 kcal/mol, which was calculated from the experimental results, is within the same order of magnitude as other studies that were reviewed.
- Testing at 1,200°C clearly shows that, from an oxidation perspective, α-SiC significantly outperforms zircaloy-4 in high-flowing superheated steam. The average weight change from the two zircaloy-4 1,200°C/30 minute tests is 15.6 percent weight gain, while the weight change for the two α-SiC 1,200°C/8 hour tests is two orders of magnitude less at 0.077 percent weight loss.
- Two 24 hour and two 48 hour 1,140°C α-SiC tests were completed, and they match the expected paralinear oxidation trend well. These tests continue to show that the SiC oxidation rate in high temperature steam is significantly lower for much longer durations than zircaloy.
- When compared to the recent tests completed by *CTP*, the α-SiC results of this study correlate well and follow the same oxidation trend which confirms that there is reproducibility between the different setups.

6.1 Oxidation Test Facility Design

The purpose of the MIT oxidation test facility is to test the oxidation rates of various materials such as zircaloy and SiC in a high temperature flowing steam environment. The facility has the ability to run high-flowing steam tests at atmospheric pressure at temperatures up to 1,600°C. Two key constraints were met in the design of the facility. First, the facility is able to generate a steady flow of high-purity, dry steam at a rate that does not starve the steam-sample reaction. Second, the samples can be safely subjected to temperatures of up to 1,600°C, although at this point, testing has only been completed at temperatures up to 1,200°C. While the majority of testing completed thus far has been done in 1,200°C steam with a steam velocity close to 1.0 m/s, the facility has the capability to produce 1,200°C steam with velocities from approximately 0.8 m/s to 6.0 m/s in its current configuration.

6.2 Oxidation Test Facility Validation

Completion of the zircaloy-4 oxidation testing and a comparison of the test results to existing models and data from past studies validates the oxidation test facility as a viable tool to test oxidation rates of SiC in high temperature flowing steam. In general, oxidation rates increased linearly with respect to $(\text{time})^{1/2}$ and at a rate that is proportional to the testing temperature. For the most intense temperature/duration test of 1,200°C for 30 minute tests, the two tested samples had an average weight gain of 15.6 percent. Also, it was seen that the NRC ECCS ECR safety limit of 17 percent was reached after approximately 20 minutes of testing at 1,200°C. Variable flow rate tests confirmed that the steam flow rate was within a regime that did not have an effect on the zircaloy oxidation rates, a result which was to be expected. By completing an SEM analysis of zircaloy-4 samples, the effect of LOCA testing on the samples by this study can be further understood and characterized to confirm that the expected reaction mechanisms and mode of attack are taking place.

6.3 Silicon Carbide High Temperature Oxidation

Six α-phase SiC oxidation tests have been completed using the modified setup of the oxidation test facility – two tests at 1,200°C for eight hours, two tests at 1,140°C for 24 hours, and two tests at 1,140°C for 48 hours, all with an approximate steam velocity of one m/s. Average weight losses of 0.077 percent, 0.282 percent, and 0.438 percent were observed for each of the

three different tests respectively, which has several implications for further research. First, the results of this study match well with the general trend of *CTP*'s LOCA study which shows that there is reproducibility between testing setups. The six tests completed at MIT thus far, show how much of an advantage SiC has over zircaloy in a LOCA environment of superheated, flowing steam. Also, the experimentally determined weight loss rate is consistent with existing models and the results of past studies. Current NRC limits allow for temperatures less than 1,200°C. However, if SiC cladding was to be implemented in future reactor fuel rod designs, from an oxidation viewpoint, normal operating and safety limit temperatures could safely be increased allowing reactors to increase power output. Although SiC cladding research and development is in its early stages and it will be years before it could safely be integrated into a nuclear reactor design, it is exciting to think of the potential performance improvements it can offer the nuclear community.

Further testing that will be completed by the MIT LOCA team using the oxidation test facility includes completing the initial test matrix of multiple time duration experiments at 1,200°C, 1,400°C, and 1,600°C, and investigating variable flow rate effects on SiC oxidation. It would also be useful to test β-phase SiC samples to determine which phase is best suited for use in nuclear reactors and determine the oxidation rate differences between different production processes, i.e., sintered or CVD. It is the intention of the MIT team to continue to look at the effect that steam flow rate has on the paralinear oxidation of SiC from 1,200°C to 1,600°C as this has not been thoroughly investigated by the scientific community under the conditions of this study.

6.4 Recommendations for Future SiC LOCA Experimentation

There have been discussions focused on whether there are competing mechanisms of corrosion versus erosion in the tests of this study. It would be useful to develop an analytical model that incorporates all of the kinetics and reaction mechanisms of SiC oxidation including the volatilization of the silica layer. This model would need to take into account several different environmental parameters including temperature, pressure, steam flow rate, and the chemical composition of the environment. An SEM analysis of SiC samples could be useful in understanding the principal reaction mechanisms that would be incorporated into the SiC LOCA model.

Although all of the future work of SiC LOCA experimentation at MIT could be completed with the oxidation test facility in its current state, there are several enhancements that could be designed into the facility to allow for a broader range of testing parameters and more precise measurement and data acquisition strategies. A weakness of the facility is that the steam flow rate cannot be precisely controlled, thus it is currently impossible for the instantaneous steam flow rate to be determined. It is only possible to calculate an averaged steam flow rate for the entire period of testing. This compromises the accuracy of experimental results and limits the accuracy of data collected from variable flow rate tests and the data analysis that follows. Two ways to improve the control over steam flow rate would be to integrate a steam flow control device into the system and revamp the steam generation process by using a pressurized vessel such as a water boiler. This would allow for longer duration tests that do not require a steam generator switch-out and would also give researchers the ability to precisely control the steam flow rate. Further, other gases could easily be added to the steam flow to look at the effects that different flow compositions have on SiC at high temperatures. If a pressurized steam generator vessel were to be used, modifications to pressurize the entire system could be undertaken.

Considerable thought and planning would have to go into these suggested design enhancements including materials integrity and suspension of the samples in the reaction tube. If implemented, it would allow for the more accurate measurement of the effect that pressure has on SiC oxidation, a critical component to postulated LOCA events and design safety in nuclear reactors. It would also be useful to install an electrical control system that provides feedback and response logic integrated into the software allowing for automated temperature monitoring and changing. This would significantly increase the accuracy of the test facility and the efficiency of testing and would benefit the researchers. Finally, if additional funding were to be available for SiC LOCA research, it is strongly recommended that the suppliers and support services of expensive and long-lead time equipment, i.e., the sample furnace, be thoroughly screened to mitigate future disruptions in the use of the test facility. This would allow the MIT team to have an operable and reliable oxidation test facility that would be available for continuing research.

References

10 CFR § 50.46. "Acceptance Criteria for Emergency Core Cooling Systems for Light-water Nuclear Power Reactors," U.S. Code of Federal Regulations (2007).

Aomi, M., M. Nakatsuka, S. Komura, T. Hirose, and T. Anegawa. "Behavior of BWR Fuel Cladding Tubes under Simulated LOCA Conditions." Proc. of 7th International Conference on Nuclear Engineering, Tokyo, Japan. 1999.

Aomi, M., M. Nakatsuka, S. Komura, T. Hirose, and T. Anegawa. "Behavior of Irradiated BWR Fuel Cladding Tubes Under Simulated LOCA Conditions." (2000).

ATI Wah Chang. *Reactor Grade Zirconium Alloys for Nuclear Waste Disposal.* Albany, OR: ATI Wah Chang, 2003.

Baker, L., and L. Just. *Studies of Metal-Water Reactions at High Temperatures.* Rep. No. ANL-6548. Argonne, Illinois: Argonne National Laboratory, 1962.

Ballinger, R., W. Dobson, and R. Biederman. "Oxidation Reaction Kinetics of Zircaloy-4 in an Unlimited Steam Environment." *Journal of Nuclear Materials* 62 (1976): 213-220.

Bauccio, Michael, Ed. *ASM Engineered Materials Reference Book.* Materials Park, OH: ASM International, 1994.

Carpenter, D., G. Kohse, and M. Kazimi. *Modeling of Silicon Carbide Duplex Cladding Designs for High Burnup Light Water Reactor Fuel.* Rep. 2008.

Carpenter, D. M. *An Assessment of Silicon Carbide as a Cladding Material for Light Water Reactors.* Ph.D. Thesis. Massachusetts Institute of Technology, 2010.

Chuto, T., F. Nagase, and T. Fuketa. "High Temperature Oxidation of Nb-containing Zr Alloy Cladding in LOCA Conditions." *Nuclear Engineering and Technology* 41.2 (2009): 163-70.

Cole-Parmer. *Bunsen Burners.* 2011/12 General Catalog.

Collier, J. G., and G. F. Hewitt. *Introduction to Nuclear Power.* Washington: Hemisphere Pub., 1987.

Deal, B. E., and A. S. Grove. "General Relationship for the Thermal Oxidation of Silicon." *Journal of Applied Physics* 36.12 (1965): 3770-778.

Dobisesky, J. P. *Reactor Physics Considerations for Implementing Silicon Carbide Cladding into a PWR Environment.* S.M. Thesis. Massachusetts Institute of Technology, 2011.

Duderstadt, J. J., and L. J. Hamilton. *Nuclear Reactor Analysis.* New York: Wiley, 1976.

Eck, J., M. Balatpichelin, L. Charpentier, E. Beche, and F. Audubert. "Behavior of SiC at High Temperature under Helium with Low Oxygen Partial Pressure." *Journal of the European Ceramic Society* 28.15 (2008): 2995-3004.

EPRI. *Program on Technology Innovation: Advanced Fuel Cycles-Impact on High-Level Waste Disposal.* Rep. No. 1016643. Electric Power Research Institute, 2008.

Feinroth, H., G. Markham, and M. Ales. Status and Future Plans for CTP Work on SiC Cladding and Joining. 21 Apr. 2011. Raw data. Ceramic Tubular Products, Meeting at ORNL.

Feng, D., P. Morra, R. Sundaram, W. Lee, P. Saha, P. Hejzlar, and M. Kazimi. "Safety Analysis of High-power-density Annular Fuel for PWRs." *Nuclear Technology* 160 (2007): 45-62.

Glasstone, S., and A. Sesonske. *Nuclear Reactor Engineering: Reactor Design Basics.* Vol. 1. Van Nost. Reinhold, 1994.

Greene, G., and C. Finfrock. "Vaporization of Tungsten-metal in Steam at High Temperature." *Experimental Thermal and Fluid Science* 25 (2001): 87-99.

Hofmann, P., S. Hagen, G. Schanz, and A. Skokan. "Reactor Core Materials Interactions at Very High Temperatures." *Nuclear Technology* 87 (1989): 146-86.

Horn, F., J. Fillo, and J. Powell. "Performance of Ceramic Materials in High Temperature Steam and Hydrogen." *Journal of Nuclear Materials* 85-86 (1979): 439-43.

Jacobson, N., E. Opila, D. Fox, and J. Smialek. "Oxidation and Corrosion of Silicon-Based Ceramics and Composites." *Materials Science Forum* 251-254 (1997): 817-32.

Jorgensen, P. J., M. E. Wadsworth, and I. B. Cutler. "Effects of Water Vapor on Oxidation of Silicon Carbide." *Journal of the American Ceramic Society* 44.6 (1961): 258-61.

Kawasaki, S., T. Furuta, and M. Suzuki. "Oxidation of Zircaloy-4 under High Temperature Steam Atmosphere and Its Effect on Ductility of Cladding." *Journal of Nuclear Science and Technology* 15.8 (1978): 589-96.

Kazimi, M. S., K. Shirvan, and R. P. Arnold. *TEPCO Annual Report on High Power Density BWR Design.* MIT. Center for Advanced Nuclear Energy Systems, 2011.

Leistikow, S., and G. Schanz. "Oxidation Kinetics and Related Phenomena of Zircaloy-4 Fuel Cladding Exposed to High Temperature Steam and Hydrogen-steam Mixtures under PWR Accident Conditions." *Nuclear Engineering and Design* 103.1 (1987): 65-84.

Mills, A. F. *Heat Transfer.* 2nd Ed. Upper Saddle River, NJ: Prentice Hall, 1999.

Munro, R. G. "Evaluated Material Properties for a Sintered α-Alumina." *Journal of the American Ceramic Society* 80.8 (1997): 1919-928.

Nagase, F., T. Otomo, M. Tanimoto, and H. Uetsuka. "Experiments on High Burnup Fuel Behavior under LOCA Conditions at JAERI." (2000).

Nero, A. V. *A Guidebook to Nuclear Reactors.* Berkeley: University of California, 1979.

NRC. *Extended Burnup Evaluation.* Topical Report BAW-10186NP-A. U.S. Nuclear Regulatory Commission, 2003.

Olander, D. R. "Light Water Reactor Fuel Design and Performance." *Encyclopedia of Materials: Science and Technology* (2001): 4490.

Opila, E. "Influence of Alumina Reaction Tube Impurities on the Oxidation of Chemically Vapor-deposited Silicon Carbide." *Journal of the American Ceramic Society* 78.4 (1995): 1107-110.

Opila, E. J., and R. E. Hann. "Paralinear Oxidation of CVD SiC in Water Vapor." *Journal of the American Ceramic Society* 80.1 (1997): 197-205.

Opila, E. "Oxidation and Volatilization of Silica Formers in Water Vapor." *Journal of the American Ceramic Society* 86.8 (2003): 1238-248.

Opila, E. *Paralinear Oxidation of SiC in Combustion Environments.* Rep. Cleveland, OH: Cleveland State University, 2006.

Opila, E. "Variation of the Oxidation Rate of Silicon Carbide with Water-Vapor Pressure." *Journal of the American Ceramic Society* 82.3 (1999): 625-36.

Opila, Elizabeth J. "Oxidation Kinetics of Chemically Vapor-Deposited Silicon Carbide in Wet Oxygen." *Journal of the American Ceramic Society* 77.3 (1994): 730-36.

Ozawa, M., T. Takahashi, T. Homma, and K. Goto. "Behavior of Irradiated Zircaloy-4 Fuel Cladding Under Simulated LOCA Conditions." *Zirconium in the Nuclear Industry: Twelfth International Symposium*. Ed. G. P. Sabol. West Conshohocken, PA: ASTM, 2000. 279-99.

Perry, R. H., and D. W. Green. *Perry's Chemical Engineers' Handbook*. 8th Ed. New York: McGraw-Hill, 2008.

Pickman, D. O. "Properties of Zircaloy Cladding." *Nuclear Engineering and Design* 21 (1972): 212-36.

Quartz Products. *Material Safety Data Sheet: Momentive Performance Materials Clear Fused Quartz*. MSDS No: 53279. Cleveland, OH, 2006.

Robinson, R., and J. Smialek. "SiC Recession Caused by SiO2 Scale Volatility under Combustion Conditions: I, Experimental Results and Empirical Model." *Journal of the American Ceramic Society* 82.7 (1999): 1817-825.

Saint-Gobain. *Hexoloy SA Silicon Carbide: Technical Data*. Rep. Niagara Falls, New York: Saint-Gobain, 2003.

Simnad, M. T. "A Brief History of Power Reactor Fuels." *Journal of Nuclear Materials* 100 (1981): 93-107.

Snead, L., T. Nozawa, Y. Katoh, T. Byun, S. Kondo, and D. Petti. "Handbook of SiC Properties for Fuel Performance Modeling." *Journal of Nuclear Materials* 371 (2007): 329-77.

Stempien, J. D. *Behavior of Triplex Silicon Carbide Fuel Cladding Designs Tested Under Simulated PWR Conditions*. S.M. Thesis. Massachusetts Institute of Technology, 2011.

Todreas, N. E., and M. S. Kazimi. *Nuclear Systems I: Thermal Hydraulic Fundamentals*. 2nd Ed. New York, NY: Taylor & Francis, 2011.

Tortorelli, P. F., and K. L. More. "Effects of High Water-Vapor Pressure on Oxidation of Silicon Carbide at 1200°C." *Journal of the American Ceramic Society* 86.8 (2003): 1249-255.

Uetsuka, H., and T. Otomo. "High Temperature Oxidation of Zircaloy-4 in Diluted Steam." *Journal of Nuclear Science and Technology* 26.2 (1989): 240-48.

Urbanic, V., and T. Heidrick. "High-temperature Oxidation of Zircaloy-2 and Zircaloy-4 in Steam." *Journal of Nuclear Materials* 75.2 (1978): 251-61.

Vasic, A. *High Temperature Properties and Heat Transfer Phenomena for Steam at Temperatures up to 5000K*. M.S. Thesis. University of Ottawa, 1993.

Vasic, A., S. Cheng, and D. Groeneveld. "A Comparison of Predictions of High-temperature Steam Properties." *Nuclear Engineering and Design* 132.3 (1992): 367-79.

Waeckel, N., P. Jacques, and R. Yang. "Effects of In-Reactor Corrosion on the 17% LOCA Criterion." Proc. of International Topical Meeting on Light Water Reactor Fuel Performance, Park City, UT. American Nuclear Society, 2000.

Welty, J. R., C. Wicks, R. Wilson, and G. Rorrer. *Fundamentals of Momentum, Heat, and Mass Transfer*. 4th Ed. New York: Wiley, 2001.

Yang, R., B. Cheng, J. Deshon, K. Edsinger, and O. Ozer. "Fuel R & D to Improve Fuel Reliability." *Nuclear Science and Technology* 43.9 (2006): 951-59.

Yueh, H. K. "Improved ZIRLO Cladding Performance through Chemistry and Process Modifications." *Journal of ASTM International* 2 (2005): 330.

Appendix

This appendix shows the request that was sent to *Ferro-Ceramic Grinding Inc.* to machine the SiC samples as discussed in section 5.1.

Request for machining to *Ferro-Ceramics Grinding, Inc.* (pg 1 of 3)

We will send you a 35.75" tube of alpha SiC with the inner and outer diameter dimensions shown below (thickness ~0.040"). We would like you to provide a quote with the price per piece to cut to height and machine the holes as shown below.

Top View

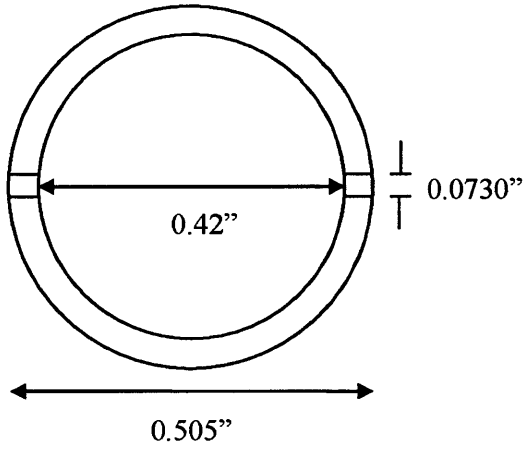

1/16" diameter rod should be able to fit through the tube holes

The diameter of the circular hole is 0.0730".

Side View

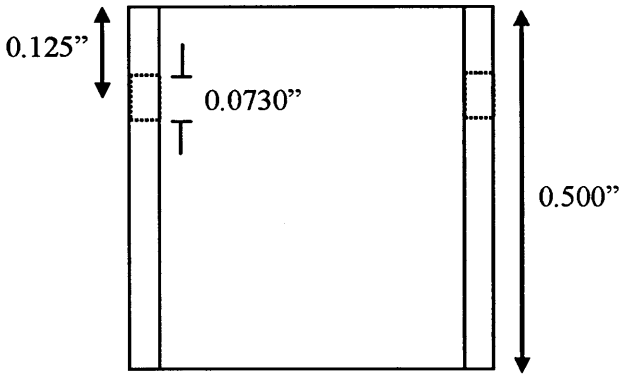

The center of the holes are 0.125" from the top of the tube.

Drawn by: Ramsey Arnold & Tom McKrell
Date: 3/14/11
Part Name: α-Sample Tubes
Material: Alpha-Phase Silicon Carbide (Provided)
Quantity: 50
Tolerances: X.XX" = ±0.010"
X.XXX" = ±0.005"
X.XXXX" = ±0.005"

Request for machining to *Ferro-Ceramics Grinding, Inc.* (pg 2 of 3)

We will send you a 1.9" long tube of beta-SiC with the inner and outer diameter dimensions shown below (thickness ~ 0.030"). We would like you to provide a quote with the price per piece to cut to height and machine the holes as shown below.

Top View

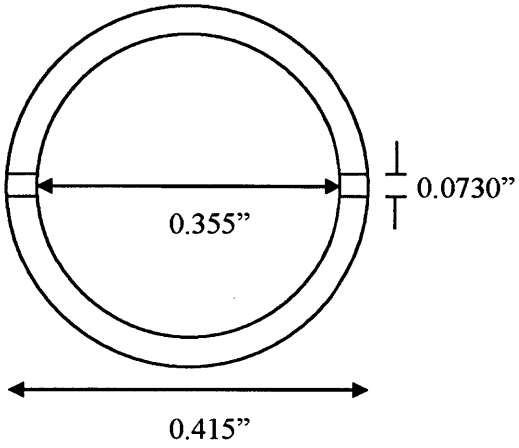

1/16" diameter rod should be able to fit through the tube holes

Side View

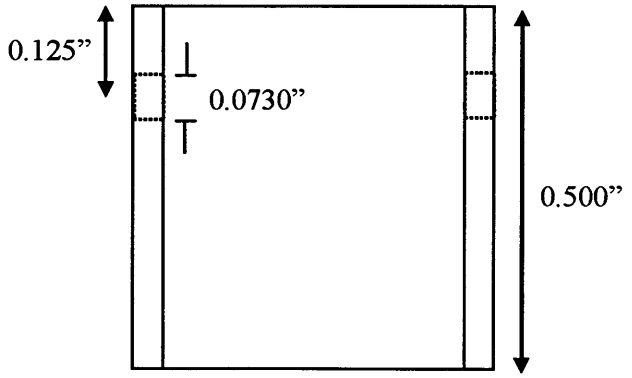

The diameter of the circular hole is 0.0730".

The center of the holes are 0.125" from the top of the tube.

Drawn by: Ramsey Arnold & Tom McKrell
Date: 3/14/11
Part Name: β-Sample Tubes
Material: Beta-Phase Silicon Carbide (Provided)
Quantity: 3
Tolerances: X.XX" = ±0.010"
X.XXX" = ±0.005"
X.XXXX" = ±0.005"

Request for machining to *Ferro-Ceramics Grinding, Inc.* (pg 3 of 3)

We will send you four (4) alpha-SiC rectangular blocks with the dimensions shown below. The widths of each piece are not the same. We would like you to provide a quote with the price per piece to machine the holes as shown below.

Side View

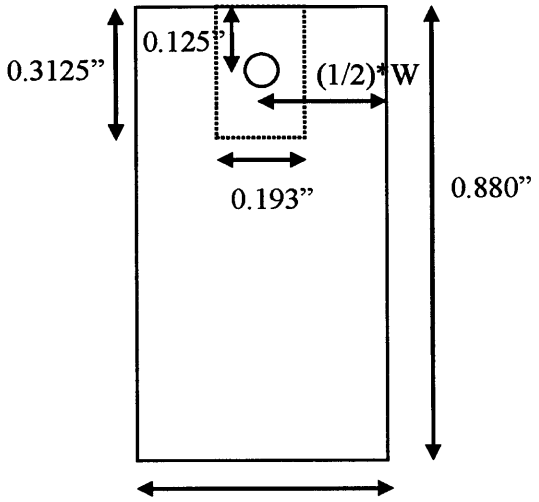

W = 0.426", 0.439", 0.470", 0.480"

Top View

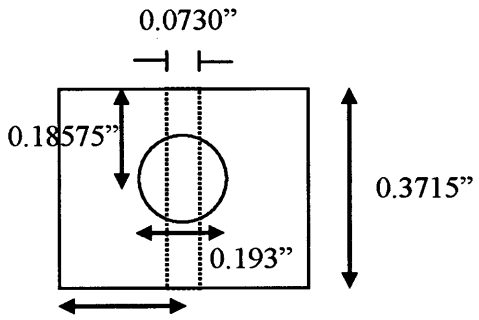

(1/2)*W = 0.213", 0.2195", 0.235", 0.240"

The horizontal circular hole has 0.0730" diameter. The center of the hole is 0.125" from the top of the block. The circular hole should be centered within the width dimension. Hence, the center of the hole should be (1/2) x W from the side faces.

The vertical circular hole has a 0.193" diameter and should be centered on the top face. The hole depth should be 0.3125".

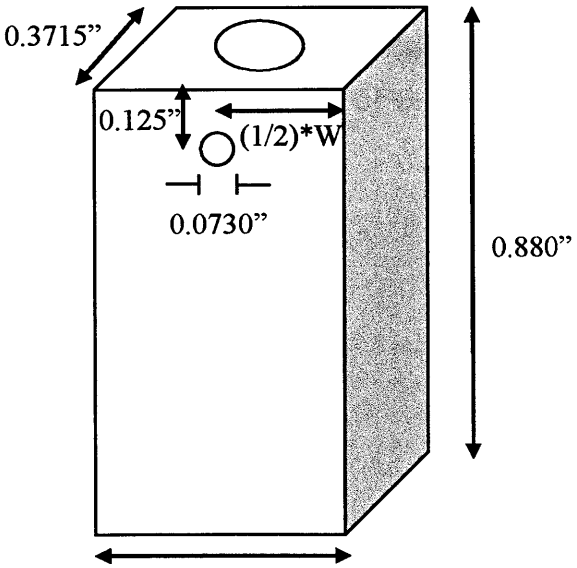

W = 0.426", 0.439", 0.470", 0.480"

Drawn by: Ramsey Arnold & Tom McKrell
Date: 3/14/11
Part Name: α-Sample Blocks
Material: Alpha-Phase Silicon Carbide (Provided)
Quantity: 4
Tolerances: X.XX" = ±0.010"
X.XXX" = ±0.005"
X.XXXX" = ±0.005"